Investigation and Optimization of Hydraulic Step-down Switched Inertance Converters with Non-uniform Inertance Tubes

A Thesis Submitted to the

College of Graduate and Postdoctoral Studies

in Partial Fulfillment of the Requirements

for the Degree of Master of Science

in the Department of Mechanical Engineering

University of Saskatchewan

Saskatoon

By

Jeremy William ven der Buhs

Permission to Use

In presenting this thesis in partial fulfilment of the requirements for a Postgraduate degree from the University of Saskatchewan, I agree that the Libraries of this University may make it freely available for inspection. I further agree that permission for copying of this thesis in any manner, in whole or in part, for scholarly purposes may be granted by the professor or professors who supervised my thesis work or, in their absence, by the Head of the Department or the Dean of the College in which my thesis work was done. It is understood that any copying or publication or use of this thesis or parts thereof for financial gain shall not be allowed without my written permission. It is also understood that due recognition shall be given to me and to the University of Saskatchewan in any scholarly use which may be made of any material in my thesis.

Requests for permission to copy or to make other use of material in this thesis in whole or part should be addressed to:

Head of the Department of Mechanical Engineering
3B48 Engineering Building
57 Campus Drive
University of Saskatchewan
Saskatoon, Saskatchewan, S7N 5A9
Canada

OR

Dean of the College of Graduate and Postdoctoral Studies
116 Thorvaldson Building
110 Science Place
University of Saskatchewan
Saskatoon, Saskatchewan, S7N 5C9
Canada

Abstract

In hydraulic systems with multiple actuators, difficulty can arise with matching the load requirements with the supply power from the system's pump. To get the desired performance at the individual loads, restrictive type valves are used to control pressure or flow by throttling the flow over a spool orifice, creating considerable power loss. This causes hydraulic systems powered off the same pump to be inefficient. Switched inertance hydraulic systems are a new technology in the field of fluid power that convert pressure and flow more efficiently than using restrictive type hydraulic valves. The step-down, or "buck", converter considered exclusively in this thesis has the ability to reduce pressure and increase flow rate to a load. The system is constructed using a digital hydraulic valve and check valve connected to the pressure supply and system reservoir respectfully. Following the valves, the system has an inertance tube, a long piece of uniform hydraulic line where fluid inertia is built up. The inertance tube also causes pressure wave propagation effects to occur since the length of the line is typically long. The performance of switched inertance converters are largely governed by the performance of the switching valve. An ideal switched inertance converter is 100% efficient at converting pressure and flow, however this would require the valve to actuate at extremely high frequency and switch instantaneously fast. This is not realizable as real valves operate up to a maximum of a couple hundred Hertz, and take a finite time to open and close, on the order of milliseconds. One of the main losses of a buck converter is the power loss across the switching valve as it transitions from open to closed and vice versa. This loss arises from the throttling of flow over the valve opening during actuation.

The research presented in this thesis looks at mitigating this loss, as well as the viscous friction loss within the inertance tube. These losses can be reduced by using an inertance tube of variable shape, a new idea introduced very recently. A shaped inertance tube is a fluid pipeline with varying cross sectional area over its length, as compared to uniform inertance tubes which have constant cross sectional area. The current gap in the research is that the tube design is not fully optimized leaving room for potential improvements in identifying better dimensions, or perhaps finding a more optimal shape. Models for comput-

ing fluid transients in uniform lines are well developed, however modelling fluid dynamics in shaped inertance tubes is an area that has not been studied as extensively. The research presented proposes a computer model for simulating fluid transients in tapered transmission line segments using the transmission line method (TLM). The current research gap in modelling tapered transmission lines is that previous models are difficult to simulate in the time domain, have poor accuracy, and have a limited range of applicability. The proposed TLM model looks to mitigate these shortcomings. When connected in succession, the tapered TLM can model shaped inertance tubes for application to hydraulic buck converters. The proposed model shows improved agreement to a numerical solution of the Navier-Stokes equations than the previous models on the topic. Validation of the model is also gained though analysis of the dynamic response in the frequency domain.

With the model now available to simulate shaped inertance tubes, a buck converter system is defined with equations presented for dynamic simulation. Initial simulations of the buck converter using parameters and design from previous research showed unoptimized performance operating at an efficiency of 47.8% for a system using a uniform inertance tube. The main objective was to optimize the shape of the inertance tube to realize increased performance using simulation studies. Genetic and pattern search algorithms were used to optimize the dimensions of the inertance tube with the goal of maximizing system efficiency while maintaining the same load. As a baseline, the uniform intertance tube design was optimized, and realized an efficiency of 64.1%, performing significantly better than the unoptimized uniform inertance tube. Further optimizations added an increasing number of tapered sections to describe the arbitrary shape of an inertance tube, up to 4 tapered segments. Significant efficiency increases were realized when using shaped inertance tubes. The best tube design increased system efficiency over 6% compared to the uniform design at a value of 70.2%. Other optimizations showed improvements in efficiency over the traditional design by reducing both valve and frictional losses in the system. The research presents a novel inertance tube design, containing a uniform section of high inertance followed by a diverging tapered section followed by another uniform section at larger diameter and low resistance. This design also proposes the idea of potential noise reduction due to the suppression of pressure fluctuations at the load.

Acknowledgements

Contents

List of Tables

List of Figures

ix

Nomenclature

1, 2	Subscript indicating inlet and outlet respectively
$A(x)$	Cross-sectional area of transmission line at axial location x
A	Orifice opening area
A_l	Load orifice area
A_{pa}	Switching valve opening area
$A_{pa,min}$	Switching valve leakage area
$A_{pa,max}$	Switching valve fully open area
A_{ta}	Check valve opening area
$A_{ta,min}$	Check valve leakage area
$A_{ta,max}$	Check valve fully open area
b	$E(s)$ transfer function scaling factor
$C_1, \ C_2$	Characteristic pressures of the TLM
C_d	Orifice discharge coefficient
c_r	Wave speed in a rigid pipe
c_e	Wave speed in an elastic pipe
c_{eff}	Effective wave speed
D	Dissipation Number (Tahmeen et al., 2001) in Chapter 2
D	Orifice opening diameter in Chapter 3
d	Inertance tube internal diameter
E	Young's modulus of elasticity of pipe material
e	Pipe wall thickness
$ETFE$	Empirical transfer function estimate
$E(s), \ F(s), \ G(s)$	TLM weighted transfer functions
f	Optimization objective function
f_{pa}	Switching valve operating frequency
f_s	Sampling frequency
$J_0, \ J_2$	Bessel functions of the first kind
j	Unit imaginary number
K	Bulk modulus of the fluid
k	Number of weighting factors
l	Length of transmission line
m	Order of MLS signal
$m_{Ei}, \ m_{Gi}$	Weighting factors
N	Frequency-dependent friction term
n_i	Weighting factors
P	Fourier transform of pressure
p	Pressure
p_a	Inertance tube inlet pressure
p_{cr}	Check valve cracking pressure
p_l	Load pressure

p_{or}	Check valve pressure override
p_s	Supply pressure
p_t	Reservoir pressure
p_{tr}	Flow regime transition pressure
$\mathbb{P}_{ab}$	Inertance tube resistance power loss
$\mathbb{P}_l$	Load power
$\mathbb{P}_{pa}$	Switching valve power loss
$\mathbb{P}_s$	Supply power
$\mathbb{P}_{ta}$	Check valve power loss
Q	Fourier transform of flow
q	Flow
q_a	Inlet flow of inertance tube
q_b	Outlet flow of inertance tube
q_l	Flow through load orifice
q_{pa}	Flow through switching valve
q_{ta}	Flow through tank sided check valve
R	Steady state resistance
R_{cr}	Critical Reynolds number
r	Pipe radius
S	Normalized Laplace operator (Tahmeen et al., 2001)
s	Laplace operator
T	Wave propagation time
T'	Modified wave propagation time
T_p	Pipe temperature
t	Time
t_o	Starting time of the switching cycle
t_p	Switching valve cycle period
t_{sw}	Switching valve actuation time
$t_{11}, t_{12}, t_{21}, t_{22}$	Transmission matrix numerical ODE terms
$t_{11}^*, t_{12}^*, t_{21}^*, t_{22}^*$	Transmission matrix approximated terms
V_p	Piezo speaker excitation voltage
V_l	Load volume
x	Axial location
Z_c	Characteristic impedance
α	Axial effect wave speed modifier
β	Dissipation number
Γ	Propagation operator (Tahmeen et al., 2001)
ϵ	Error
η_{sys}	Buck converter system efficiency
η_{vol}	Buck converter volumetric efficiency
θ	Taper angle
κ_{pa}	Switching valve operating duty cycle
λ	Taper ratio
ν	Kinematic viscosity
ν_p	Poisson's ratio of pipe material

ξ	Convergence/divergence parameter (Tahmeen et al., 2001)
ρ	Fluid density
τ	Wave propagation time modifier
Ω	Number of frequency points on which the optimization is performed
ω	Frequency

Chapter 1

Introduction

This chapter will introduce the background information and motivation behind this project. The history of research of this technology along with discussions on the current methods for increasing performance will be presented in a detailed literature review. The research objectives and expected contributions will be discussed, then will be followed by an overview of the thesis as a whole.

1.1 Background

Hydraulic systems are common-place in industrial settings and on heavy-duty mobile equipment. There are many reasons these systems are used so often, some notable ones are their high power-to-weight ratio and simple power train compared to mechanical systems. While extremely effective at transmitting power, hydraulic systems suffer from losses, as do any other mechanical or electrical system. Hydraulic losses occur in three main places: actuators such as pumps, motors, and cylinders; controls like directional, pressure, and flow control valves; and conveyances like lines, hoses, and fittings. Most hydraulic systems are powered by the same pump with multiple actuators requiring different operating conditions, therefore control valves are used to throttle flow to match the desired load performance to the operators input. While there are systems, such as load-sensing (LS) and pressure compensated (PC) pumps, that have been designed to better match input power to required power at the load, the use of restrictive type control valves to throttle pressures and flows are still required if multiple loads are present. Significant hydraulic power is lost across these valves, and power

is released as heat into the valve components, the environment, and the hydraulic fluid. With the need for hydraulic systems to become more efficient due to dwindling resources, increasing fuel costs, and stricter emissions regulations, newer technologies are being developed to better control pressures and flows without the need for inefficient restrictive control valves.

One such technology is the switched inertance converter, a digital hydraulic system that efficiently controls pressure and flow using switching control and fluid inertial properties. Inertia is cyclically built up and released by accelerating and decelerating fluid in a long tube called an inertance tube, which allows for the suction of fluid from a reservoir, or dumping it to effectively reduce or increase pressure. There are two main configurations that operate differently depending on what type of control is needed. A step-down or "buck" converter lowers pressure and boosts flow from the supply, while the other configuration, a step-up or "boost" converter, increases pressure while reducing flow. A buck converter can perform similar control as typical restrictive pressure and flow control valves, however with significantly greater efficiency. Boost converters can have more specialized applications where an increase in pressure is required elsewhere in the circuit. The buck converter will be specifically focused on in this dissertation.

Switched inertance converters are based on their electrical equivalent, the switched-mode power supply, a technology that has been well developed today. The hydraulic domain of these converters were initially conceived by Montgolfier (1803) (co-inventor of the manned hot-air balloon) with his invention of the hydraulic ram pump, a large scale boost converter. Modern applications to fluid power systems began with Brown (1987), indicating a significant gap in development from the early 19th century to the late 20th century. This gap in development is believed to be due to switching valve technology which, still to this day, has been one of the main limiting factors in commercializing the technology. The limiting factor with hydraulic valves is the speed at which they operate. One of the major losses in a switched inertance converter is the loss across the partially open valve as it switches from open to closed. While specialized high speed-valves have been developed for research purposes that reduce this loss, commercially available valves have limited bandwidth and actuate on the order of milliseconds, which can be significant.

Proposed ideas to mitigate this loss focus on instilling resonance inside the inertance tube

using half-cycle or near half-cycle resonance, which has shown to have good results (Pan et al., 2014a; Scheidl and Hametner, 2003; Wang et al., 2011; Wiens, 2015). Other novel ideas by Wiens (2015, 2016) have shown that adjusting the reservoir flow check valve location and using full-cycle resonance with shaped inertance tubes have reduced this loss and increased efficiency. Using shaped inertance tubes is a novel idea that exploits wave propagation effects within the line and internal reflections to gain improved efficiency characteristics, and its effects have not yet been fully investigated or optimized until this point. This method of loss mitigation is the main focus of this thesis.

1.1.1   Configuration and Operation of A Buck Converter

Hydraulic buck converters can be constructed using two different valve configurations to achieve the same flow boosting effect. A common configuration uses a 2-position 3-way valve as the main switching valve as shown in Figure 1.1 (a). This valve has two inlets, and one outlet port. One inlet is connected to the high pressure supply, and the second inlet is connected to the low pressure supply. The outlet of the valve is then connected directly to the inlet of an inertance tube, a long piece of small diameter hydraulic line. This configuration is popular due to its simplicity in only having 1 valve component; however it does add complexity with respect to valve control and timing. The other common configuration, which has also been studied extensively, uses a simple digital hydraulic valve (2-position, 2-way) in combination with a check valve as shown in Figure 1.1 (b). The inlet of the switching valve is connected to the high pressure supply, with the check valve connected to the reservoir to allow flow from the reservoir into the inlet of the inertance tube at a tee junction. This configuration is simpler to control due to the passive actuation of the check valve.
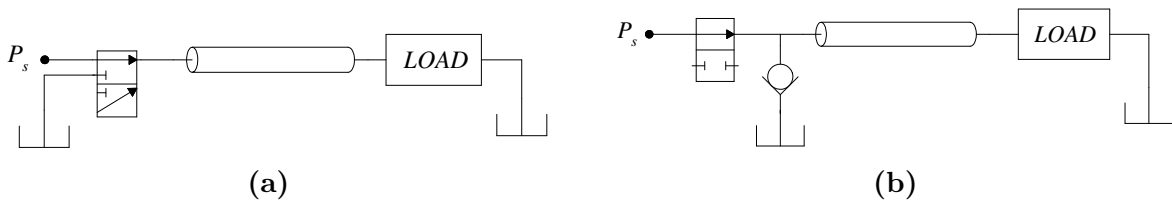
Figure 1.1: (a) A buck converter using a 2-position, 3-way directional control valve. (b) A buck converter with a digital hydraulic valve in combination with a check valve.

Configuration (b) is considered exclusively in this thesis. The operation is visualized in

Figure 1.2, with the flow paths indicated in green. Figure 1.2 (a) shows the acceleration of fluid through the long inertance tube when the switching valve is open. Once the valve shuts, the fluid tends to continue in the forward direction creating suction at the check valve, pulling fluid from the low pressure reservoir into the inlet of the instance tube shown in Figure 1.2 (b). As a result, more fluid is introduced into the system, increasing output flow, and decreasing pressure due to the exposure to the lower reservoir pressure. Even though the flows through the switching and check valves are rapidly switching from low to high, and vice versa, the load flow is maintained to a near constant value as indicated in Figure 1.2 (c). The valve is actuated with a pulse-width modulated (PWM) signal, at a specific frequency and duty cycle. While this explanation is simplified, other effects such as wave propagation in the long inertance tube have shown to have a large influence on the performance of the system if not designed carefully.

1.2   Literature Review

As previously mentioned, switched inertance technology was introduced centuries ago, but modern research and applications to fluid power have only progressed within the last 30 years or so. Brown first introduced the circuit in 1987 where he extensively highlighted the similarities between the hydraulic converters and their electrical counterparts. He also pointed out its potential energy savings over typical resistive control. Ideal switched inertance systems theoretically can achieve 100% efficiency, whereas ideal resistive control is based off the ratio of supply and load pressures which inherently leads to very poor efficiency. Consider a simple hydraulic circuit having a supply pressure of 25 MPa, tank pressure of 10 MPa, and a desired load pressure of 16 MPa for some arbitrary load. This circuit theoretically has an ideal efficiency of 40% when using a restrictive-type pressure reducing valve (PRV) to set the load pressure. Using a switched inertance converter in place of this PRV can have significant efficiency gains. Brown (1987) also pointed out that realistic implementations of a converter will suffer from losses such as resistive losses within long inertance tubes, and dynamic losses across switching valves.

The technology has been researched quite recently at the University of Bath by Johnston
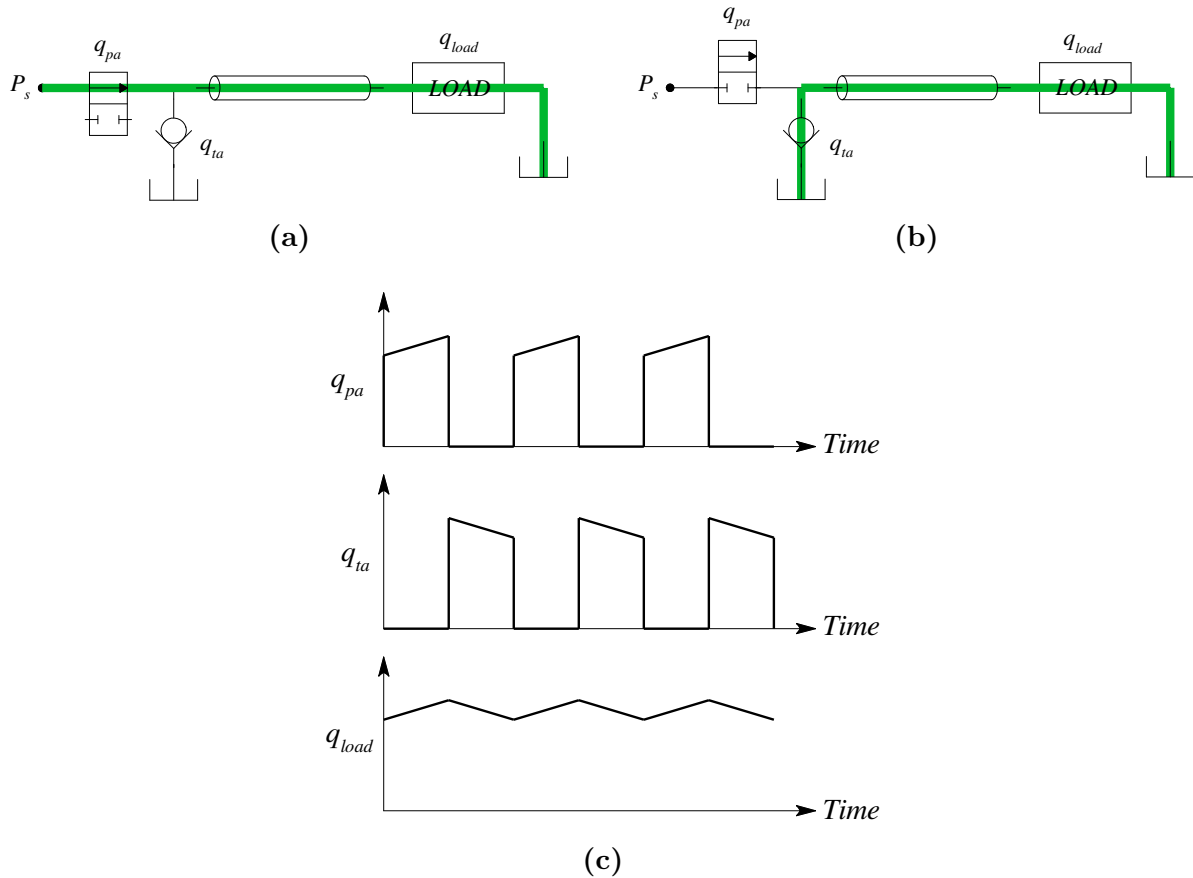
Figure 1.2: (a) Flow path of the converter with the switching valve open. (b) Flow path with the switching valve closed. (c) Flows of an idealized converter over 3 cycles (Johnston, 2009).

(2009) and Pan et al. (2014a,b) looking at theoretical analysis as well as experimental results. One of the biggest challenges with theoretical simulations of the converter is the model of the inertance tube, which has numerous effects that can affect performance. Simpler models are available, but in order to truly model realistic dynamic flow, Johnston et al. (2014) developed the enhanced transmission line method (TLM), which is a complex network of linear transfer functions and time delays that simulate pressure and flow dynamics within inertance tubes. They use this model extensively in their research to compare to experiments, where the results have been very good. More information on transmission line modelling will be presented in the following chapter.

Research at Johannes Kepler University Linz by Kogler and Scheidl (2008) looked at theoretical and experimental analysis of both buck and boost converters. Extensive work by

Kogler (2012) looked specifically at the buck converter, and also designed compact commercial prototypes within his Ph.D dissertation. In his work, he studied the function of every component within the buck converter circuit developing models for each. His simulations compared very well to experimental results of several prototype converters, which achieved very good efficiency characteristics.

Most of the research in this area has looked at theoretically simulating and experimentally testing switched inertance converters and evaluating their performance. As an outcome of this research it has been pointed out that one of the major losses within the circuit is the throttling of flow as the main switching valve transitions from open to closed and vice versa (Pan et al., 2014a). Topics of very recent research have been to minimize this loss to make switched inertance systems more efficient. The "soft-switching" concept stores the fluid that would normally be throttled across the valve in a capacitive element, and then allows it to flow out when the valve is fully open at its most efficient state (Rannow and Li, 2012; Yudell and de Ven, 2016). This technique has shown to significantly reduce power losses across the valve at the expense of increased number of components and circuit complexity. Looking at wave propagation effects within the inertance tube is another area which has sparked different approaches when it comes to optimization. Analysis of wave propagation effects due to digital valve switching has been investigated by Kogler et al. (2015) and Pan et al. (2014a) indicating that wave propagation must be seriously considered in the design and performance of these systems. Wave propagation effects generally relate to the transient propagation of flow and pressure waves from inlet to outlet and vice versa.

One idea is to remotely locate the check valve away from the switching valve at some location along the inertance tube (Wiens, 2015, 2016). This isolates wave propagation effects occurring at the valve and at the check valve, which has indicated better performance by separating these wave events. Very recent research has also looked at optimizing the diameter and length of the inertance tube to better exploit inertial and wave propagation effects (Pan, 2017). Other investigations have shown that instilling standing wave resonance in the inertance tube, either by adjusting the length of the tube or tuning the switching frequency, is very beneficial to the performance of the system (Scheidl and Hametner, 2003; Wang et al., 2011; Wiens, 2015).

Resonance can be created two different ways in order to gain efficiency benefits. First, the inertance tube can be designed to exploit soft boundary reflections off the open end of the tube using near half-cycle resonance with a tube of length $\frac{t_p c}{4}$ assuming a duty cycle of 50%. Here, t_p is the switching period and c is the wavespeed in the inertance tube. This configuration causes inverted pressured waves to reflect off the open end of the pipe. When the switching valve is open to the high pressure supply, a positive pressure wave travels along the pipe and arrives at the open end where a compressible volume or accumulator is located. As a result, the pressure wave inverts and begins to travel back to the switching valve and check valve as a suction wave. This occurs approximately half a cycle later when the switching starts to close. This tends to pull more fluid through the check valve giving better volumetric performance. However it can pull more fluid through the switching valve during closure, thus increasing the flow rate over the partially open valve, and increasing the valve loss. Due to the standing wave resonance, the opposite occurs as a positive pressure wave arrives as the switching valve opens, which reduces the flow across the valve during actuation, reducing valve loss, and increasing system efficiency (Wiens, 2015).

The second method of instilling resonance can be realized by reflecting non-inverted waves off the end of the inertance tube and arriving back approximately one full cycle later. As the valve opens, the positive pressure wave travels to the end of the tube and back reflecting as a positive pressure wave, thus reducing flow across the valve during opening and improving system efficiency. Also, when the valve closes, the suction wave travels to the end of the tube and reflects back as a suction wave the following cycle, therefore pulling more fluid through the check valve and improving volumetric performance. This design, proposed by Wiens (2015), requires the tube to be shaped having a sudden shift from low impedance to high impedance at a length of approximately $\frac{t_p c}{2}$. The design is a diverging-converging tube with the contracting section at the specified location. The current gap in the research is that the tube design is not fully optimized having room for potential improvements in identifying better dimensions, or perhaps finding a more optimal shape. Also, modern research into switched inertance converters utilizes the widely accepted and validated TLM inertance tube model developed by Johnston et al. (2014), which Wiens did not use in his simulation as the TLM had not yet been developed for tubes of varying cross section. As a result, the following

research will look at proposing the TLM for tapered transmission lines, opening the door to modelling inertance tubes of arbitrary shape. The current research gap in modelling tapered transmission lines is that existing models are difficult to simulate in the time domain, have poor accuracy, and have a limited range of applicability. Developing the TLM for tapered lines has potential for faster simulation times and more accurate results. When connected together, arbitrary tube shapes can be created and analyzed using individual tapered TLM segments. Following the development of the TLM for tapered lines, optimizations of the inertance tube shape within the application of switched inertance converters will be performed. The goal of this research is to evaluate the potential efficiency increases due to shaped inertance tubes over typical designs that employ simple uniform inertance tubes.

1.3   Research Objectives

The main objective of this research is to find the optimal shape of a hydraulic inertance tube for the use in switched inertance converters in order to maximize efficiency of the system. The optimized shape should clearly indicate improved efficiency over using standard uniform inertance tubes that have been optimized the same way. Within the scope of this project, simulation studies will be performed to demonstrate the performance of the hydraulic converter with experimental investigations suggested as topics of future research. It is expected that using shaped inertance tubes may be more complex and costly to manufacture, however if theoretical research shows improvement in the performance of the converter, justifications could be made to proceed with physical prototyping.

As a secondary objective, an accurate and validated model that describes the fluid dynamics through inertance tubes of varying cross section is required to proceed with simulations and optimizations of shaped inertance tubes. Therefore, a literature search into previous transmission line models is performed, and a model using the TLM will be proposed. It is also desired to have the model experimentally validated in order to have confidence in the results.

1.4 Thesis Overview

This section briefly outlines the contents of this thesis. The current chapter, Chapter 1, provides an introduction to the research including background information on the problem, a detailed literature search on the previous and current developments on the technology, and research objectives. Chapter 2 will review the current models in tapered transmission line modelling, and propose a new, more accurate model using the transmission line method (TLM). Experimental validation will also be performed in order to have confidence in the proposed model. Chapter 3 will introduce the dynamic models used for simulations of a switched inertance buck converter, as well as the equations that quantify its performance. Chapter 4 will propose the optimization scheme used to find the best shape for an inertance tube, and will present and discuss the results of that analysis. Finally, Chapter 5 will provide some conclusions about the presented research and propose topics for future research.

Chapter 2

Proposed Tapered Transmission Line Model

This chapter will review the current models for simulating pressure and flow dynamics within tapered transmission lines, and propose a more accurate model using the transmission line method (TLM). An extensive error analysis is performed, comparing the proposed model to the Navier-Stokes equations that describe the flow. The model is developed for both rigid and elastic fluid lines. An experiment was designed to compare real measurements to the flow equations on which the model is approximated. Lastly, time domain simulations are performed, demonstrating the step response of the model.

2.1 Chapter Preface

The research presented in this chapter has been presented by the Author at the 15th Scandinavian International Conference on Fluid Power (SICFP'17) which took place in Linköping, Sweden in June of 2017. The research has been published in the proceedings of the conference (ven der Buhs and Wiens, 2017a). The conference paper has also been expanded to include experimental results as well as elastic pipeline considerations, which has been submitted to the American Society of Mechanical Engineers (ASME) for inclusion in the Journal of Dynamic Systems, Measurement, and Control (ven der Buhs and Wiens, 2017b). The Author performed the investigation into the shortcomings of previous models and proposed improvements using the TLM. All of the detailed analysis, prototype manufacturing,

10

experimental work, and full paper composition were also performed by the Author. The co-author, Wiens, contributed the concepts of numerically solving the differential equations and weighting factor optimization. Wiens also proposed the conceptual experimental procedure and provided some specialized computer code that generates the excitation signal. Wiens provided detailed review of the papers before submission as well. At the time of publication of this thesis, the journal paper is currently in review. The model proposed in this chapter has also been applied to the detection of pipeline weakening and defects by analyzing fluid pressure dynamic response using elastic pipeline considerations. That research has been presented by the Author at the 2017 Maintenance, Engineering and Reliability / Mine Operators Conference (MEMO 2017) in Saskatoon, Canada and published in the conference proceedings (ven der Buhs and Wiens, 2017c). For this paper, the Author contributed the dynamic model, analysis, research into previous technologies, and composition of the paper. Wiens contributed the original concept and application to pipeline monitoring, and provided detailed review before submission.

2.2 Introduction

Modelling transmission lines has been a topic of research within the fluid power area for a long time. The idea that pressures and flows within a pipe propagate dynamically over its length was an idea initially introduced by Whitehurst (1775) and Montgolfier (1803) with their inventions and implementations of hydraulic ram pumps. Their inventions would prove that fluid inertia and propagation effects in long water transmission lines could be exploited to elevate pressure head at the expense of reducing volumetric efficiency. These initial findings were the basis of what is called the "waterhammer" effect, which is the basis of all transmission line models developed today. While these initial ideas where mostly observed experimentally, extensive research into the theory behind this phenomenon has been developed more recently in the latter half of the 1900's up to as recently as 2014. Transmission line research is commonly performed for uniform lines; a pipe with a constant radius. However there has been limited research into modelling tapered lines, where the radius varies linearly over its length. While the Navier-Stokes equations that describe water hammer in pipes has been

well developed and verified over the years, they cannot be solved in the time-domain very easily. Typically, some sort of approximation method is employed to allow pipelines to be solved in the time domain, and interface well with other, potentially non-linear, component models. There are numerous approximation methods, and they all have their own strengths and weaknesses. Effects such as the pipe material, pipe wall thickness, and viscous friction model have shown to have significant effects on the accuracy of today's transmission line models. An excellent comparative study prepared by Soumelidis et al. (2005) compares all of the modern day techniques used for modelling fluid transients in uniform transmission lines, where some of these techniques have been applied to the tapered problem.

2.3 Previous Models

A schematic of a rigid tapered transmission line is shown in Figure 2.1. Within a tapered transmission line, the radius varies linearly from inlet to outlet given by Eqn. (2.1):

$$r(x) = r_1 + \frac{(r_2 - r_1)x}{l}. \tag{2.1}$$

The differential equations that describe one-dimensional laminar flow, Q, and pressure, P, through the tapered tube are the equations of motion and continuity. The derivation of these equations is rather complex, but it is well documented in Viersma (1980) for uniform lines. The same equations result for tapered lines, however with terms now depending on
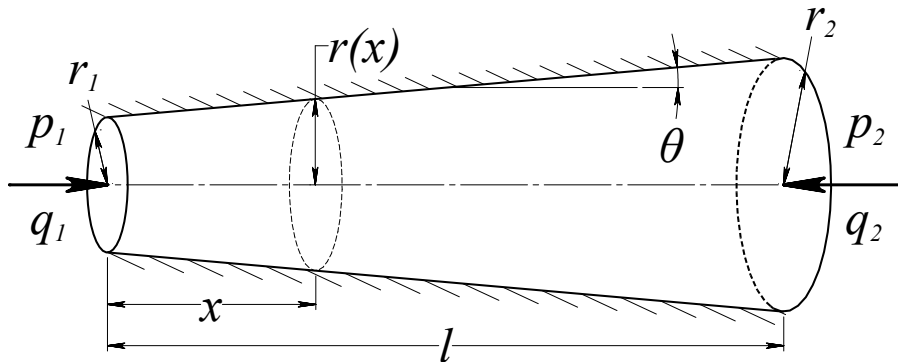
Figure 2.1: Schematic of a rigidly walled tapered transmission line. For one-dimensional flow, θ is assumed to be small.

axial location, x. These equations are expressed in the Laplace domain, respectively:

$$\frac{\partial P(x,s)}{\partial x} + \frac{\rho s}{A(x)} Q(x,s) N(x,s) = 0 \tag{2.2}$$

$$P(x,s) + \frac{\rho c_r^2}{A(x)s} \frac{\partial Q(x,s)}{\partial x} = 0 \tag{2.3}$$

where ρ is the fluid density, c_r is the wave speed within the rigid pipe defined by

$$c_r = \sqrt{\frac{K}{\rho}}, \tag{2.4}$$

K is the bulk modulus, and s is the Laplace variable. N is the frequency-dependent friction term, commonly used in previous research (Krus et al., 1994; Johnston, 2012; Johnston et al., 2014; Zielke, 1968; Muto et al., 1981; Tahmeen et al., 2001; Viersma, 1980) defined as:

$$N(x,s) = -\frac{J_0\left(jr(x)\sqrt{\frac{s}{\nu}}\right)}{J_2\left(jr(x)\sqrt{\frac{s}{\nu}}\right)}, \tag{2.5}$$

where ν is the kinematic viscosity of the fluid, and $J_{0,2}$ are Bessel functions of the first kind.

In hydraulic system analysis, it is common for researchers to assume quasi-steady distributed friction within the fluid lines, such as given by Krus et al. (1994):

$$N(s) = \frac{R}{Z_c T s} + 1. \tag{2.6}$$

Where R is the resistance of the line, Z_c is the characteristic impedance, and T is the time it takes for a wave to travel from inlet to outlet. This assumption simplifies the modelling of fluid lines, and while this is more than adequate for systems that operate at steady state, it is not a very accurate assumption for systems that continuously oscillate. Realistic viscous friction inside fluid pipelines is inherently frequency-dependent, and models that implement it have shown to be significantly more accurate than models that assume steady friction (Johnston, 2012; Krus et al., 1994; Zielke, 1968).

The presented differential Equations (2.2) and (2.3) cannot be analytically solved in the time domain or frequency domain, largely due to the complex ratio of Bessel functions present in the term for the frequency dependent friction, $N(x,s)$. As a result, a major portion of the research into the simulation of fluid lines has been the development of numerical approximate

models. The first approximation of tapered lines began with Zielke (1968) where he proposed a method of characteristics (MOC) solution. Within the MOC, the equations of motion and continuity in the time domain are transformed into ordinary differential equations using finite difference methods. These equations are then integrated along characteristic lines that represent the propagation of waves along the pipe. Figure 2.2 shows the characteristic lines, c^+ and c^-, for this application which correspond to the wave propagation in either driection in the transmission line.
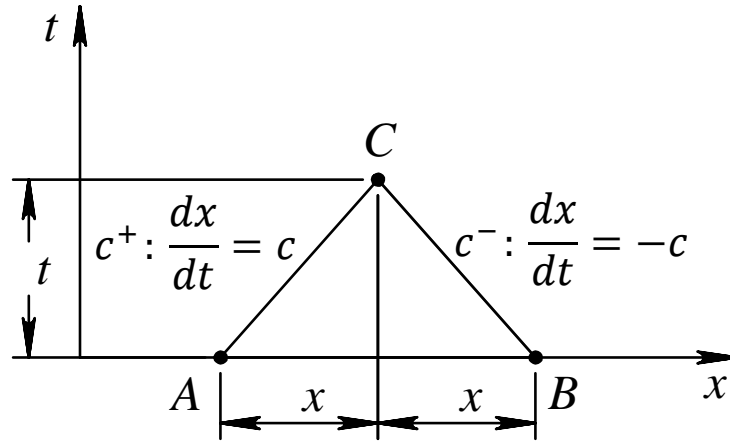
Figure 2.2: Characteristic lines c^+ and c^- used for the MOC. Time steps are determined by the speed of sound in the pipe, c, (Johnston, 2006).

While the equations for the MOC were proposed for tapered lines in Zielke's paper, it was not solved nor investigated experimentally. His work on tapered lines was taken further by Washio et al. (1974) where they computed the MOC for tapered lines and performed experiments to validate the theory. Their experimental results only looked at the first harmonic resonance in the frequency domain, which compared very well. This method has shown to accurately model the effects of frequency dependent friction as well, however, it can be computationally intensive since it calculates pressures and flows at nodes throughout the length of the line. The MOC is also restricted to fixed-step solvers, which is undesirable as most modern day simulations use advanced variable-step solvers that can significantly reduce simulation times (Johnston, 2006).

An approximate analytical solution to the differential equations was then proposed by Muto et al. (1981). Their solution, represented as a transmission matrix in the frequency

domain, was generated by rejecting higher order terms of a Taylor series expansion which allowed for a closed form solution. This model is in nondimensional form with all parameters nondimensionalized with respect to the inlet radius, r_1. The transmission matrix Muto et al. derived is defined as:

$$
\begin{pmatrix} P_1 \\ \\ Q_1 \end{pmatrix} = \begin{pmatrix} \cosh\Gamma - \dfrac{\xi\lambda_o}{DS\sqrt{N}}\sinh\Gamma & Z_c\sqrt{N}\sinh\Gamma \\ \dfrac{1}{Z_c\sqrt{N}}\sinh\Gamma & \cosh\Gamma + \dfrac{\xi\lambda_o}{DS\sqrt{N}}\sinh\Gamma \end{pmatrix} \begin{pmatrix} \dfrac{P_2}{1-\xi\lambda_o} \\ \dfrac{Q_2}{1+\xi\lambda_o} \end{pmatrix} \tag{2.7}
$$

where,

$$
\Gamma = DS\gamma_o[1+\xi(1-\lambda_o)], \;\; D = \frac{\nu l}{c r_1^2}, \;\; Z_c = \frac{\rho c \gamma_o}{\pi r_1^2},
$$

$$
\lambda_o = \frac{1}{2}\left[1 - \left\{\frac{\chi_o(\gamma_o^2-1)}{2\gamma_o}\right\}^2\right], \;\; t_o = \frac{r_1^2}{\nu}, \;\; S = st_o, \tag{2.8}
$$

$$
\gamma_o = \left[-\frac{J_o\left(j\sqrt{S}\right)}{J_2\left(j\sqrt{S}\right)}\right], \;\; \chi_o = \sqrt{S}, \;\; \xi = \frac{\theta l}{r_1}.
$$

As presented, the model proposed by Muto et al. cannot be solved in the time domain. Further approximation of this transmission matrix is required in order to perform simulations. Muto and Kayukawa (1986) progressed their research where they made further approximations to their transmission matrix. They used an approximation proposed by Brown (1962) to allow them to determine response curves for the impulse and step response. Their approximations allowed them to model tapered lines within the taper parameter range of $|\xi| < 0.1$. It is important to note that this region of applicability is fairly limiting. Their research also only allows the simulation of the impulse and step response of a line, and does not permit the interfacing with other component models in a hydraulic system.

The approximate transmission matrix, Equation (2.7), was taken further by Tahmeen et al. (2001) by performing a different approximation technique to allow for simulation in the time domain and interfacing with other system components. This is the most recent development on tapered transmission line modelling. In their paper, they used modal analysis (MA) and rational polynomial transfer function approximations (RPTFA) to approximate

the hyperbolic and transcendental functions in the solution. This required the rearrangement of the transmission matrix into every possible configuration of input and output. This approximation is tabulated in detail in their paper. Tahmeen et al. were able to perform simulations in the time domain, with good agreement to the results in Muto et al. (1981) and Muto and Kayukawa (1986). However it is important to note that this approximation has the same limitations as previous, and that it is also based on the approximated transmission matrix proposed by Muto et al. which has some shortcomings due to providing asymmetrical solutions.

An important factor with simulation models that interface with other components is solving symmetrically. This means that by maintaining the same boundary dimensions and conditions, the model should provide the same solution even if the ends are swapped. Consider the two cases visualized in Figure 2.3. Case 1 has a diverging tapered pipeline with the outlet of the line blocked (i.e. $q_2 = 0$). This case has an open inlet, where the pipeline is excited with an input signal. Case 2 is essentially a flipped version of Case 1, having a converging tube with a blocked inlet (i.e. $q_1 = 0$). Case 2 has an open outlet, where the tapered line is excited with an input signal. Both cases have the larger radius blocked (indicated with cross hatching), the smaller radius open, and the same length, l.
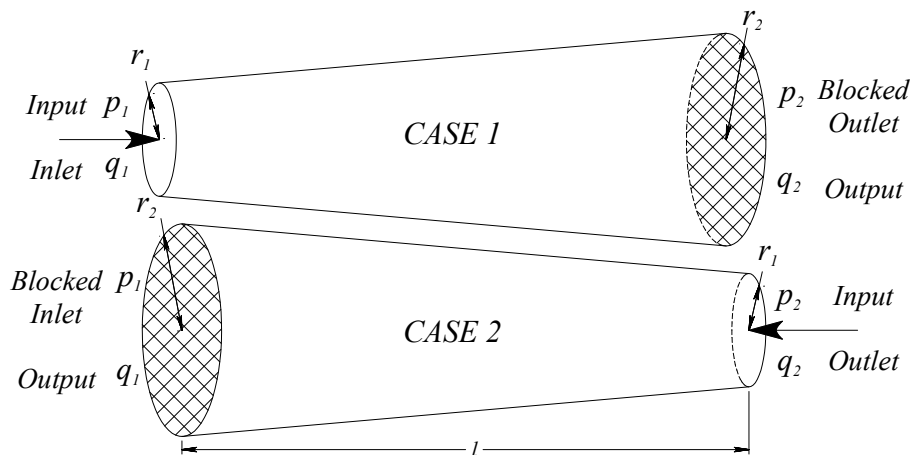
Figure 2.3: Visual representation of the two tapered line cases.

The *Output/Input* transfer function of pressure was computed for both cases using Equations (2.7) and (2.8), and is shown in Figure 2.4. The results show that between Cases 1 and 2, the frequency response is not the same as the resonant frequencies are shifted. Since

16

Case 2 is a flipped version of Case 1, keeping all things constant, the realistic result should show the transfer functions be identical. The same study was performed using a numerical solution to the differential Equation (2.9) defined as:

$$\frac{\partial^2 Q(x,s)}{\partial x^2} - \frac{1}{A(x)}\frac{dA(x)}{dx}\frac{\partial Q(x,s)}{\partial x} - \frac{s^2}{c_r^2}N(x,s)Q(x,s) = 0 \qquad (2.9)$$

which is the second order form of Equations (2.2) and (2.3) when the equations are combined. The differential equation is computed with a numerical boundary value solver, explained in a later section. The results of that investigation yielded the same transfer functions for both cases, which is also plotted in Figure 2.4. As a result of this case study, confidence in the previous model was low as asymmetry in the dynamic model leads to errors in further approximations and implementations in the time domain.
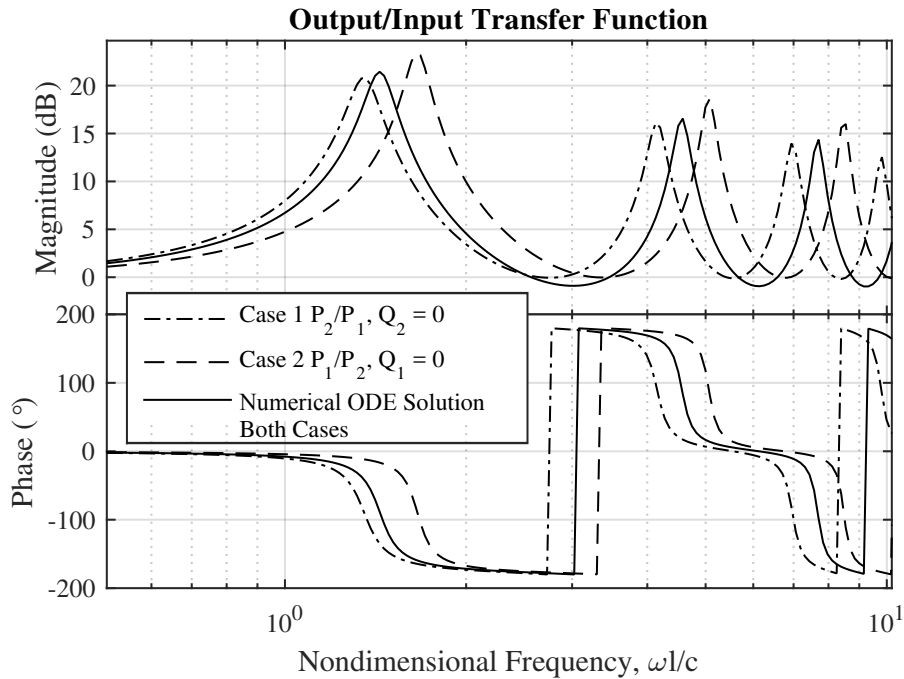
Figure 2.4: Asymmetry of the transfer functions in the previous models. The ODE numerical solution for both cases is shown for comparison.

Another shortfall of the previous models is inaccuracy at higher resonant frequencies. Looking at the Case 1 transfer function in Figure 2.4, the first harmonic peak compares well to the numerical ODE solution, but higher frequencies do not match well. This error becomes greater as the amount of taper in the line increases.

2.4 Proposed Model

The proposed model uses the recently developed enhanced transmission line method (TLM) proposed by Johnston et al. (2014). The TLM is a method of modelling fluid transients in long pipelines using a network of linear transfer functions and time delays. The TLM is a popular technique that was initially proposed by Krus et al. (1994) and further improved by Johnston (2012) to accurately include frequency dependent friction effects. The network of transfer functions is arranged as shown in Figure 2.5. The transmission matrix relating pressures and flows from the inlet to outlet is represented by the following equation:
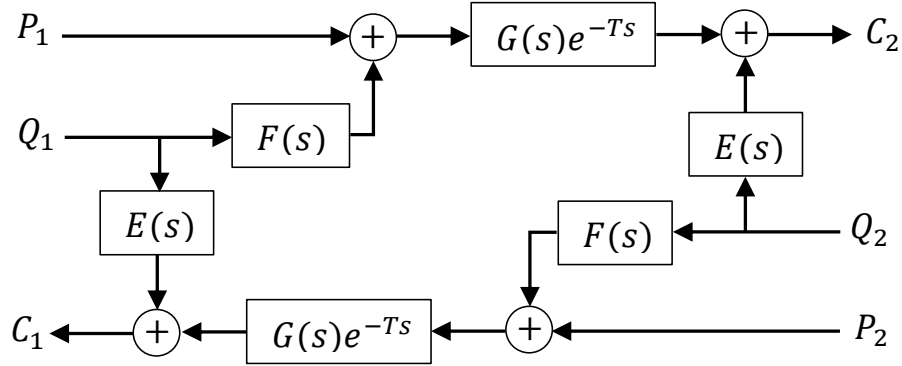
Figure 2.5: Block diagram of the TLM. (Krus et al., 1994).

$$\begin{pmatrix} P_1 \\ Q_1 Z_c \end{pmatrix} = \begin{pmatrix} t_{11} & t_{12} \\ t_{21} & t_{22} \end{pmatrix} \begin{pmatrix} P_2 \\ Q_2 Z_c \end{pmatrix} \tag{2.10}$$

where the characteristics C_1 and C_2 are related to the pressure, flow, and the line's characteristic impedance, Z_c, by:

$$P_1 = C_1 + Z_c Q_1 \tag{2.11}$$

and

$$P_2 = C_2 + Z_c Q_2. \tag{2.12}$$

The characteristic impedance of a tapered line is derived using the definition proposed by Krus et al. (1990), where wave propagation time, T, is divided by the capacitance of the

transmission line. Within the derivation, the internal volume of the line is required, which is that of a right circular cone frustum for a tapered line. Therefore:

$$Z_c = \frac{3\rho c_r}{\pi r_{max}^2} \left(1 + \lambda + \lambda^2\right)^{-1} \tag{2.13}$$

where the taper ratio, λ, is a quantification of how much the line is tapered defined as:

$$\lambda = \frac{r_{min}}{r_{max}}. \tag{2.14}$$

The taper ratio is a quantity that does not change if the tube is either converging or diverging as it is defined by the minimum radius divided by the maximum radius. As a result, the proposed tapered TLM is symmetric by design, a desired quality absent in the previous models. Another important parameter is the line's dissipation number, β, a number quantifying the amount of oscillation and damping in the pipeline. A higher dissipation number indicates the fluid response is damped greater than a fluid pipeline with a smaller dissipation number. Dissipation, in this case, is referring to the dissipation of fluid kinetic energy as heat. It is calculated with the laminar resistance of the line, R, and the characteristic impedance given by:

$$\beta = \frac{R}{8Z_c} = \frac{\nu l}{c_r r_{max}^2} \left[\frac{(1 + \lambda + \lambda^2)^2}{9\lambda^3}\right] \tag{2.15}$$

where the laminar resistance of the tapered line is determined by the integration of uniform Hagen-Poiseuille pressure drops over the full length of the transmission line. This is considered acceptable according to Lubrication theory, stating that the change in radius over a small element dx is considerably smaller than the size of the pipe itself. The laminar resistance is given as:

$$R = \frac{8\rho \nu l}{\pi r_{max}^4} \left[\frac{1 + \lambda + \lambda^2}{3\lambda^3}\right]. \tag{2.16}$$

These definitions of the critical TLM parameters are also valid for a uniform line that has a taper ratio of $\lambda = 1$. The characteristic impedance, dissipation number, and laminar resistance equations would simplify to the definitions used in Johnston (2012) and Johnston et al. (2014).

The $E(s)$, $F(s)$, and $G(s)$ transfer functions that comprise the enhanced TLM are summations of weighted transfer functions, and are arranged in the block diagram shown in Figure 2.5. The linear transfer functions defined by Johnston et al. (2014) are given as:

$$E(s) = Z_c \sum_{i=1}^{k} \frac{m_{Ei}}{n_i + Ts}, \tag{2.17}$$

$$F(s) = Z_c + bE(s), \tag{2.18}$$

$$b = 1 - \frac{8\beta}{\sum_{i=1}^{k} \frac{m_{Ei}}{n_i}}, \tag{2.19}$$

and

$$G(s) = 1 - \sum_{i=1}^{k} \frac{m_{Gi}Ts}{n_i + Ts}. \tag{2.20}$$

The transmission time, T, is scaled by a factor τ which has shown to give improved results:

$$T' = \tau T = \tau \frac{l}{c_r}. \tag{2.21}$$

The factors m_{Ei}, m_{Gi}, and τ are determined through a constrained optimization explained in detail in the following section. The weighting factors, n_i, are the same as given in Johnston et al. (2014):

$$n_1 = \frac{0.3}{1 + 3\beta}, \quad n_{i+1} = 3n_i. \tag{2.22}$$

In this case the $F(s)$ transfer function is scaled from the $E(s)$ transfer function in order to accurately compute the correct pressure drop during steady state conditions. It is also possible to specify separate weighting factors for $F(s)$, but it provided no improvement in accuracy and added considerable time to the optimization.

Working from the TLM diagram in Figure 2.5, the TLM functions can be expressed in transmission matrix form (Johnston et al., 2014). This form is used in the optimization procedure to compare the TLM to the numerical ODE solution:

$$t_{11}^* = \frac{(E + Z_c)G^{-1}e^{j\omega T'} + FGe^{-j\omega T'}}{E + Z_c + F}, \tag{2.23}$$

20

$$t_{12}^* = \frac{(E + Z_c)^2 G^{-1} e^{j\omega T'} - F^2 G e^{-j\omega T'}}{E + Z_c + F}, \tag{2.24}$$

$$t_{21}^* = \frac{G e^{-j\omega T'} - G^{-1} e^{j\omega T'}}{E + Z_c + F}, \tag{2.25}$$

and

$$t_{22}^* = -t_{11}^*. \tag{2.26}$$

Tapered transmission lines have an asymmetrical geometry as compared to uniform lines, which led to research into separating the transfer functions for the inlet or outlet such as $E_1(s)$ and $E_2(s)$. This was performed in order to see if improved accuracy of the tapered TLM could be realized. The following were investigated:

- Separate $G(s)$ transfer functions with separate weighting factors. This resulted in no increase in accuracy, and increased optimization effort.

- Separate wave propagation times T' for either direction. This resulted in increased error if the optimization ended in a local optimum with unequal T'.

- Separate $E(s)$ transfer functions, with the corresponding $F(s)$ transfer function scaled from it. This resulted in no increase in accuracy, and increased optimization effort.

- Separate $E(s)$ and $F(s)$ transfer functions where $F(s)$ is not scaled off $E(s)$. This resulted in significant error in magnitude and phase, as well as substantial increase in optimization effort.

While it was believed that these scenarios would improve accuracy, investigations showed that no improvement in accuracy could be achieved, and in all cases significant computation time was added. As a result, the standard form of the enhanced TLM was used for application to the tapered problem.

2.5   Weighting Factor Optimization

The optimization objective function is similar to the one proposed by Johnston et al. where they minimize the error in the t_{12} and t_{21} transfer functions, however they omit t_{11} and t_{22}.

The equation proposed here includes the t_{11} and t_{22} transfer functions, minimizing the error between the TLM transmission matrix of Equations (2.23) - (2.26) and the numerical ODE solution computed from the differential Equation (2.9). Here, terms with an asterisk indicate the TLM terms, and terms without indicate the results of the numerical ODE solution. The optimization function is:

$$f(m_{Ei}, m_{Gi}, \tau) = \sum_{0.01 \leq \omega T \leq n_k} \frac{\left| \frac{t_{12} - t_{12}^*}{Z_c} \right|^2}{\omega T} + \sum_{0.01 \leq \omega T \leq n_k} \frac{|(t_{21} - t_{21}^*)Z_c|^2}{\omega T} +$$

$$\sum_{0.01 \leq \omega T \leq n_k} \frac{|(t_{11} - t_{11}^*)|^2}{\omega T} + \sum_{0.01 \leq \omega T \leq n_k} \frac{|(t_{22} - t_{22}^*)|^2}{\omega T} + \epsilon_E + \epsilon_G, \quad (2.27)$$

where ϵ_E and ϵ_G are soft constraints put in place to ensure the parameters are consistent and well behaved:

$$\epsilon_E = \sum_{i=3}^{k} \left[\max(0, m_{Ei} - 3m_{Ei-1}) \right]^2, \tag{2.28}$$

and

$$\epsilon_G = 10 \left[\max\left(0, \sum_{i=1}^{k} (m_{Gi}) - 1 \right) \right]^2. \tag{2.29}$$

The optimization procedure requires the ODE solution to the problem, which was computed numerically using boundary value solution of the differential equation (2.9). The Matlab® m-files `ExactSolutionforOpt.m`, `t11t21venderBuhsExact.m`, and `t12t22ven derBuhsExact.m` in Appendix B.3, B.4 and B.5 respectively contain the algorithms used to compute the numerical ODE solution. It uses `bvp4c()` as the numerical solver to find the t_{xx} entries of the transmission matrix. Setting Q_2 to 0 allows for t_{11} and t_{21} to be found, and by setting P_2 to 0 allows for the solution of the other two entries, t_{12} and t_{22}. The boundary value problem is solved for every value of frequency given in Table 2.1. Solving the boundary value problem adds significant computation time to the optimization procedure, therefore if the Parallel Computing Toolbox is available, it is recommended to solve the transmission matrix in parallel using `parfor` loop structure. Once the numerical solution is solved, the tapered TLM parameters (m_{Ei}, m_{Gi}, and τ) are optimized using `fmincon()`, a constrained numerical optimization algorithm. The only rigid constraint on the optimization is a lower

bound of 0, ensuring all the parameters are positive, a similar constraint used in Johnston et al. (2014). The output of the optimization algorithm is typically a local minimum, not global, however in this case the results appear to have adequate accuracy.

Initial investigations showed that the same TLM weighting factors would result if the same dissipation number and taper ratio were held constant for tapered lines of different dimensions. Similar to Johnston et al. where the TLM parameters only vary with dissipation number, a tabulation of the parameters allows for fast interpolation to select the parameters for a given transmission line without repeating the optimization. In Johnston et al. (2014), a one-dimensional look-up table is used to find the parameters. However, here a two-dimensional look-up table is used due to the addition of the taper ratio parameter. The table was generated using the m-file `TableGenerate.m` provided in Appendix B.1. The algorithm is better visualized as a flow chart provided in Figure 2.6. The range of parameters for the optimizations are given in Table 2.1. The range of dissipation number, β, is logarithmically spaced with 8 points per decade, and the taper ratio, λ, is spaced linearly with 10 points. The number of TLM parameters were 13, corresponding to $k = 6$. It has been shown that varying the number of parameters has a significant effect on accuracy, which is also expected here (Johnston et al., 2014). However, with $k = 6$ it is believed that adequate accuracy is achieved without significantly increasing computation times.

Table 2.1: Range of parameters used for optimization

Parameter	Range
Frequency	$0.01 \leq \omega T \leq n_k$
Dissipation number	$10^{-4} \leq \beta \leq 10^0$
Taper ratio	$1 \geq \lambda \geq 0.5$

It was desired to have a smooth transition with the TLM parameters from one optimization to another, as it allows for interpolation for in-between values. Therefore the initial guess for optimizations were the result from the previous optimization. The optimization intially selects a value of β and $\lambda = 1$ using the initial guess from Johnston (2014) and Johnston et al. (2014) for uniform transmission lines. The following optimization at the same dissipation number and $\lambda = 0.95$ uses the result from $\lambda = 1$ as the initial guess, and
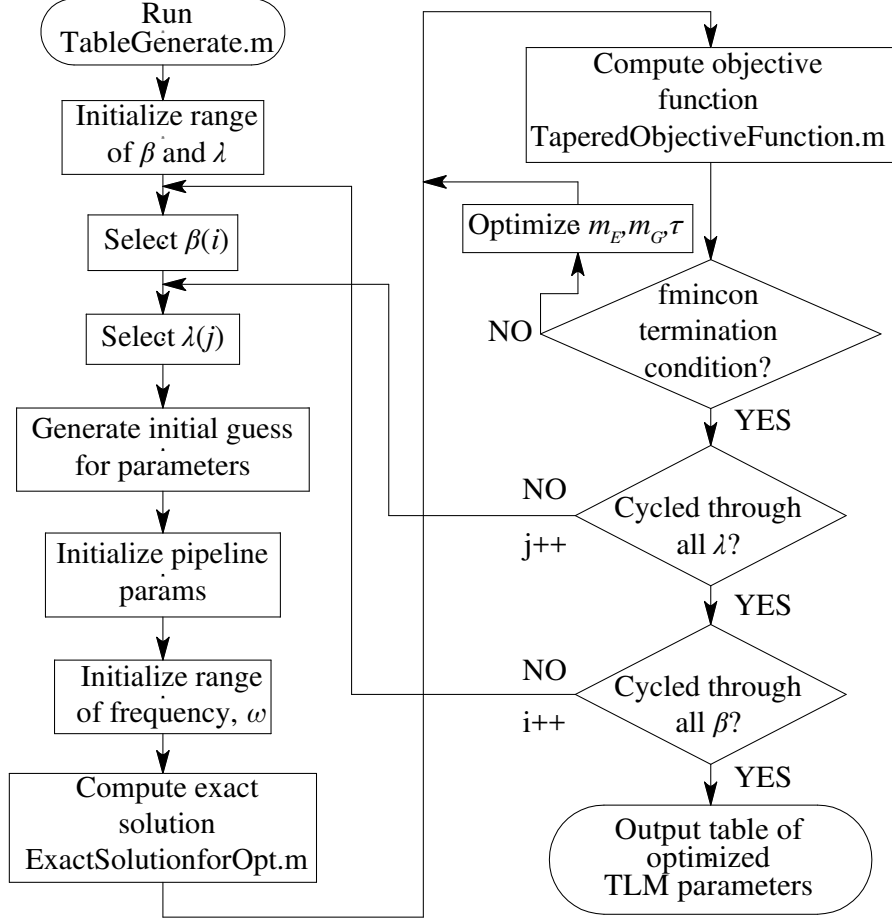
Figure 2.6: Flow chart of the tapered TLM parameter optimization procedure.

so on for all successive iterations. The output of `TableGenerate.m` are 2 three-dimensional matrices containing m_E and m_G factors, and 1 two-dimensional matrix of τ factors. The three-dimensional matrices are split up into individual two-dimensional matrices, and are included in this thesis in Appendix A along with the τ factors. The interpolation algorithm is provided in Appendix B.10, allowing for the look-up of any tapered TLM parameter set within the given range.

2.6   Frequency Domain Results

The transmission matrix for a tapered line with a dissipation number of 10^{-3} and taper ratio of 0.75 is plotted in Figure 2.7. The anti-diagonal terms of the TLM transmission matrix (t_{12} and t_{21}) compare very well to the numerical ODE solution. The principal diagonal terms (t_{11}

and t_{22}) are accurately approximated in both phase and magnitude, however not to the same extent as the the anti-diagonal terms. In the principal diagonal terms, it can be seen that the first resonant peak is not perfectly aligned, while all subsequent resonances are matched well. Also, there is a slight magnitude shift in the numerical ODE solution, which is not followed by the TLM approximation. In all terms, the proposed tapered TLM approximation is more accurate than the previous models by Muto et al. (1981) and Tahmeen et al. (2001).
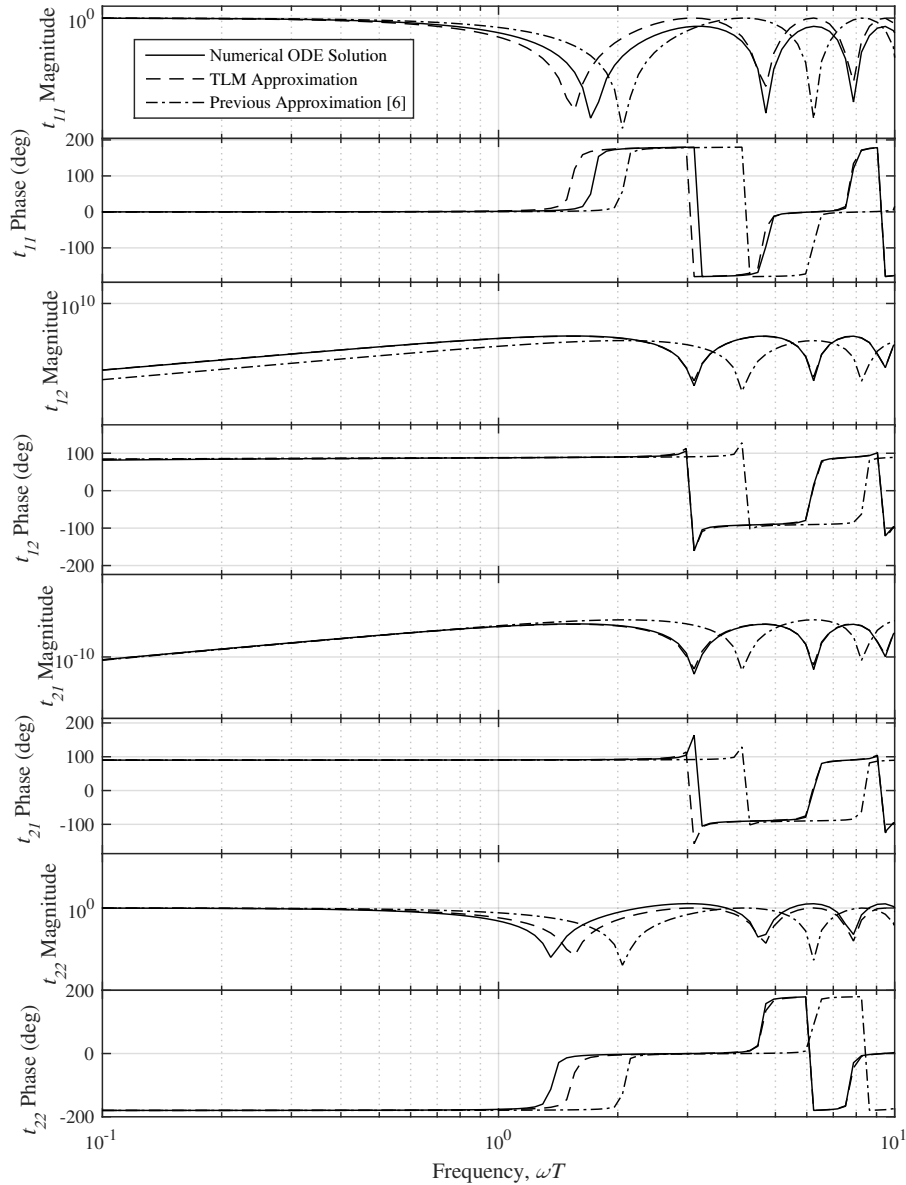
Figure 2.7: Transmission matrix frequency response for $\beta = 0.001$ and $\lambda = 0.75$.

A tapered line with less taper ($\lambda = 0.9$) and a higher dissipation number ($\beta = 10^{-1}$) has

its transmission matrix plotted in Figure 2.8. As shown, there is a better approximation of the first resonant peak within the principal diagonal terms, and the anti-diagonal terms are very closely represented.
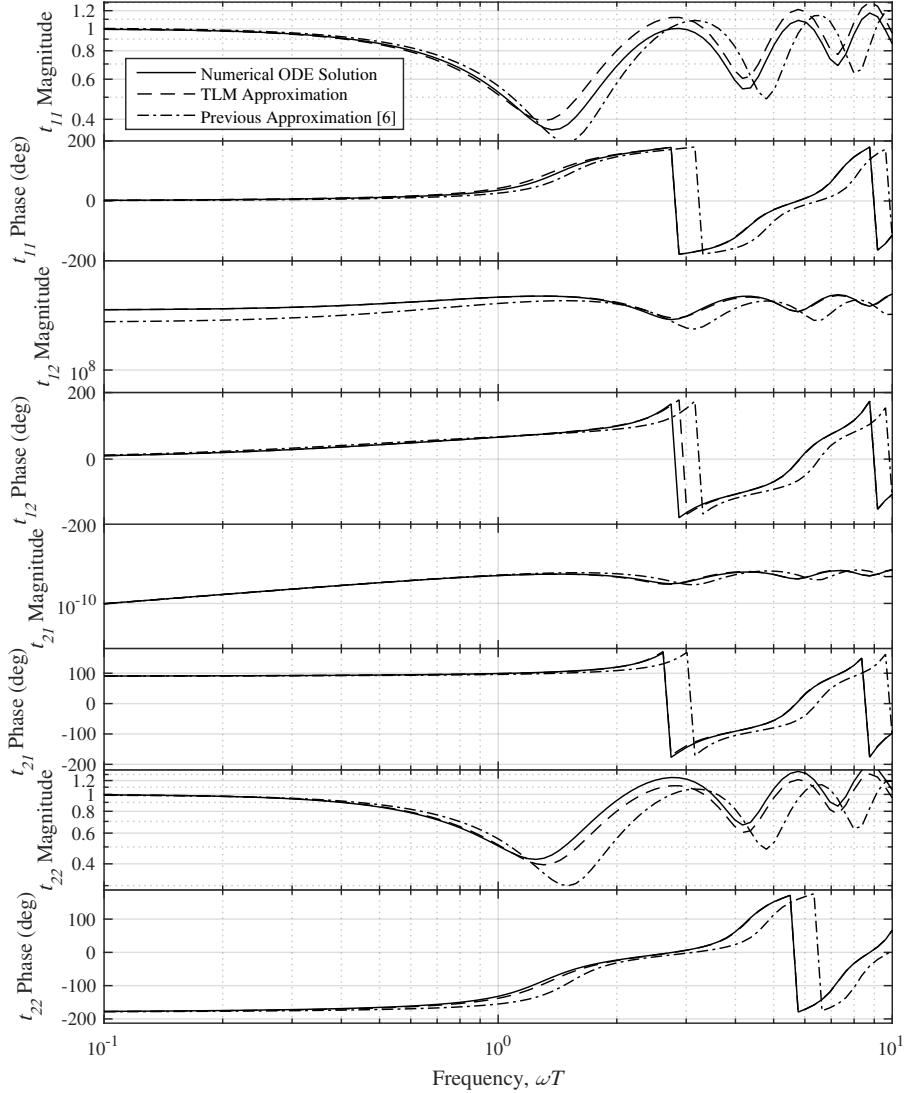
Figure 2.8: Transmission matrix frequency response for $\beta = 0.1$ and $\lambda = 0.9$.

While two transmission matrices were shown to highlight the accuracy of the proposed tapered TLM, an overall investigation into the error was desired. The following investigation looks at the error over the full range of taper ratio and dissipation number. An overall error value was defined and is used to compare the proposed tapered TLM to the numerical ODE solution, and also to compare the previous model to the numerical ODE solution. A different error value was chosen instead of using the optimized minimum from Equation (2.27) as

the proposed error value is not scaled by frequency. This gives an overall quantification of the accuracy of fit over the entire frequency range. The error function is defined as the difference between the transmission matrix terms where the anti-diagonal terms are scaled with characteristic impedance:

$$\epsilon = \frac{1}{\Omega} \sum_{i=1}^{\Omega} \left[\left| \frac{t_{12}(\omega_i) - t_{12}^*(\omega_i)}{Z_c} \right| + |[t_{21}(\omega_i) - t_{21}^*(\omega_i)] Z_c| + |t_{11}(\omega_i) - t_{11}^*(\omega_i)| + |t_{22}(\omega_i) - t_{22}^*(\omega_i)| \right].$$
(2.30)

where Ω is the number of frequency points used in the optimization. Therefore this error value is an average value not scaled by frequency. Figure 2.9 shows a color map indicating the error value over the full range of dissipation number and taper ratio. In general, the amount of error between the tapered TLM and the numerical ODE solution increases with the amount of taper (i.e. decreasing λ) and with increasing dissipation number. The TLM proposed by Johnston et al. (2014) was considered acceptable for $\beta \leq 0.5$. So by following the error value from $\lambda = 1$ to $\lambda = 0.5$, an approximately triangular region, shown as a black contour, of acceptable error is found. Therefore it is recommended to use this model within the specified acceptable error contour at an error value $\epsilon < 0.5$.

Equation (2.30) is used again to compare the previous model of Muto et al. (1981) and Tahmeen et al. (2001) to the numerical ODE solution to demonstrate the improvement of the proposed model. The error plot is shown in Figure 2.10, with the same error contour plotted at $\epsilon = 0.5$. Overall, the amount of error is greater than the previous figure, with the color map up to an error value of $\epsilon = 22$. What can be seen is that the error is extremely low around $\lambda = 1$, this is due to the fact that their approximate transmission matrix analytically becomes the ODE solution when there is no taper. As taper and dissipation number increase, the error increases rapidly. The error contour indicates a very small range of applicability of the previous model as compared to the same contour of the proposed TLM model. As a result, it is demonstrated that the proposed tapered TLM is more accurate and more applicable than the previous models when compared in the frequency domain to the numerical ODE solution.
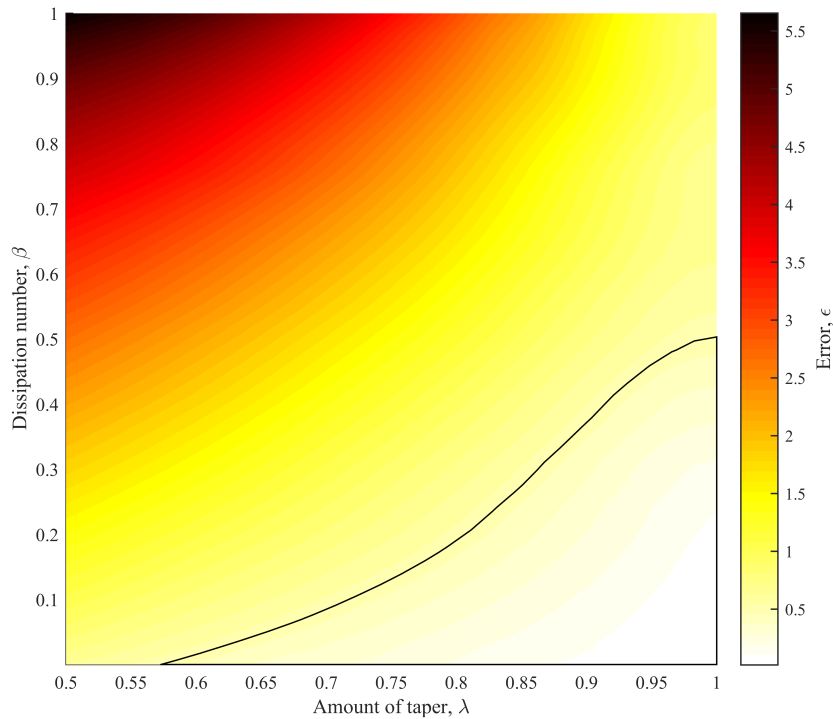
Figure 2.9: Error analysis for tapered TLM. The black lines show the enclosed region of acceptable error as defined by $\epsilon < 0.5$.
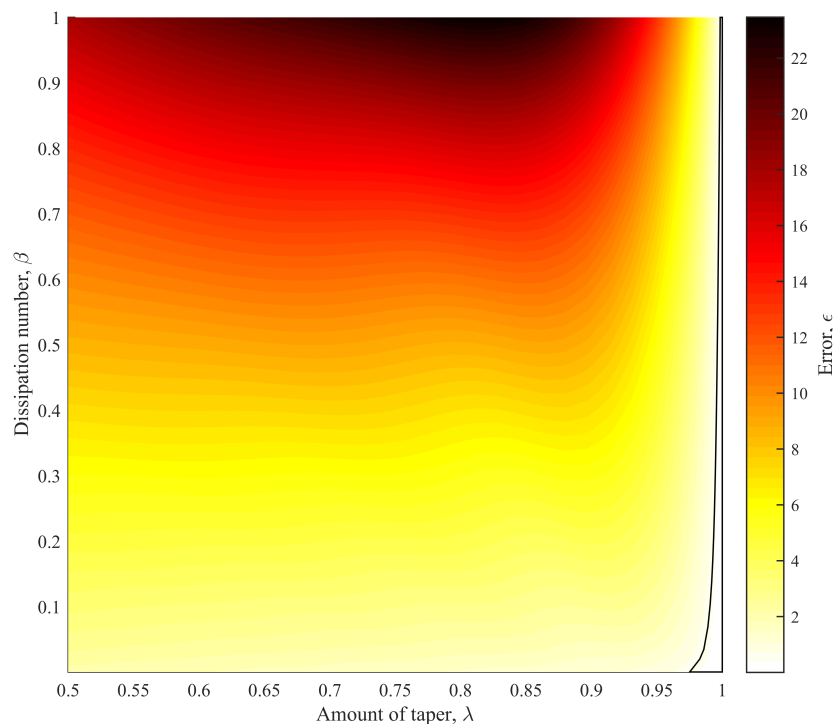
Figure 2.10: Error analysis for approximate solution from Muto et al. (1981). The black lines show the enclosed region of acceptable error, as defined by $\epsilon < 0.5$. Note that the error color scale is different than the scale in Fig. 2.9

2.7   Elastic Pipe Wall Considerations

A schematic of a tapered transmission line with finite wall effects is shown in Figure 2.11. The transmission lines studied up until this point has assumed a rigid pipe wall. Therefore the wave speed, c_r, is computed using only the compressibility of the fluid since the wall is perfectly stiff. For lines with flexible elastic walls, the wave speed is not only a function of the fluid compressibility, but is also a function of the wall elasticity. While a rigid assumption is reasonably acceptable for steel lines with a thick wall such as common hydraulic lines, the assumption is not valid for different materials such as plastics or weaker metals.
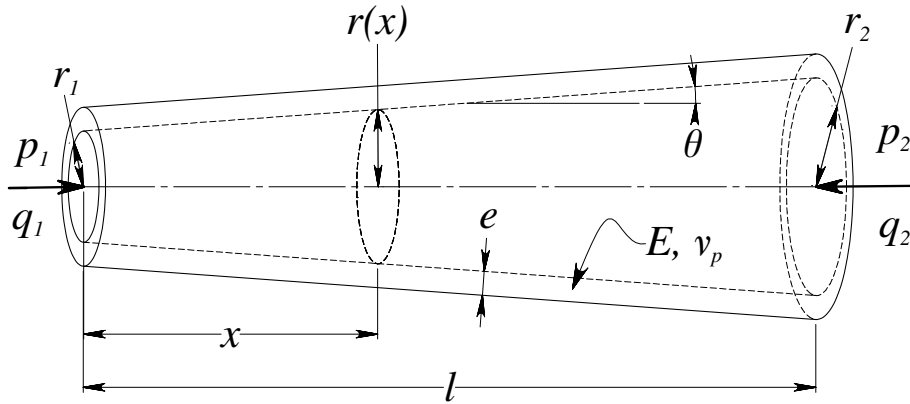
Figure 2.11: Schematic of a tapered transmission line with elastic wall effects. Note that constant wall thickness is maintained throughout the length of the pipe.

The differential equation that quantifies wave speed with both wall and fluid compliance is given by Ghidaoui et al. (2005):

$$\frac{1}{c_e^2} = \frac{d\rho}{dP} + \frac{\rho}{A}\frac{dA}{dP},$$

(2.31)

where $\frac{d\rho}{dP}$ corresponds to the fluid's compressibility, and $\frac{\rho}{A}\frac{dA}{dP}$ corresponds to the pipe wall's elasticity. For rigid pipes, this term is set to 0. Following the derivation in Ghidaoui et al. (2005) an equation computing the wave speed as a function of pipe and fluid parameters results. This equation also accounts for axial effects depending on how the pipe is restrained, however assuming no inertial effects of the line due to physical vibration. A fluid-structure interaction (FSI) model, such as in D'Souza and Oldenburger (1964), would have to be used. This is not within the scope of this research however.

Elastic wave-speed as a function of axial position, x, is given as:

$$c_e(x) = \sqrt{\frac{\dfrac{K}{\rho}}{1 + \alpha \dfrac{2Kr(x)}{eE}}} \qquad (2.32)$$

where axial effects are calculated by:

$$\alpha = \begin{cases} 1 - \dfrac{\nu_p}{2} & \text{Anchored upstream,} \\[2mm] 1 - \nu_p^2 & \text{Anchored throughout,} \\[2mm] 1 & \text{Anchored with expansion joints.} \end{cases} \qquad (2.33)$$

As indicated in Equation (2.32), the wave speed is a function of axial location due to the dependence on the varying internal radius, $r(x)$. This dependence was initially pointed out by Zielke (1968) for tapered pipes, but not studied. Therefore, a study into how elastic effects change the wave speed over the length of the pipe was performed in order to get a better understanding of what the pressure waves are doing inside the tapered pipeline. The study looked at 3 different tapered transmission lines of similar geometry made with materials of different Young's modulus. The Young's modulus of steel is around 180 GPa, whereas some polymers such as polyvinyl chloride (PVC) and acrylonitrile butadiene styrene (ABS) have a significantly lower Young's modulus of around 2 GPa. Figure 2.12 shows that the slope of the wave speed curve tends to 0 as the wall becomes more rigid. It also indicates that there can be a significant variation in the wave speed in pipes that have very flexible walls.

Figure 2.13 shows the linearity of the wave speed curve for the 3 cases investigated. The curve indicates that as the pipe becomes stiffer, the wave speed curve tends toward linearity, and for pipes that are very flexible the wave speed curve can be nonlinear.

As shown, the wave speed in an elastic tapered transmission lines varies over its length with a non-linear relationship. In order to apply the tapered TLM parameters to this problem, a singular value of wave speed is required to compute the dissipation number, β, characteristic impedance, Z_c, and wave propagation delay, T. The proposed approach is to use the effective wave speed, c_{eff}, to determine these parameters. Effective wave speed is defined as the total length of the line divided by the total time it takes for the wave to travel through the tube
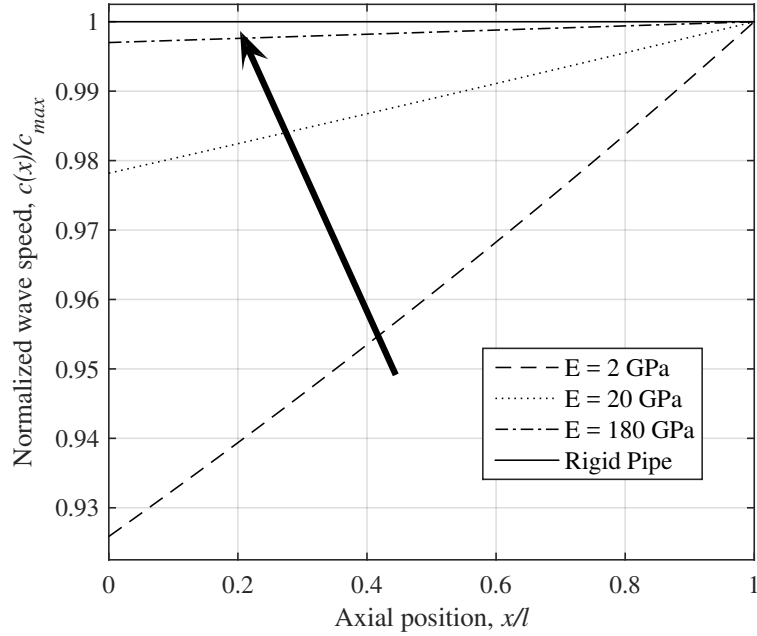
Figure 2.12: Normalized wave speed as a function of axial position within a tapered elastic pipe for different pipe stiffness values. Shows trend as pipe becomes more rigid, the wave speed slope tends to 0. Fluid properties and pipe dimensions are given in Table E.1.
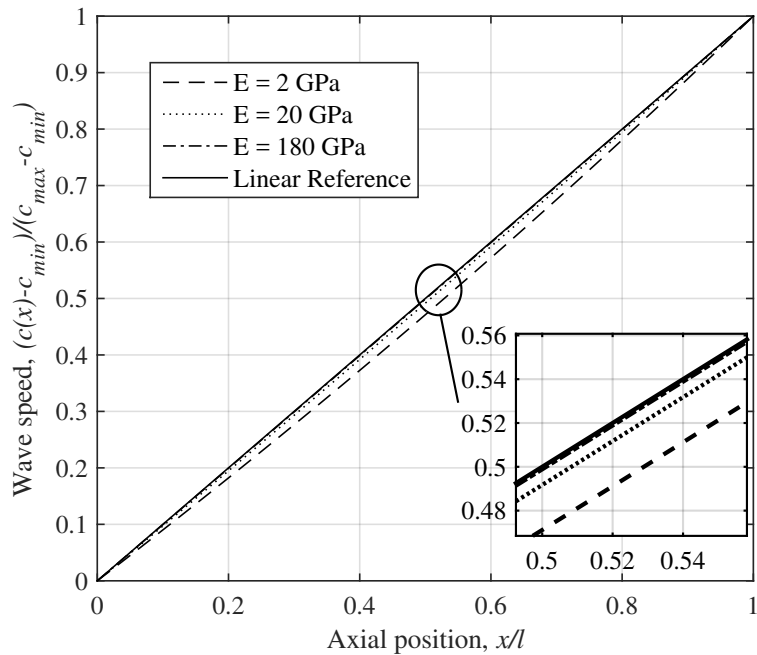
Figure 2.13: Scaled wave speed as a function of axial position within a tapered elastic pipe for different pipe stiffness values. Shows as pipe becomes more rigid, the wave speed function also tends towards linearity. Fluid properties and pipe dimensions are given in Table E.1.

from one end to the other. Due to the non-linearity of the wave speed function, the curve must be integrated to get the total propagation time. Effective wave speed is defined as:

$$c_{eff} = \frac{l}{\int_0^l \frac{1}{c_e(x)} dx}. \tag{2.34}$$

An analytical solution to Equation (2.34) is not proposed here, as numerically integrating has shown to be sufficiently accurate. The `integral()` function in MATLAB has shown to compute the integral quickly and accurately. Using c_{eff} in computing the dissipation number in Equation (2.15), characteristic impedance in Equation (2.13), and transmission time in Equation (2.21) in the tapered TLM was compared to a numerical ODE solution using $c_e(x)$ instead of c_r in Equations (2.2) and (2.3). The second order differential equation is given as:

$$\frac{\partial^2 Q(x,s)}{\partial x^2} - \left(\frac{1}{A(x)} \frac{dA(x)}{dx} - \frac{2}{c_e(x)} \frac{dc_e(x)}{dx} \right) \frac{\partial Q(x,s)}{\partial x} - \frac{s^2}{c_e(x)^2} N(x,s)Q(x,s) = 0, \tag{2.35}$$

which was solved using the same algorithm as previously described.

The comparison between the elastic tapered TLM and the numerical ODE solution showed similar accuracy to the transmission matrix plots in Figures 2.7 and 2.8. Therefore, the tapered TLM can be modified by using the effective wave speed to include the effects of elastic wall flexibility on the fluid dynamics.

2.8 Experimental Results

Validation experiments have been performed previously for rigid tapered pipes, but only for the first peak of resonance (Muto et al., 1981; Washio et al., 1974). While the first peak has been validated, higher bandwidth has not been investigated. In order to have confidence in the ODE solution used to compute the tapered TLM parameters, an experimental apparatus was manufactured to allow the investigation of high frequency dynamics. A schematic of the apparatus is given in Figure 2.14, and labelled photos of the apparatus in Figures 2.15 and 2.16.

Manufacturing a tapered pipeline would prove to be very difficult, an observation also made by Washio et al. (1974). However, through trial and error, a successful design of ta-
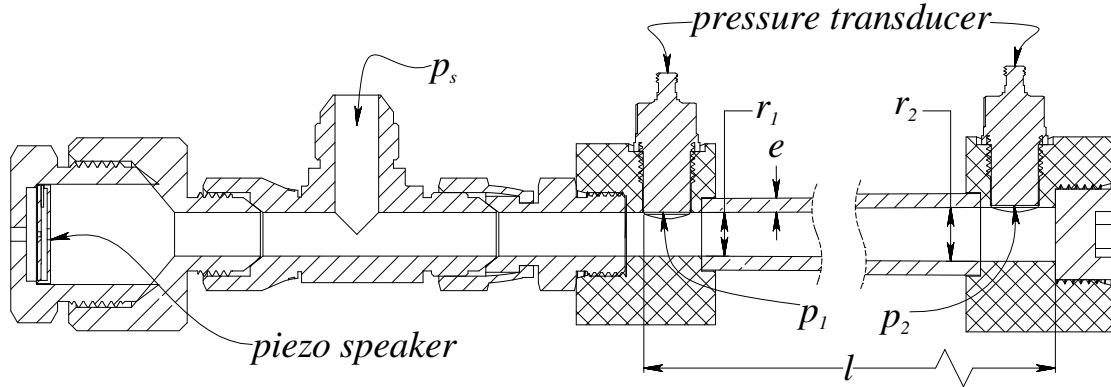
Figure 2.14: CAD schematic of tapered transmission line test rig. Note there is a break in the drawing.

pered pipe sections (TP-08-02 and TP-08-03) and end caps (TP-08-01 and TP-08-04) were manufactured using a MakerBot® Replicator™ 2X experimental 3D printer using acrylonitrile butadiene styrene (ABS) filament. Detailed manufacturing drawings of the experimental apparatus TP-08 are included in Appendix C. The end caps have standard o-ring boss (ORB) ports printed into them to allow the connection of standard fittings. At the inlet of the line, a tee fitting was installed to allow the application of a static pressure, p_s, and the connection of the exciter PT-02. The exciter contains a small piezoelectric speaker element epoxied inside of a -16[1] JIC plug. The assembly is then fastened into a -16 to -8 reducer, making up the pipeline's exciter. The outlet of the transmission line was blocked with a -10 ORB hollow hex plug to hold the outlet flow rate at 0. A small bleed screw was installed in the outlet plug to bleed the air and ensure the line was filled completely with hydraulic oil.

Pressure was measured using fast responding Kistler 606A piezoelectric transducers with Kistler 504A charge amplifiers. All control and data measurement was done with a National Instruments™ data acquisition system (NI-DAQ). Both inlet and outlet pressure signals were filtered using a 2-channel first-order resistor-capacitor (RC) filter bank, set at the Nyquist frequency. This was done to prevent aliasing when the signals were sampled. The parameters of the experimental apparatus are given in Table E.1.

It was desired to use an excitation signal that could provide even power throughout the

---

[1]The "Dash Size" is a common metric that describes the size of hydraulic fittings, hoses, and lines. The number indicates the nominal inner diameter in 1/16 of an inch increments. For example, -08 is 8/16 of an inch which reduces to 1/2 of an inch.
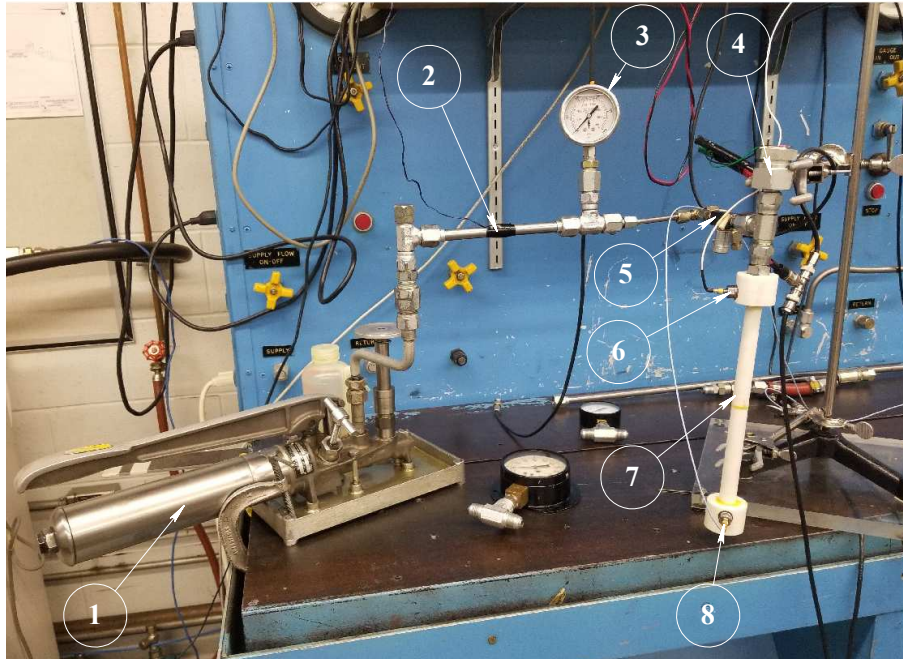
Figure 2.15: Photo of the experimental apparatus showing: ① dead weight tester, ② thermocouple, ③ pressure gauge, ④ PT-02 exciter, ⑤ needle valve, ⑥ inlet pressure sensor, ⑦ TP-08 tapered transmission line, ⑧ outlet pressure sensor.
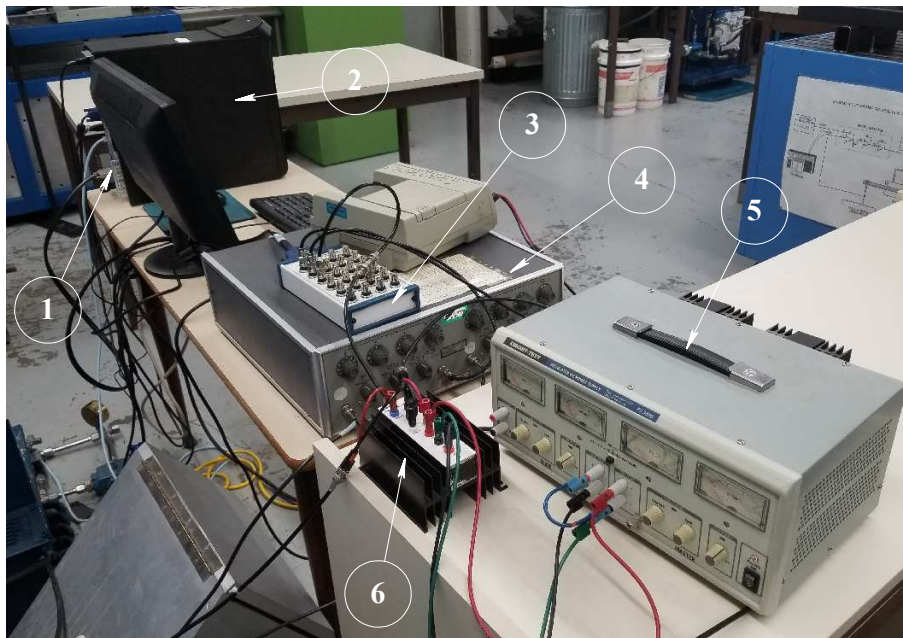
Figure 2.16: Photo of the experiment's electronics showing: ① National Instruments NI PCIe-625 DAQ, ② computer, ③ National Instruments BNC-2111 connector box, ④ 2-channel RC filter bank, ⑤ laboratory power supply, ⑥ LM12 power amplifier.

bandwidth investigated. A maximum length sequence (MLS) is a digital pseudo-random binary sequence that has a perfectly white, flat spectrum. The MLS is generated using linear feedback shift registers (LFSR) using MATLAB® code created by Wiens (2009) and LSFR feedback values from Koopman (n.d.). The length of an MLS signal is $2^m - 1$ where m is the order of the sequence. Figure 2.17 shows the first 20 samples of a 9th order MLS implemented in the time domain with a command signal applied to the exciter.
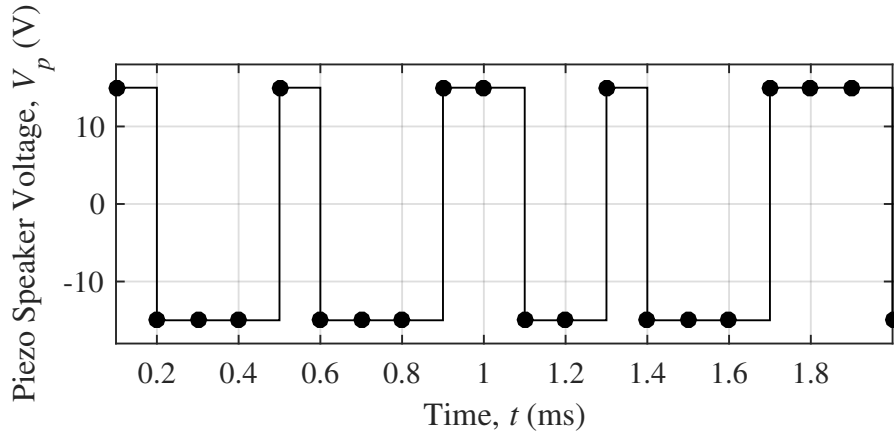
Figure 2.17: A MLS sequence represented in the time domain with 20 samples shown at a sampling frequency of 10 kHz.

In order to have confidence in the theory, the experiment compares the t_{11} transfer function of the numerical ODE solution to the empirical transfer function estimate (ETFE) measured experimentally. The relationship is given by the following equation:

$$ETFE = \frac{P_2}{P_1} = \frac{1}{t_{11}}.$$
(2.36)

where P_1 and P_2 are the fast Fourier transform (FFT) of the pressure signals at the inlet and outlet respectively.

The excitation signal was repeated 24 times in succession with the first run discarded to ensure all runs have the same initial excited state. The exciter instilled very small pressure waves in the transmission line, and as a result the measured pressure signals had very small magnitude, however still within the specified range of the transducers. To reduce random noise, the signals were averaged in the time domain before applying the FFT. Averaging in the time domain, as performed here, may lead to inaccuracy with the FFT if the equipment

35

exciting and sampling the system are run on a different clock. As a result, the samples would not be aligned resulting in skewed phase and incorrect magnitudes. This, however, is not an issue here as the NI-DAQ that was used played the MLS signal and sampled the pressure signals all on the same clock at a sampling frequency of $f_s = 10\text{kHz}$.

Good confidence in the theory for the first resonant peak has been assured in previous research (Muto et al., 1981; Washio et al., 1974), but validation of the presence of higher frequency peaks is desired. Figure 2.18 shows how the ETFE compares with the t_{11} term of the numerical transmission matrix computed from the ODE. The second resonance peak is the one shown at 1.85 kHz, the third at 3.13 kHz, and the fourth at 4.31 kHz. Good agreement can be seen between experiment and theory for the second and start of the fourth harmonic peak in both magnitude and phase, however the third harmonic peak is not represented in the theory. An obvious notch frequency is present at around 3.13 kHz, which is strongly believed to be the result of line vibration. Line vibration effects have been quantified by D'Souza and Oldenburger (1964), and the notch present here looks very similar to the vibration phenomenon they measured in their experiments. The apparatus TP-08 was not rigidly restrained during testing, allowing the transmission line to vibrate. This presence of the notch frequency in the response was expected, and since the TLM or numerical ODE solution does not account for these effects, it cannot be computed theoretically. If the apparatus would have been rigidly anchored, it is believed the frequency response would follow the theory closely, as observed in D'Souza and Oldenburger (1964) when they anchored their apparatus. In the end, confidence in higher order resonances is gained through this experiment.

2.9   Time Domain Simulations

Dynamic simulations were performed in MATLAB® SIMULINK®, with the models available for download from Wiens and ven der Buhs (2017). The overall arrangement of transfer functions is shown in Figure 2.19, where the $E(s)$, $F(s)$, and $G(s)$ transfer functions were implemented with summations of individual `Transfer Fcn` blocks, and the time delays, $e^{-j\omega T}$, were implemented with `Transport Delay` blocks set to a delay of T'.

There are 4 possible arrangements of the TLM shown in Figure 2.20 that can be used
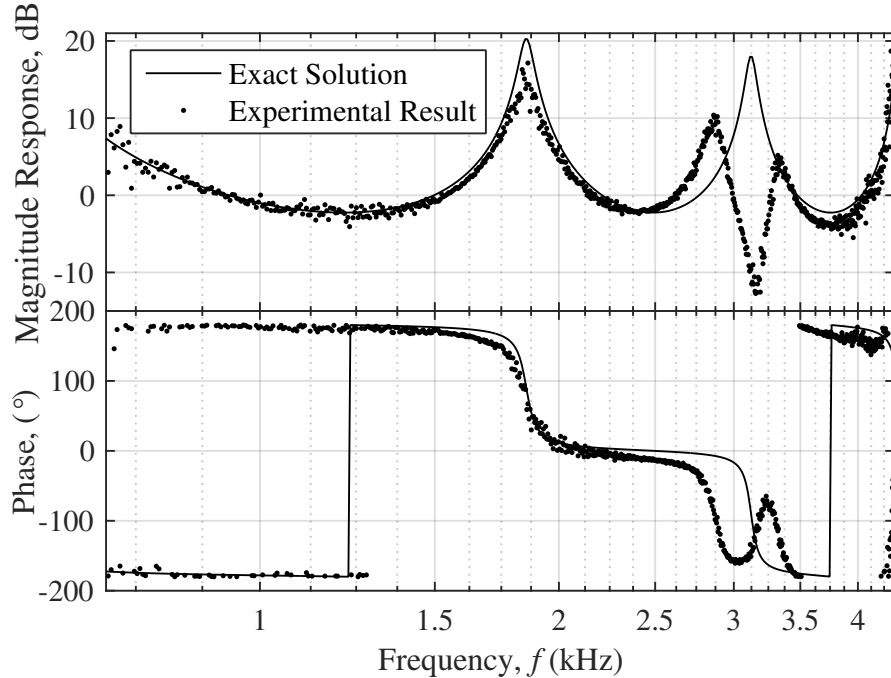
Figure 2.18: Comparison between the observed experimental result and the numerical ODE solution. Note the notch at 3.13 kHz, this is confidently believed to be the result of line vibration, a phenomenon extensively studied and quantified by D'Souza and Oldenburger (1964).

depending on how it needs to fit in a dynamic simulation. To generate the different configurations, the boundary Equations (2.11) and (2.12) are applied at the inlet and outlet to solve for the desired states.

The simulation study performed here only considers one arrangement of inputs and outputs. The inputs are inlet flow and outlet pressure, and the outputs are outlet flow and inlet pressure. The outlet pressure was maintained at 0, and inlet flow was given a step input. The solver was MATLAB®'s `ode23t()` with a relative tolerance of 10^{-6}, a stiff solver commonly used for simulating transmission line dynamics. Using non-stiff solvers, such as `ode45()`, add considerable computation time to the simulation. The same parameters used for computing the transmission matrices in Figures 2.7 and 2.8 were used for the dynamic simulations. The results of the simulations are inlet pressure and outlet flow, where the flow response is normalized by dividing by the step change in flow. The pressure response is normalized with the step change in flow multiplied by the characteristic impedance of the line. Figure 2.21 shows the results for a tapered transmission line with low dissipation and large taper. The flow
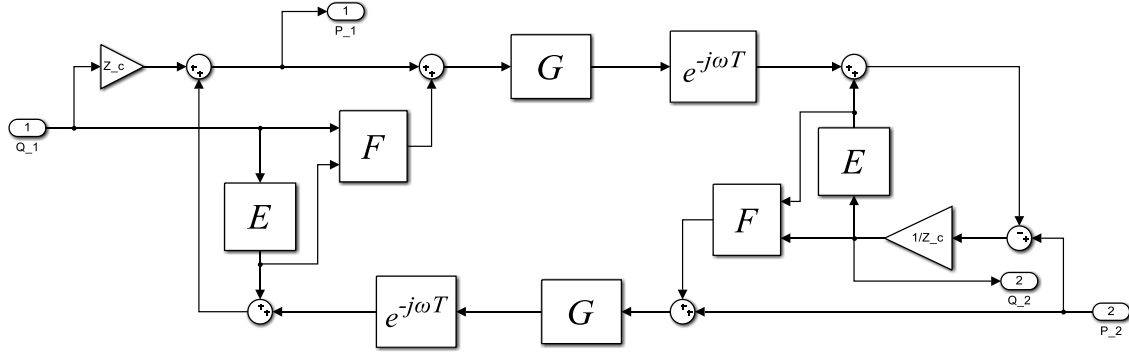
Figure 2.19: MATLAB® SIMULINK® model of the tapered TLM.
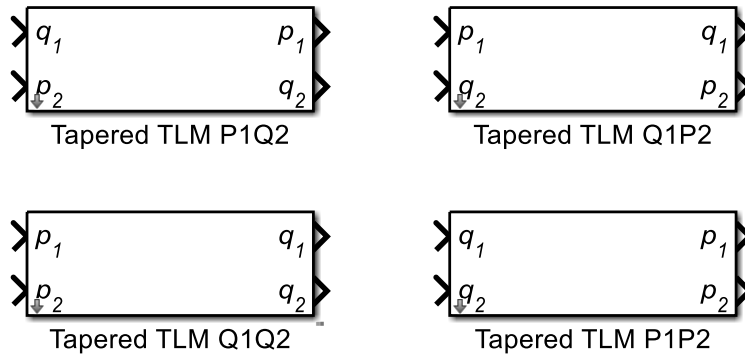
Figure 2.20: The 4 arrangements of inputs and outputs for the TLM.

response oscillates around a value of 1, indicating proper flow continuity. The response of the line is also stable when applied with a step input, an important quality as these models are typically used in system with high frequencies present. Figure 2.22 shows the reposes of a highly dissipative transmission line with less taper, and again the same qualities within the response as the previous simulation are also present. These responses also look similar when compared to the response of uniform lines (Johnston, 2012; Johnston et al., 2014).

The TLM has been used in previous research within simulations of hydraulic switched inertance converters (Johnston et al., 2014; Wiens, 2016). It is believed that the proposed tapered TLM will also suit well for simulations and optimizations of shaped inertance tube designs, which will be discussed in the following sections.
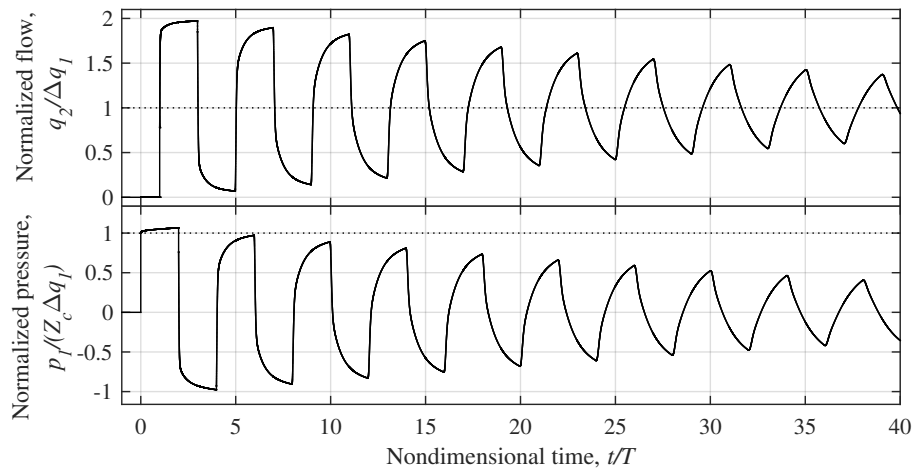
Figure 2.21: Simulated results for $\beta = 0.001$ and $\lambda = 0.75$.
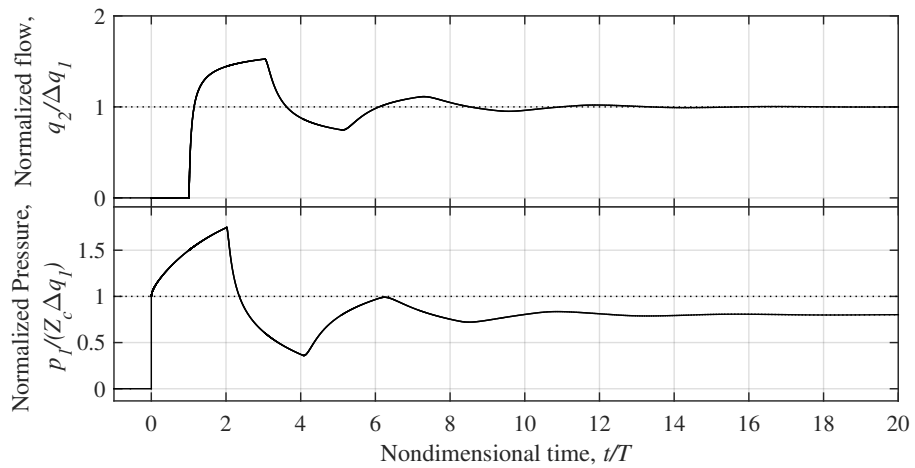
Figure 2.22: Simulated results for $\beta = 0.1$ and $\lambda = 0.9$.

Chapter 3

Analysis of a Switched Inertance Converter

This chapter will introduce the design of the hydraulic buck converter used for the analyses and optimizations in the latter part of this thesis. The dynamic equations of the individual components will be introduced and justified. Performance of the system is quantified by identifying the different power losses in the system, and also by defining volumetric efficiency. Finally, dynamic simulation of the system is performed using parameters from previous research, with detailed analysis provided to quantify its performance.

3.1 Configuration and Operation

Previous research within the fluid power research group at the University of Saskatchewan has analyzed and improved the performance of a simulated buck converter with the reservoir flow going through a passive check valve (Wiens, 2015, 2016). As a result, the same converter will be studied in this research. This will allow for comparisons of previous models and studies to the new developments presented here. The converter studied in this research has a detailed schematic shown in Figure 3.1 with the states and direction of positive flow indicated on the diagram.

The converter studied in this research contains a 2-position, 2-way digital hydraulic valve, passive check valve, inertance tube, and a load. The load is an ideal compressible volume in combination with a turbulent orifice. Each component of the converter has an equation or
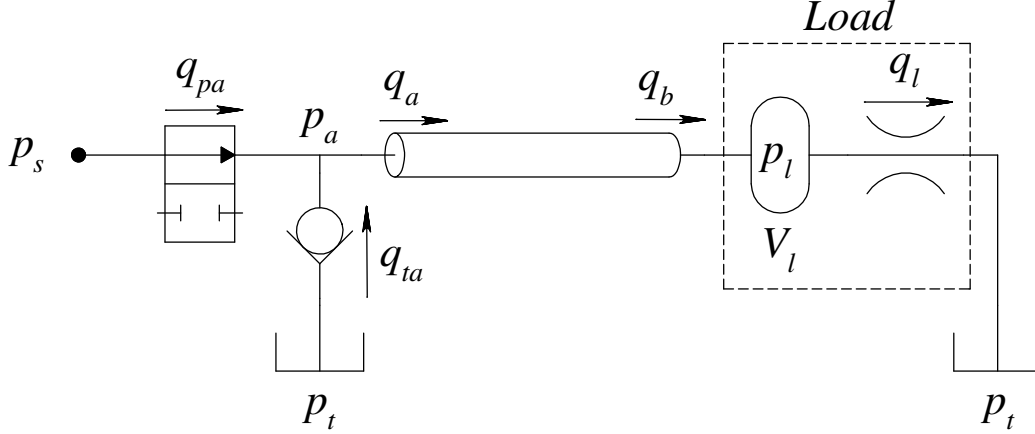
Figure 3.1: Detailed schematic of a hydraulic buck converter with a check valve configuration. Pressure and flow states are indicated including the direction of positive flow.

model that describes its performance. The following section will describe each component, and define the non-linear equations.

3.2 Non-linear Dynamic Model

The model that describes a hydraulic buck converter is inherently non-linear due to the components that describe the pressure and flow states throughout the system. The following section will define the equations and models used for simulation of the hydraulic buck converter.

3.2.1 Orifices

The dynamic models used for the switching valve, check valve, and load orifice all assume a turbulent orifice, however with different parameters. Typically, the turbulent orifice equation is given as:

$$q(\Delta p) = \text{sgn}(\Delta p) C_d A \sqrt{\frac{2}{\rho} |\Delta p|} . \tag{3.1}$$

This formulation is more than acceptable for computing steady flows and flows that are unidirectional. However, it creates complications within numerical solvers during dynamic

41

simulation when the pressure differential, Δp, nears 0 as the flow changes direction. The reason lies in the derivative of this function, which tends to infinity as the pressure difference across the orifice nears 0. This causes modern Jacobian-based variable-step solvers to significantly reduce the step size during this part of the simulation, significantly increasing computation time while also consuming more system resources. A proposed solution by Ellman and Piché (1999) is to include a laminar region near the singularity of the turbulent orifice equation with a smooth transition between the laminar and turbulent regions. First, one must compute the transition pressure, p_{tr}, the pressure at which the regime switches to fully turbulent flow given by:

$$p_{tr} = \frac{9R_{cr}^2 \rho \nu^2}{8C_d^2 D^2} \tag{3.2}$$

where R_{cr} is the critical Reynold's number for the flow, C_d is the turbulent discharge coefficient, and D is the hydraulic diameter of the orifice opening. Once computed, the pressure difference across the orifice is then compared to the transition pressure to determine which regime the flow should be in. This piecewise function is given by:

$$q(\Delta p) = \begin{cases} \text{sgn}(\Delta p) C_d A \sqrt{\frac{2}{\rho}|\Delta p|} & \text{if } |\Delta p| > p_{tr}, \\ \text{sgn}(\Delta p) \dfrac{3A\nu R_{cr}}{4D} \left(\dfrac{|\Delta p|}{p_{tr}}\right)\left(3 - \dfrac{|\Delta p|}{p_{tr}}\right) & \text{if } 0 \le |\Delta p| \le p_{tr}. \end{cases} \tag{3.3}$$

A comparison between the traditional purely turbulent model and the Ellman-Piché model is shown in Figure 3.2 with the axes scaled. One can see that the Jacobian of the purely turbulent orifice tends to infinity when approaching $\Delta p = 0$ while the 2-regime orifice has a linear region within the bounds $|\Delta p| < 1$.

3.2.2 Switching Valve

The buck converter contains a simple digital (on/off) hydraulic valve as its only control valve. The valve has two ports (inlet and outlet) and two possible spool positions (through or blocked). Often in system simulation, valves are approximated as a turbulent orifice with a time-varying orifice area. Here the Ellman-Piché orifice is used as described previously with the following parameter relations: $A = A_{pa}(t)$, $D = \sqrt{\dfrac{4A_{pa}(t)}{\pi}}$, $\Delta p = p_s - p_a$, and $q = q_{pa}$.
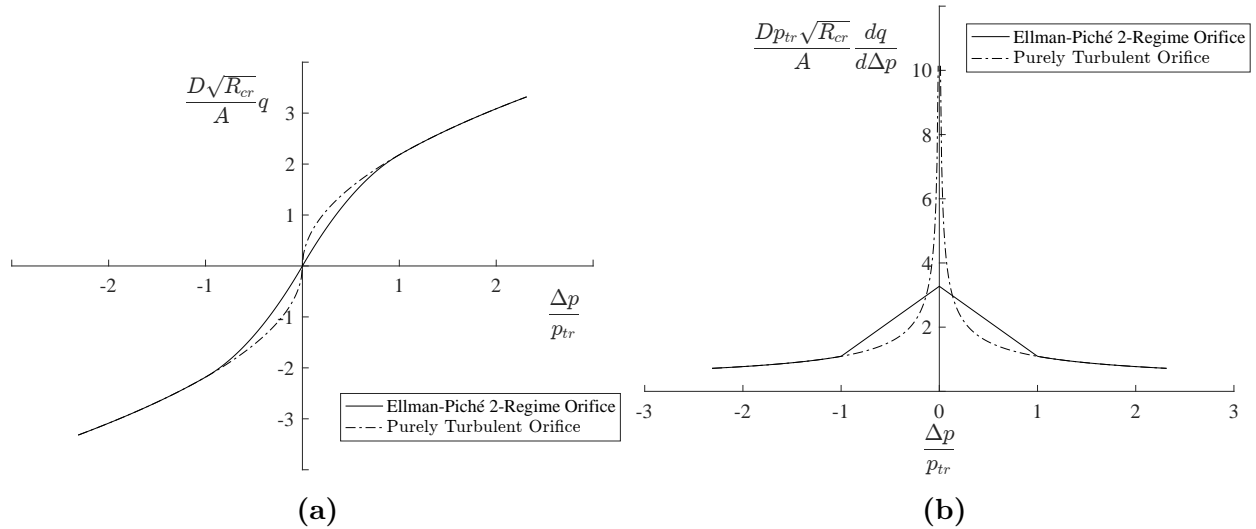
Figure 3.2: Comparison between the Ellman-Piché 2-regime orifice, and the standard purely turbulent orifice. (a) Shows how the flow though the orifice varies with the pressure drop across it. (b) Shows the Jacobian of the two equations. Note that the Jacobian of the purely turbulent orifice tends to infinity when approaching zero pressure drop.

The orifice area function, $A_{pa}(t)$, is a rate-limited pulse-width modulated (PWM) signal that alternates between the valve's fully open area $A_{pa,max}$ and leakage area $A_{pa,min}$. A small leakage area is specified to maintain numerical integrity of the Ellman-Piché orifice flow equation which is undefined when $A = 0$. The switching valve operates at a frequency of $f_{pa} = \frac{1}{t_p}$ at a duty cycle of κ_{pa} quantifying the fraction of time that the switching valve is open. The slew rate of the signal is dependent on the valve's switching time, t_{sw}, which can be on the order of a fraction of a millisecond for specialized high performing valves, or a few milliseconds for commercially available options. This valve area curve is visualized in Figure 3.3, and has been used in other research of similar application as a simplified approximation of the valve dynamics (Pan et al., 2014a; Wiens, 2015; Kogler et al., 2015).

3.2.3 Check Valve

The hydraulic check valve is a directional control valve that limits the flow of fluid in one direction, thus eliminating back flow through the line except for a small amount of leakage. In a buck converter circuit, the valve is installed to allow the free flow of fluid from the low pressure reservoir to a tee coupling just before the inertance tube. The check valve orifice area
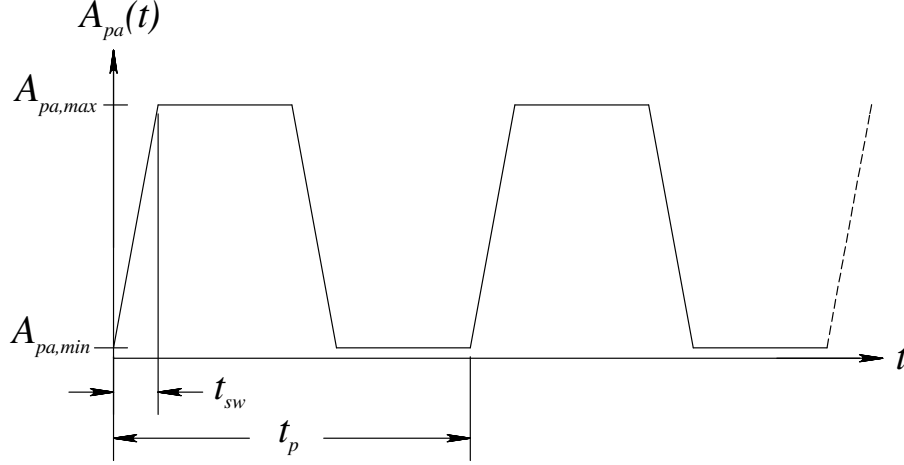
Figure 3.3: Valve switching area curve.

function, $A_{ta}(\Delta p)$, that is used for simulation is one that has been used in previous research on the topic (Wiens, 2015, 2016), and is also similar to that implemented in commercially available simulation packages (MathWorks, 2006a). The check valve is considered an Ellman-Piché two regime orifice with a valve opening dependent upon the differential pressure across it. The parameter relations are: $A = A_{ta}(\Delta p)$, $D = \sqrt{\dfrac{4A_{ta}(\Delta p)}{\pi}}$, $\Delta p = p_t - p_a$, and $Q = Q_{ta}$ where,

$$
A_{ta}(\Delta p) = \begin{cases} A_{ta,min} & \text{if } \Delta p \leq p_{cr} \\ A_{ta,max} & \text{if } \Delta p \geq p_{cr} + p_{or} \\ A_{ta,min} + \dfrac{\Delta p - p_{cr}}{p_{or}}\left(A_{ta,max} - A_{ta,min}\right) & \text{otherwise} \end{cases} \tag{3.4}
$$

where the fully open valve area is $A_{ta,max}$, and the leakage area is $A_{ta,min}$. The two characteristic pressures of the valve are the cracking pressure, p_{cr}, and the pressure override p_{or}. The valve is typically constructed of a poppet or ball on a seat inside of an in-line cartridge. When the pressure difference is greater than the cracking pressure, the ball moves off the seat allowing fluid to flow in the favoured direction. The area of the valve continues to open as the pressure difference becomes greater until the ball hits the end of its possible stroke inside the cartridge. At this point the check valve has also overcome its pressure override, and is fully open. When the pressure difference across the valve is less than the cracking pressure, the ball is fully on the seat closing the valve, thus blocking the flow in the opposite

direction. Again, a small leakage area is specified to maintain numerical integrity. The area curve of the check valve is provided in Figure 3.4.
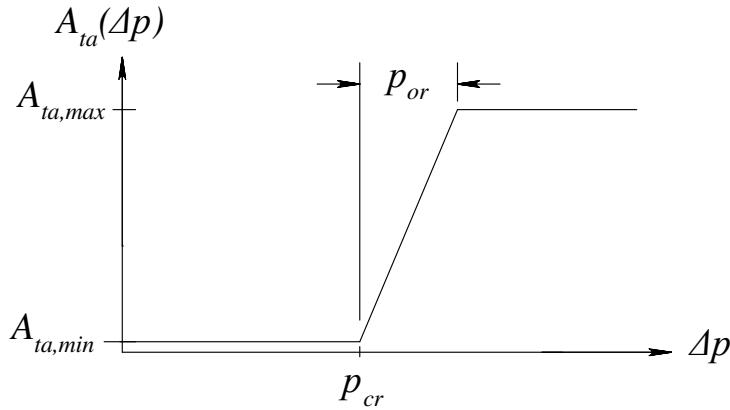
Figure 3.4: Check valve area curve.

There are some notable assumptions built into this model. The check valve has an instantaneous response to changes in pressure across it. This is is a simplification to the model as it allows the inertial effects of the poppet to be neglected. The model also assumes that the orifice area varies linearly with the differential pressure across the valve when transitioning from closed to open and vice versa. The choice of this model is to provide the best case scenario in performance, and can also allow for the design of a controller when swapped with active switching such as using a 2-position 3-way valve, or another digital valve on the reservoir line (Wiens, 2016).

3.2.4 Inertance Tube

The inertance tube serves an extremely important role in the operation and performance of a switched inertance converter. Previous research by Wiens (2015) into the effects of a shaped inertance tube on the performance of a buck converter used a lumped element method (LEM) style of model. This is where the pipeline is broken up into segments of uniform radius where each segment contains an inertance, laminar steady resistance, and a compressible volume. The schematic for a single element as well as 4 segment transmission line is shown in Figure 3.5. The transmission line is constructed by connecting these elements in series, where the pressure and flow into the element is equal to the pressure and flow at

the outlet of the previous element, and so on. The LEM is a popular choice for modelling fluid transmission lines due to its simplicity and availability in commercial packages such as in MATLAB® SIMSCAPE™ in the SIMULINK® environment (MathWorks, 2006b). However, since pressures and flows are calculated at nodes over the length of the line, there is extra computational load. Also, this model has low accuracy due to 3 main causes. The first cause of inaccuracy is due to the fact that it does not model the effects of frequency dependent friction. Another inaccuracy is that the LEM does not model higher frequencies well. Finally, there is a significant increase in noise (i.e. numerical instability) in the solution.
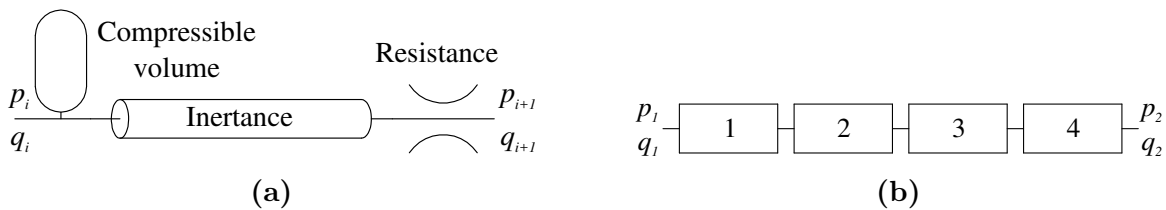
Figure 3.5: (a) A single element of the LEM containing a compressible volume, inertance, and a laminar resistance. (b) A 4 segment LEM pipeline model with elements from (a) connected in series.

While the LEM approach is simple to use, better accuracy is required for the simulation studies performed in this thesis. Therefore the inertance tube model proposed here employs the tapered TLM that was presented in previous section as its base model for computing the fluid dynamics. The main goal of this research is to investigate the effects of a shaped inertance tube on the performance of the converter, and optimize its dimensions. As a result, the tapered TLM needs to be applied in a way to allow the specification of shape all while keeping errors low.

In order to reduce the number of parameters in the following study, a rigid inertance tube is assumed. This assumption is valid for pipes with thicker walls and stiff material such as steel. It is desired to operate the tapered TLM within a region of low error specified by the error contour in Figure 2.9. As a result, the model must ensure that a minimum taper ratio is met. For sections with a taper ratio smaller than the required minimum, the length is repeatedly segmented until the taper ratio of the individual segments are greater than or equal to the specified minimum. The algorithm is described using the flow chart in Figure 3.6. An analytical expression was derived to solve for first segmented diameter while

maintaining the same taper ratio, which is given by:

$$d_{seg,1} = (d_i^{j-1} d_{i+1})^{\frac{1}{j}}; \tag{3.5}$$

where d_i and d_{i+1} are entries i and $i+1$ in the specified diameter look-up table $\boldsymbol{d}$. The integer j is the number of segments required to meet the minimum taper ratio. Sequential segment diameters are found by dividing the taper ratio, λ, by the diameter immediately before it for a diverging section, or multiplying if converging:

$$d_{seg} = \frac{\lambda}{d_{previous}} \text{ or } d_{seg} = \lambda d_{previous} \tag{3.6}$$
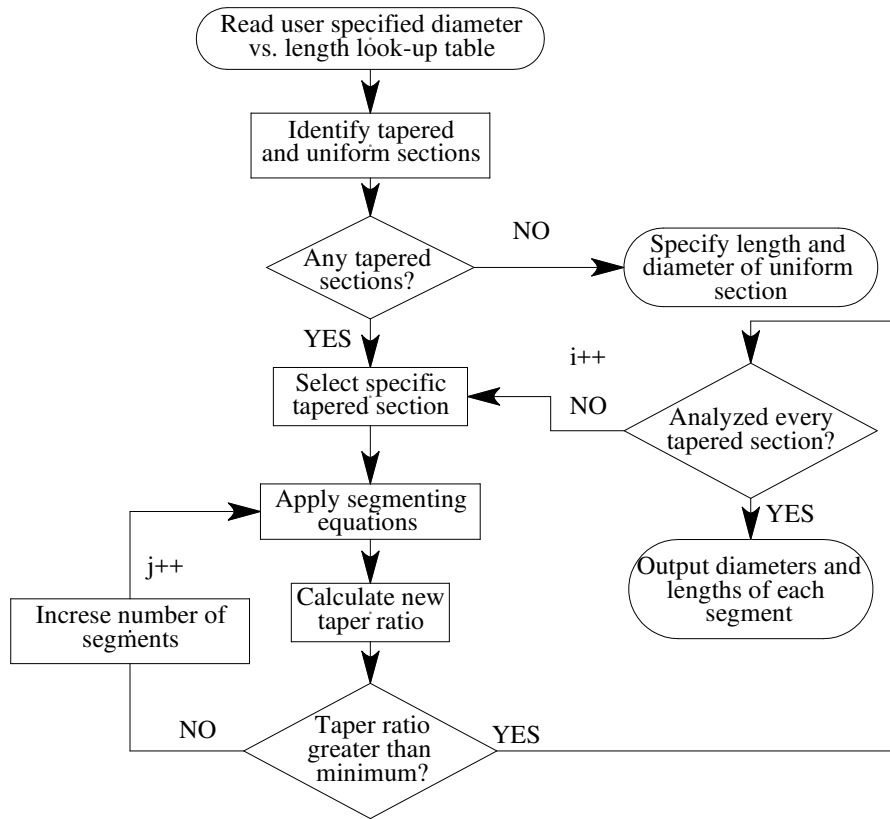
Figure 3.6: Flow chart describing the shaped inertance tube segmenting algorithm.

This allows the user (or optimization algorithm) to specify any arbitrary shape while using the tapered TLM in a region of low error. The minimum taper ratio specified was $\lambda_{min} = 0.75$. The segmenting algorithm is included in Appendix D.1 for reference. The one

downside to performing segmentation is the increase in computation time when simulating, due to the addition of more equations and states into the problem.

3.2.5   Load

The load is comprised of two components, a compressible volume and a turbulent orifice. The compressible volume is assumed to be ideal, meaning it is contained inside of a rigid container, is filled completely with hydraulic fluid with no air pockets, and has constant bulk modulus. The model also assumes there is no heat transfer. The equation that describes the dynamics of this component is well established in the literature, and is given as:

$$p_l = \frac{K}{V_l} \int (q_b - q_l) \, dt. \tag{3.7}$$

The load orifice is described using the Ellman-Piché orifice equation with the following parameter relations: $A = A_l$, $D = \sqrt{\frac{4A_l}{\pi}}$, $\Delta p = p_l - p_t$, and $q = q_l$

3.3   Quantification of performance

The performance of a hydraulic switched inertance converter is characterized by two main metrics, system efficiency and volumetric performance. Figure 3.7 shows an account of all the power losses present within the system. There are three power losses within the proposed system: power loss across the switching valve, power loss across the check valve, and power loss due to viscous friction within the inertance tube. Out of these three losses the most significant are the switching valve loss and the inertance tube line loss. The majority of the valve loss occurs when switching from open to closed and vice versa due to the throttling of the flow over the partially opened orifice. The check valve loss will be shown to be nearly negligible in the following analyses.

Since a hydraulic buck converter is constantly oscillating due to the switching action between high and low pressure, the system needs to be analysed and averaged over one cycle. Since the dynamic model is solved using a variable-step numerical solver, one cannot average the output over one cycle directly due to concentration of points near non-linear
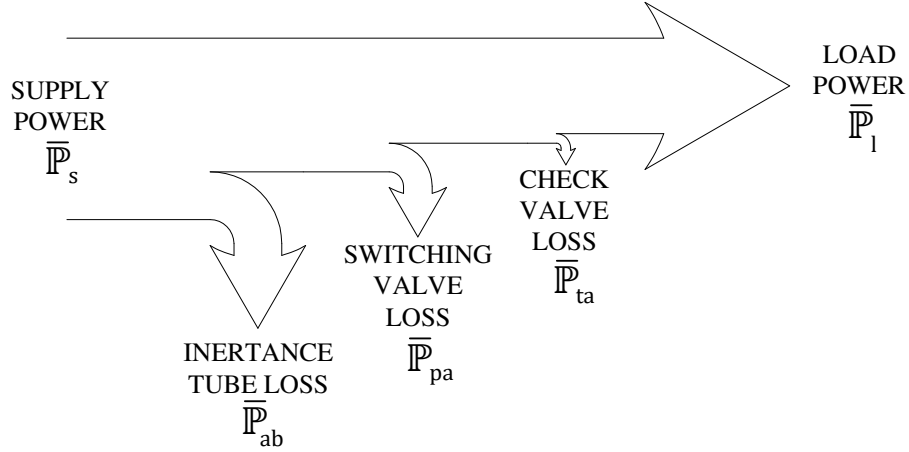
Figure 3.7: An account of power losses within the hydraulic buck converter.

events requiring higher fidelity in the response. As a result, the output must be numerically integrated. The `trapz()` function in MATLAB® is a trapezoidal integration method which has shown to work well. The switching valve power loss, check valve power loss, and inertance tube power loss are respectively defined as:

$$\overline{\mathbb{P}}_{pa} = \frac{1}{t_p} \int_{t_o}^{t_o+t_p} q_{pa} \left(p_s - p_a\right) dt, \tag{3.8}$$

$$\overline{\mathbb{P}}_{ta} = \frac{1}{t_p} \int_{t_o}^{t_o+t_p} q_{ta} \left(p_t - p_a\right) dt, \tag{3.9}$$

and

$$\overline{\mathbb{P}}_{ab} = \frac{1}{t_p} \int_{t_o}^{t_o+t_p} \left(q_a p_a - q_b p_l\right) dt, \tag{3.10}$$

where t_o is the chosen starting time of the switching cycle.

System efficiency quantifies the ratio of power consumed at the load to power supplied to the switching valve, and is defined as:

$$\eta_{sys} = \frac{\overline{\mathbb{P}}_l}{\overline{\mathbb{P}}_s} = \frac{\dfrac{1}{t_p} \displaystyle\int_{t_o}^{t_o+t_p} q_l \left(p_l - p_t\right) dt}{\dfrac{1}{t_p} \displaystyle\int_{t_o}^{t_o+t_p} q_{pa} \left(p_s - p_t\right) dt}. \tag{3.11}$$

One of the main functions of the hydraulic buck converter is to boost the flow rate at the outlet compared to the supply flow. To quantify the volumetric performance of the system,

49

volumetric efficiency is defined as the fraction of flow supplied to the load divided by the ideal flow through the switching valve (Wiens, 2016).

$$\eta_{vol} = \frac{\overline{q}_l \kappa_{pa}}{\overline{q}_{pa}} = \frac{\dfrac{\kappa_{pa}}{t_p} \displaystyle\int_{t_o}^{t_o+t_p} q_l \, dt}{\dfrac{1}{t_p} \displaystyle\int_{t_o}^{t_o+t_p} q_{pa} \, dt}. \tag{3.12}$$

Assuming a buck converter is operating at a duty cycle of 50%, in order to have 100% volumetric efficiency, the flow rate at the load would have to be twice, or $\frac{1}{\kappa_{pa}}$ times, the mean flow rate through the switching valve, $\overline{q}_{pa}$. Operating at this volumetric efficiency is not realizable, however, due to the limited speed of switching valves and the dynamics of realistic passive check valves.

3.4   Simulated Results

Simulations were performed using MATLAB® with the dynamic equations implemented within the SIMULINK® graphical programming environment. Initial simulations were performed using parameters from Wiens (2016, 2015) for initial investigation into the model and to ensure the model is solving correctly. These parameters are provided in Table E.2 in Appendix E. The main goal of this simulation is to operate the load at a pressure of 16 MPa; as a result the duty cycle of the switching valve was adjusted to 54% to achieve this target. The pressure states in the system are plotted in Figure 3.8. One can see the load pressure is maintained around an average value of 16 MPa. The pressure at the inlet of the inertance tube, p_a, transitions between the low pressure and high pressure supplies as the valve opens and closes.

The flow response of the system over one cycle can be seen in Figure 3.9. One can see that as the flow through the switching valve decreases to zero during valve closure, the check valve opens, sucking fluid from the low pressure reservoir into the system. Load flow, q_l, oscillates slightly, but is relatively smooth due to the compressible volume at the inlet of the load orifice.

The two peaks in flow through the switching valve occur during valve opening and closure, which is undesirable performance. This is caused by not switching the valve at the correct
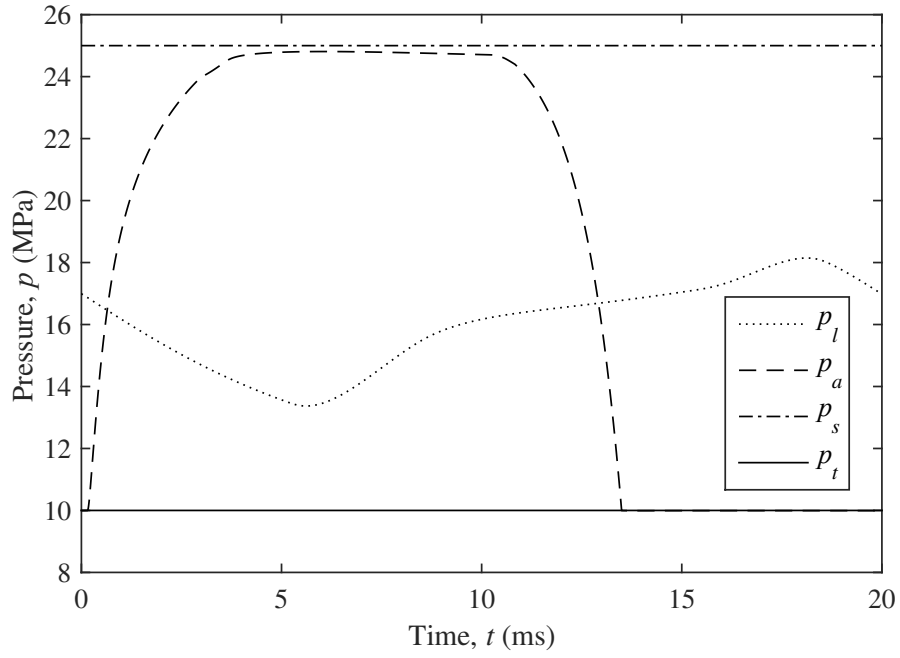
Figure 3.8: Simulated pressures for one cycle at steady state.
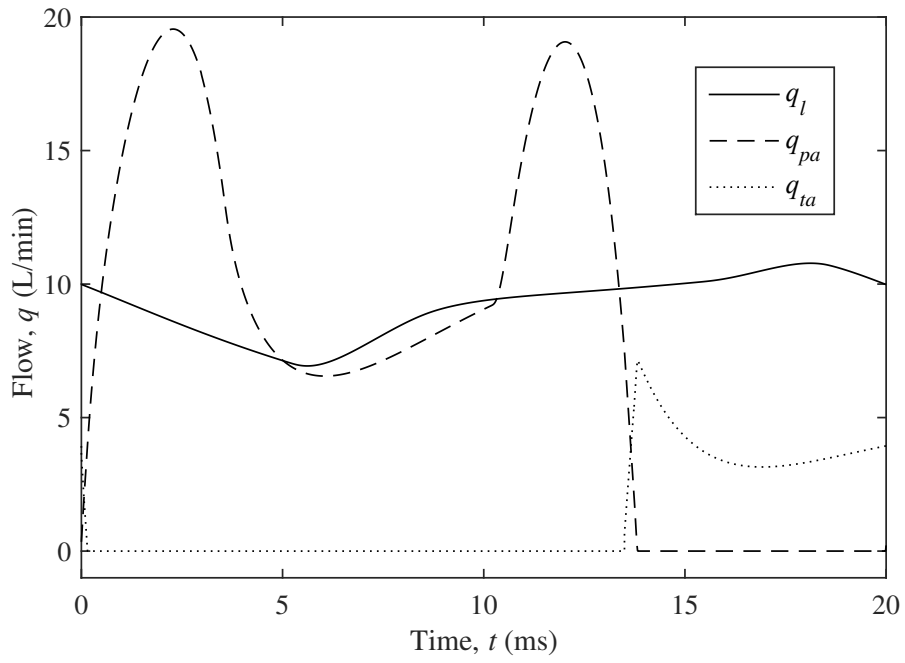
Figure 3.9: Simulated flows for one cycle at steady state.

51

frequency for the chosen inertance tube length, and as a result the wave resonance of the tube has a deleterious effect on performance for this case. The suction wave reflected off the end of the tube is arriving too early, thus increasing the flow over the partially open valve and increasing the power loss during closure. Also, the power loss across the valve upon opening is high since the downstream pressure, p_a, is still low, and pulling fluid through the check valve. The high power loss through the switching valve can be visualized in Figure 3.10. The valve opening and closing events are highlighted with a shaded region within the figure. As can be seen, the power loss through the valve is increased during valve actuation, which is the main cause of the power loss through the switching valve. The power through the inertance tube is also shown, which shows that due to its capacitance it stores and releases power dynamically throughout the response, but averaged over a cycle, there is a net power loss caused by the resistance of the line. The load power is held to a near constant value, which is due to the compressible volume at the load smoothing out the load pressure.
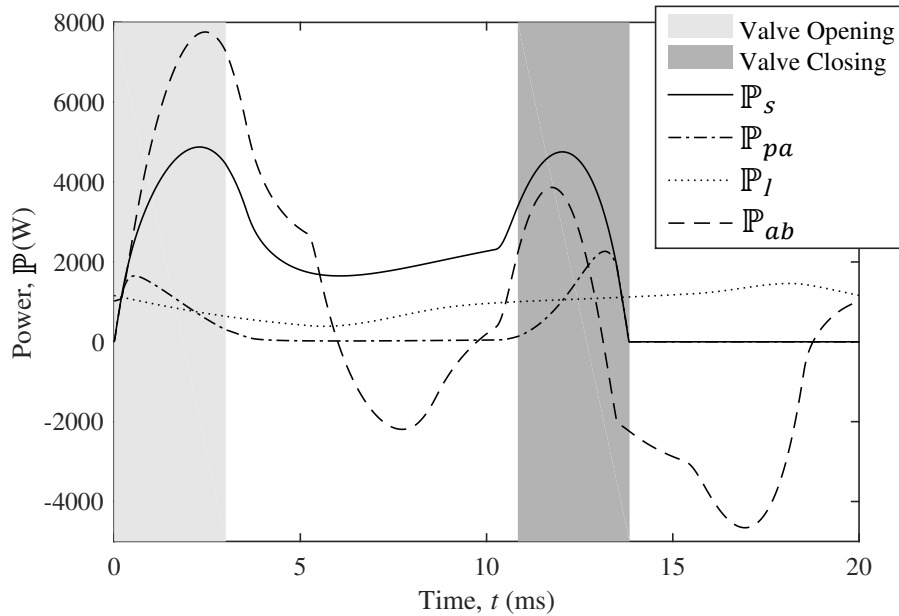
Figure 3.10: Calculated powers for one cycle at steady state. Note the check valve power, $\mathbb{P}_{ta}$, is not shown since it is relatively small.

All the powers present in the system were averaged over a cycle using numerical integration, and the results are given in Table 3.1. What can be seen is that with this converter, the majority of the power loss comes from the switching valve and the inertance tube resistance.

52

The check valve loss is very small relative to the other losses. As a result, this non-optimized system is operating at an efficiency of 47.8% with a volumetric efficiency of 63.0%.

Table 3.1: Energy account for initial simulations

Power	Value	Net
$\overline{\mathbb{P}}_s$	1972.3 W	Input
$\overline{\mathbb{P}}_{pa}$	352.7 W	Loss
$\overline{\mathbb{P}}_{ta}$	0.2 W	Loss
$\overline{\mathbb{P}}_{ab}$	677.4 W	Loss
$\overline{\mathbb{P}}_l$	942.0 W	Output

Chapter 4

Inertance Tube Optimization

This chapter discusses the optimization scheme used to find the optimal dimensions of shaped inertance tubes for the hydraulic buck converter system. The objective function is defined, and the optimization algorithms are described. The optimizations are performed with an increasing number of parameters, and the results are tabulated. A discussion on the results is provided, where the optimal designs are compared to the traditional design using only uniform inertance tubes. Finally, a recommended design is suggested.

4.1   Optimization Scheme

This section will look at the algorithms and fitness function used to optimize the shape of a non-uniform inertance tube. The optimization algorithms that were used were a genetic algorithm and a pattern search algorithm. The problem involves the optimization of a highly non-linear SIMULINK® model, and as a result, the gradient of the problem is not known. These two algorithms used in combination does provide the search of a large sample space providing robustness in finding well performing parameters, however there is no guarantee that the optimal solution is a global result. The two optimization algorithms presented in the following sections work well for these types of problems as they do not require knowledge of the gradient. The objective function contains a solver that maintains a desired load pressure for any inertance tube shape by adjusting the duty cycle of the digital valve. This creates a nested optimization, which does increase computation time significantly. This is the reason for the 2-stage optimization using a genetic algorithm and then followed by a pattern search

for parameter refinement.

4.1.1   Genetic Algorithm

A genetic algorithm (GA) is a type of evolutionary algorithm that is very robust in finding the global minima of an optimization problem, however not guaranteed. The genetic algorithm emulates the biological processes of selection, crossover, and mutation to successively gravitate towards an optimal solution. An initial population of points within the parameter space is generated randomly, and the optimization function is computed at these points. The best points within the initial generation are used as parents to breed successive generations of new child parameters using the mentioned biological processes. Selection is a process that chooses the best parameters for reproduction, the points that have a better efficiency value are selected over points that result in poor efficiency. Crossover swaps certain values from the selected parent parameters to create offspring, mimicking biological recombination. Lastly, mutation modifies the parameters by some random factor, which introduces diversity in the optimization (Mitchell, 1998).

The genetic algorithm is a black-box search, or derivative-free, algorithm useful for the application of optimizing the inertance tube design. Also, since the GA is a good choice for finding the global minimum of a problem, it is well suited for this problem which has shown to have numerous local minima and basins of attraction which would cause other algorithms to return poorer solutions. A major downfall of using the GA is computation time. Since the GA computes a fixed population size for each generation, the amount of fitness evaluations can be extremely high. The genetic algorithm has been used previously for the optimization of switched inertance converters, and has shown to provide excellent robustness (Pan, 2017).

The algorithm specifically used in this thesis is `ga()` available in the GLOBAL OPTIMIZATION TOOLBOX within MATLAB®. The algorithm allows for the specification of several options. To try to mitigate the amount of computation time, the average change in the best fitness function over a number of stall generations was 10^{-2} with the number of stall generations set to 5. To further refine the result, `patternsearch()` from the same toolbox was used to refine the solution.

4.1.2 Pattern Search

Pattern search, also known as direct-search, is a type of optimization algorithm that starts at a specified point and varies the parameters in either direction by the same magnitude to find a possible better optimum. The step size is then reduced if a better point cannot be found, and it's repeated until the function tolerance is met. With the result from the genetic algorithm as an initial starting point, `patternsearch()` iteratively converges to a locally optimal result. This allows for good convergence on an optimum without excessive computations that would otherwise be computed by `ga()`. The algorithm is set to stop if the relative change between the best fitness is 10^{-6}. Pattern search is similar to the genetic algorithm since it is also a derivative-free method, which works well for the presented problem. Pattern search is vulnerable to finding local minima rather than the global minimum, making the algorithm less robust than the genetic algorithm. This is the reason for its use as a secondary algorithm to refine the solution and save computation time. A simplified flow chart showing how the genetic and pattern search algorithms work is shown in Figure 4.1.

4.1.3 Objective/Fitness Function

The main goal of the optimizations is to run the load of the buck converter at 16 MPa using the least amount of power possible by adjusting the inertance tube shape (i.e. by maximizing system efficiency). Therefore, the objective function will take inputs of inertance tube dimensions (i.e. lengths and diameters), and will output the system efficiency obtained while running the load at the desired pressure. The duty cycle of the valve is adjusted at each iteration to ensure the desired load pressure is maintained. A simple zero finding algorithm in Matlab® called `fzero()` is used to find the duty cycle that gives an average of 16 MPa at the load over 1 cycle. Once the desired load pressure is found, the system efficiency at that setting is output to the optimization algorithm. A flow chart of the objective/fitness function is given in Figure 4.1.
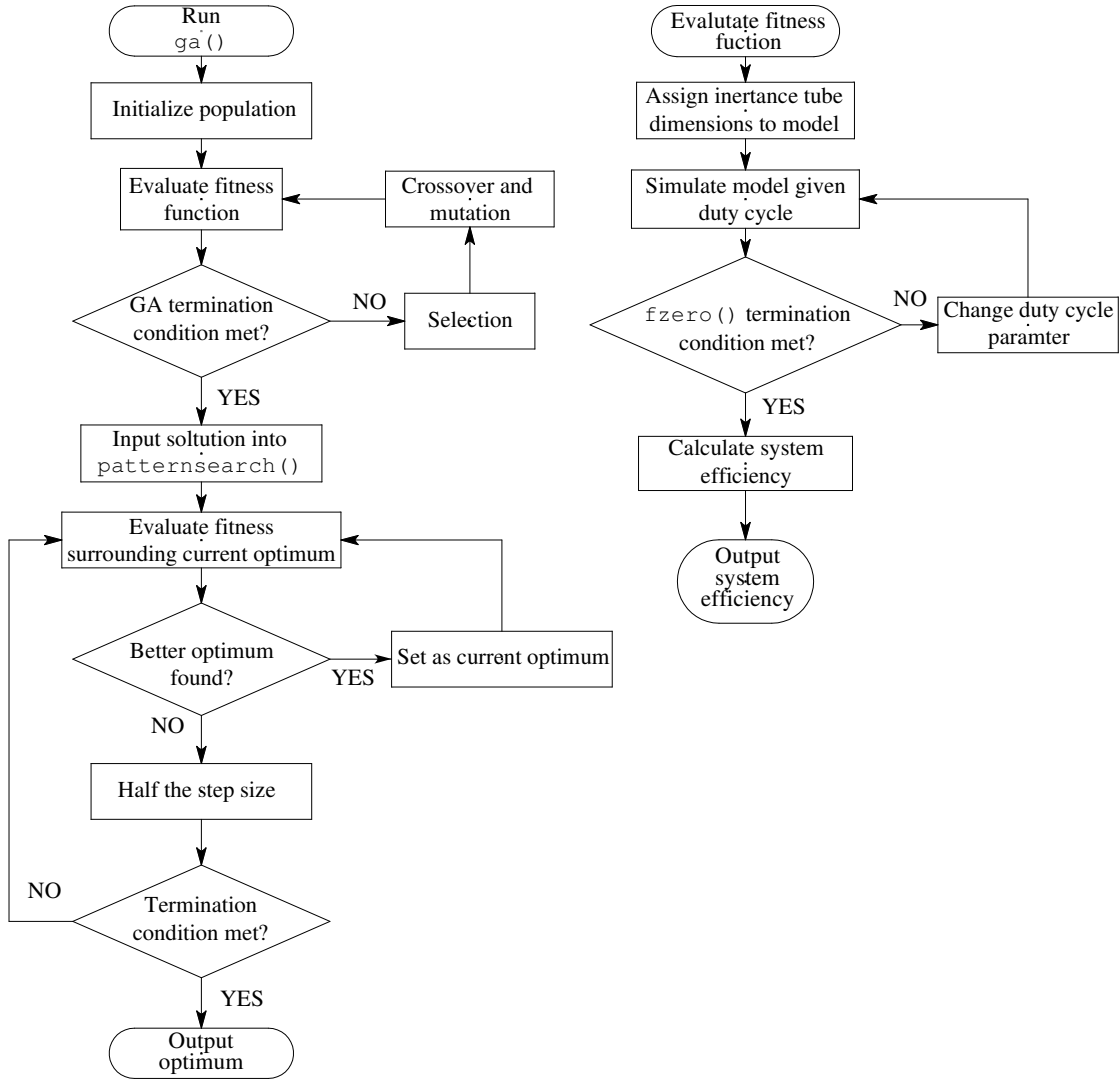
Figure 4.1: Flow chart of the optimization algorithm (left) and objective function (right)

4.2 Results

This section will present the results of the optimizations for five cases. The first case is optimizing a uniform inertance tube, indicating the best case performer of the current and widely used design. The optimizations following are shaped tubes with an increasing number of look-up dimensions. The number of parameters for each shaped tube optimization is given

by the following equation:

$$n = 2N + 1 \qquad\qquad (4.1)$$

where N is the number of segments, and n is the total number of optimization parameters. For all shaped inertance tube cases, there are N section length parameters, and $N + 1$ tube diameter parameters. Each tapered TLM segment requires the specification of a length and both inlet and outlet diameters. Within a shaped inertance tube, it is assumed that the outlet diameter of one section becomes the inlet diameter of the following section. The uniform inertance tube optimization only has two parameters, being its length and constant diameter. Table 4.1 contains the optimized dimensions of the optimization cases, where $\boldsymbol{d}$ and $\boldsymbol{x}_d$ are the diameter and axial position look-up tables respectively. Sketches of each optimized inertance tube is also provided in Table 4.4. Table 4.3 contains the energy account and efficiencies of the optimized buck converter systems.
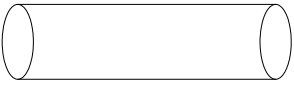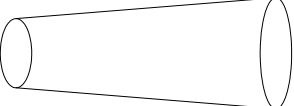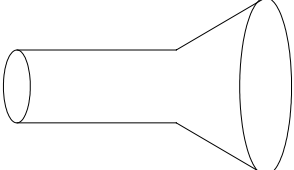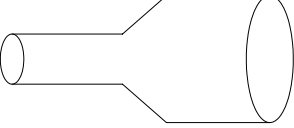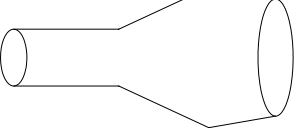
4.2.1 Discussion

Using a uniform transmission line is the current standard design that has been used extensively in most modern research into hydraulic switched inertance converters. As discussed, the uniform inertance tube used in the previous chapter for initial simulations caused the converter to perform rather poorly resulting in a low value of system efficiency. The optimization algorithm was applied to the design of the uniform inertance tube, with the optimized parameters given in Table 4.1 - Optimization 1. To maintain the load pressure at 16 MPa averaged over a cycle, the duty cycle of the valve was set to 33.8%. By keeping all other parameters constant, the converter yielded a system efficiency of 64.1%, an improvement of over 16% compared to the converter simulated in Chapter 3. The pressure and flow responses over one cycle are shown in Figures 4.2 and 4.3 respectively. This converter is considerably more efficient than the converter simulated in the previous chapter as the valve loss is reduced significantly along with the inertance tube line loss. The reduction in valve loss can be noticed in the flow and pressure responses. As the valve opens, the pressure downstream of the valve, p_a, is high at around 17.5 MPa which reduces the flow through the valve, q_{pa},

Table 4.1: Optimal dimension look-up tables for inertance tube optimizations. Note, for all optimizations the load pressure was constant at an average of 16 MPa over one cyle.

Optimization	Sections	$\boldsymbol{x}_d$ (m)	$\boldsymbol{d}$ (mm)	κ_{pa} (%)
1	1 Uniform	[0, 6.52]	[6.8, 6.8]	33.8
2	1 Tapered	[0, 11.32]	[5.0, 16.2]	38.5
3	2 Tapered	[0 5.18, 9.13]	[7.9, 7.0, 29.9]	27.3
4	3 Tapered	[0, 3.94, 5.51, 12.80]	[9.2, 8.9, 21.2, 21.6]	25.1
5	4 Tapered	[0, 2.10, 5.19, 9.93, 14.96]	[6.7, 6.9, 7.5, 29.7, 20.6]	31.4

Table 4.2: Sketches of optimal inertance tube designs. Note the sketchs are not drawn to scale.

Table 4.3: Energy account and efficiencies for inertance tube optimizations

Optimization	$\overline{\mathbb{P}}_s$ (W)	$\overline{\mathbb{P}}_{pa}$ (W)	$\overline{\mathbb{P}}_{ta}$ (W)	$\overline{\mathbb{P}}_{ab}$ (W)	$\overline{\mathbb{P}}_l$ (W)	η_{sys} (%)	η_{vol} (%)
1	1538.5	141.0	0.5	410.9	986.1	64.1	49.7
2	1493.8	199.1	0.5	338.0	956.2	64.0	58.9
3	1365.8	131.5	0.8	301.4	932.1	68.2	46.2
4	1339.5	181.7	1.0	216.4	940.4	70.2	43.0
5	1362.6	110.4	0.8	319.6	931.8	68.4	53.2

and as a result reduces the power loss. In the previous simulation, the downstream pressure was low as the valve opened, and as a result more fluid flows through the valve increasing the throttling loss. Another mitigation of valve loss occurs when the valve closes. Looking at flow rates in Figure 4.3, there is a short delay at around 10 ms from when the valve fully closes to where the suction wave pulls fluid through the check valve. This delay is evidence that the suction wave reflected off the end of the inertance tube is timed adequately so as to not pull more fluid through the switching valve as it closes. This is a noticeable improvement over the previous simulation where hydraulic fluid is pulled through the check valve and the switching valve simultaneously as it closes thus increasing the valve loss. The improvement of this optimized design is largely due to the length of the inertance tube being increased to 6.5 m in combination with the correct valve duty cycle.

The other improvement in the design is a reduction in the inertance tube power loss, where there is a savings of around 266 W with the optimized design. This is due to the decrease in laminar resistance of the line caused by increasing the inertance tube diameter from 5 mm to 6.8 mm. One might propose that the inertance tube diameter be increased to a large value in order to significantly decrease the line loss imposed by using smaller diameter tubes. While this is a valid proposition, this would largely affect the dynamic characteristics of the line, especially the line's inertance which is inversely proportional to the cross sectional area of the inertance tube (Durfee et al., 2015). For lines with large cross sectional area, the fluid inertia is reduced significantly which has adverse effects on the suction wave that pulls fluid through the check valve. The loss through the check valve is increased slightly with this improved design, however, only by a fraction of a Watt.
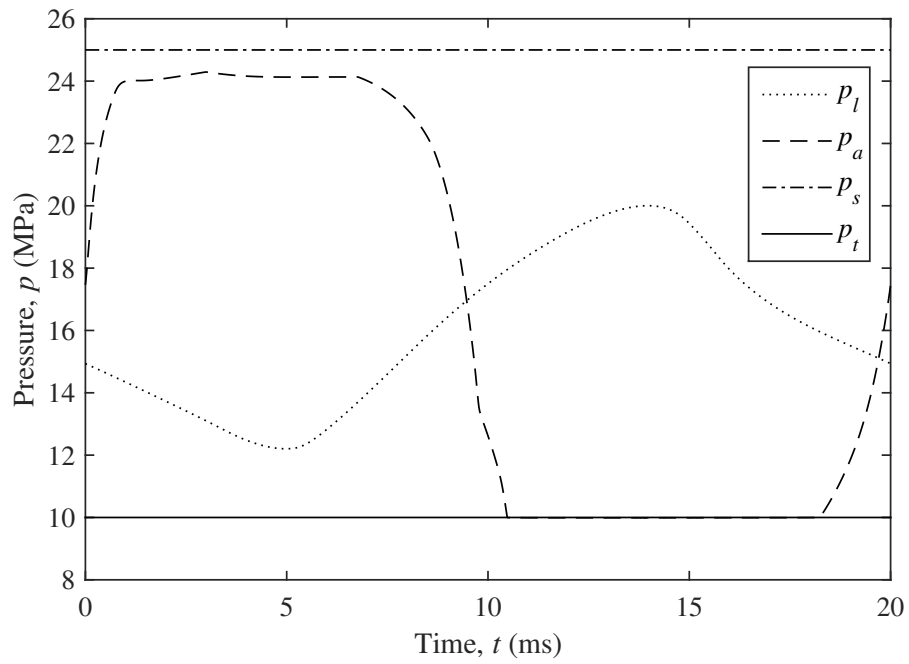
Figure 4.2: Pressure responses over one cycle for the optimized uniform inertance tube
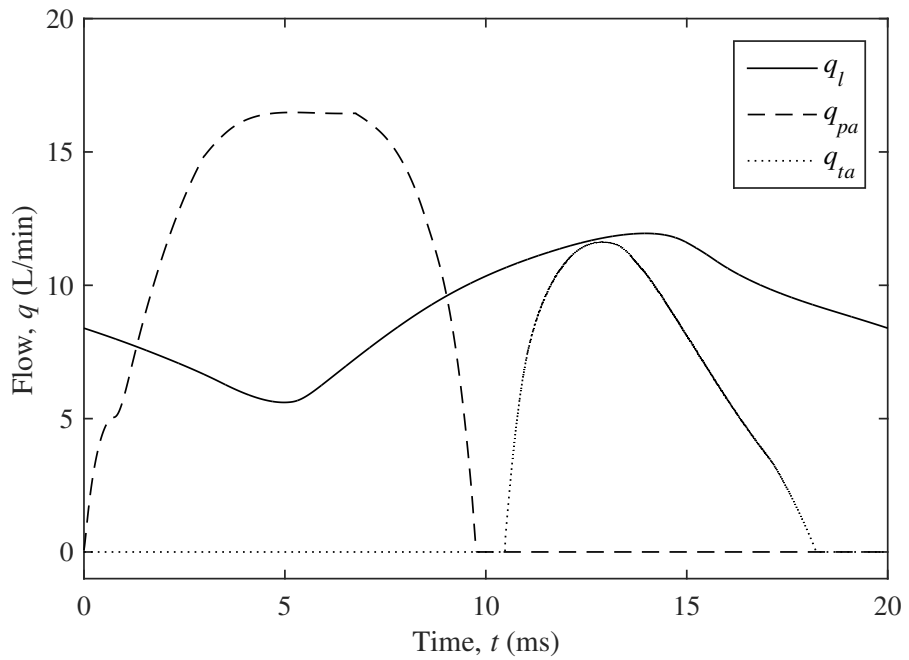
Figure 4.3: Flow responses over one cycle for the optimized uniform inertance tube

Optimization 2 looked at what the performance would be if the traditional design, a uniform inertance tube, was changed to using one single tapered segment as the converter's inertance tube. The optimization converged to the dimensions given in Table 4.1 running at 38.5% duty cycle. This design indicates no clear improvement over the traditional design when looking at the system efficiency, running at a similar 64.0%. The volumetric efficiency is improved slightly, indicating increased check valve flow. What can be seen is that the valve loss is increased from the traditional design, however the line loss is reduced. With the check valve loss unchanged, these two losses trade off against each other to give similar efficiency. This configuration, however, runs the load at lower power and therefore requries less input power. The pressure and flow traces over one cycle are shown in Figures 4.4 and 4.5 respectively. What can be seen in the flow response is that as the switching valve closes, the check valve opens, having flow occur at the same time. This indicates that a suction wave is arriving as the digital valve closes, which increases the valve loss as more fluid is pulled over the partially open valve. Also, as the digital valve opens, the pressure downstream of the valve is low, unlike in Figure 4.2 where the pressure is high as the valve opens at the start of the cycle. As a result, flow is not decreased across the valve as it opens, again creating more valve loss. The shape of Optimization 2 contains a large amount of taper, having its diameter increase from 5.0 mm to 16.2 mm over a length of 11.32 m. This increase in diameter is the reason for the lower line loss, as the resistance of the line decreases over its length from inlet to outlet.

The third set of calculations optimized the dimensions of two tapered sections. The results of this optimization are also provided in Tables 4.1 and 4.3. This inertance tube design shows a significant jump in performance over the previous two optimizations, with an improvement of over 4% in system efficiency. In this case, both the valve and line losses are decreased over the previous two designs, with the check valve loss increased slightly. Pressure and flow over one cycle can be seen in Figures 4.6 and 4.7 respectively. Similar effects as Optimization 1 can be seen here. The valve loss is reduced as the valve opens since the downstream pressure is high, decreasing flow though the partially open orifice. While the valve closes, the downstream pressure is significantly higher than previous, reducing the valve loss even further than the first optimized deign. The shape of this tube is a near-uniform
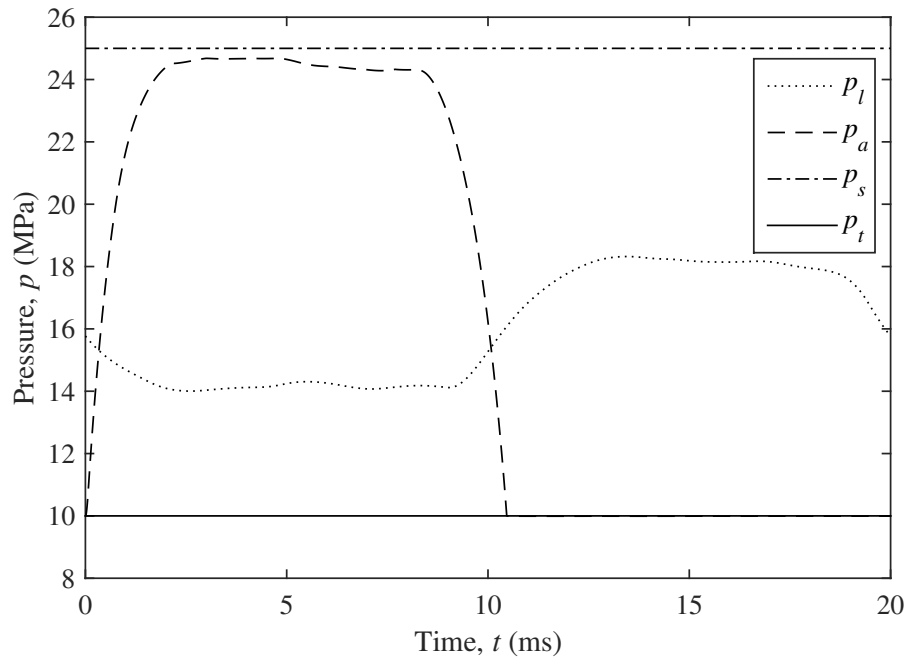
Figure 4.4: Pressure responses over one cycle for the optimized shaped inertance tube with one tapered segment.
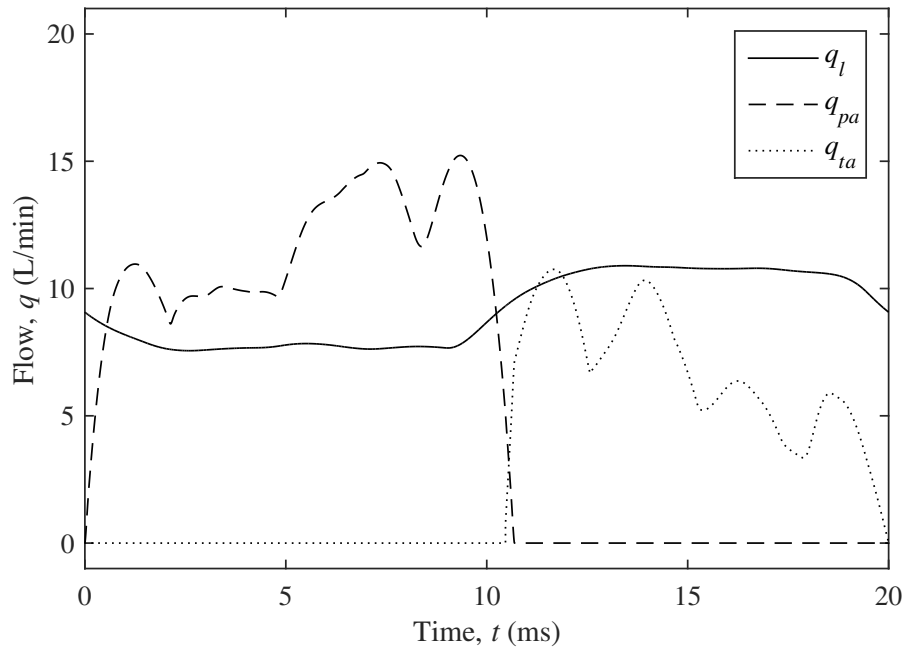
Figure 4.5: Flow responses over one cycle for the optimized shaped inertance tube with one tapered segment.

63

section followed by a largely diverging tapered section. The combination of the total tube length and valve duty cycle here allow for the precise timing of waves in the line to reduce the valve loss, and the increased internal diameter through the near-uniform and diverging section account for the decreased line loss.

The optimized dimensions for an inertance tube with three tapered sections (Optimization 4) are given in Table 4.1. With this inertance tube design, the converter runs at a duty cycle of 25.1% to maintain the desired load pressure. This converter operates at an efficiency of over 6% better than a using a uniform line, and 2% better than using a tube with two tapered sections. The system also operates at a volumetric efficiency of 43.0%. The pressure and flow responses for this design are given in Figures 4.8 and 4.9. The pressure and flow response, again, show similar traits to previous optimizations when it comes to the dynamics. As the valve opens the pressure downstream of the valve is high, and there is also a delay from when the valve closes to when the suction wave pulls fluid though the check valve. The interesting result from this optimization is that the valve loss is not reduced compared to the optimal uniform design, however the line loss is significantly reduced compared to all optimizations. The optimized shape is a near uniform section followed by a diverging tapered section, to a larger diameter uniform section. This result is interesting as it indicates that it is beneficial to have a uniform section of small diameter with high inertance immediately after the switching valve, similar to Optimization 3. The tube then diverges to a section of large diameter and low line resistance all while maintaining the proper dynamics to boost flow and overall length for proper resonance. This inertance tube design style could be potentially simple to manufacture as only one tapered section would have to be made, with the rest of the inertance tube being uniform.

The final set of computations looked at optimizing the dimensions of the inertance tube using four tapered sections (Optimization 5). This optimization contained nine parameters defining the tube dimensions. Optimization 1 took on the order of a couple hours to compute, with successive optimizations appearing to take exponentially longer to converge to an optimal solution. The final optimization took significant computation time to solve the problem, on the scale of multiple days. As a result, this optimization was slated to be the final parameter set due to time constraints. The dimensions and energetic performance are
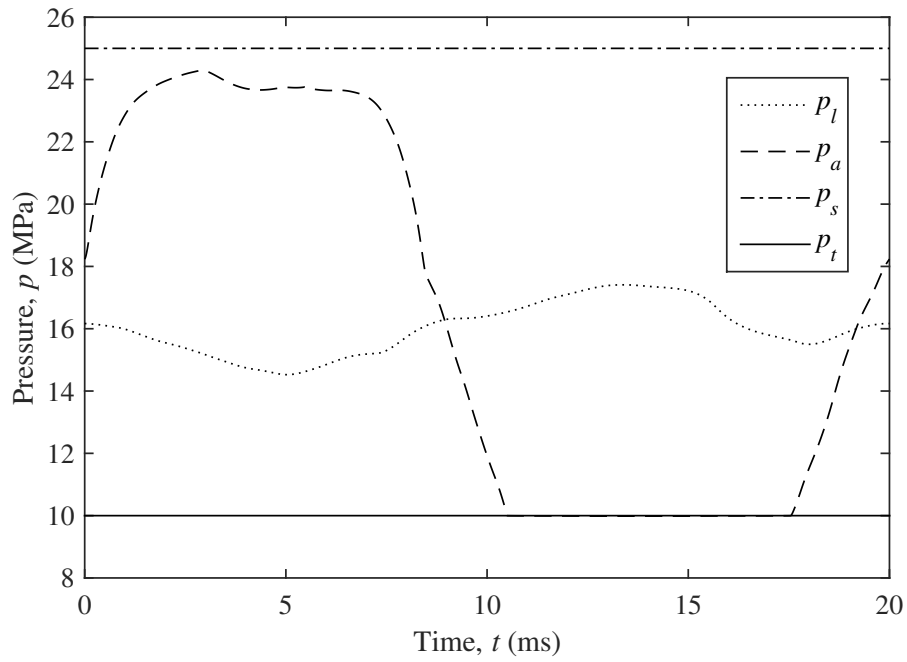
Figure 4.6: Pressure responses over one cycle for the optimized shaped inertance tube with two tapered segments.
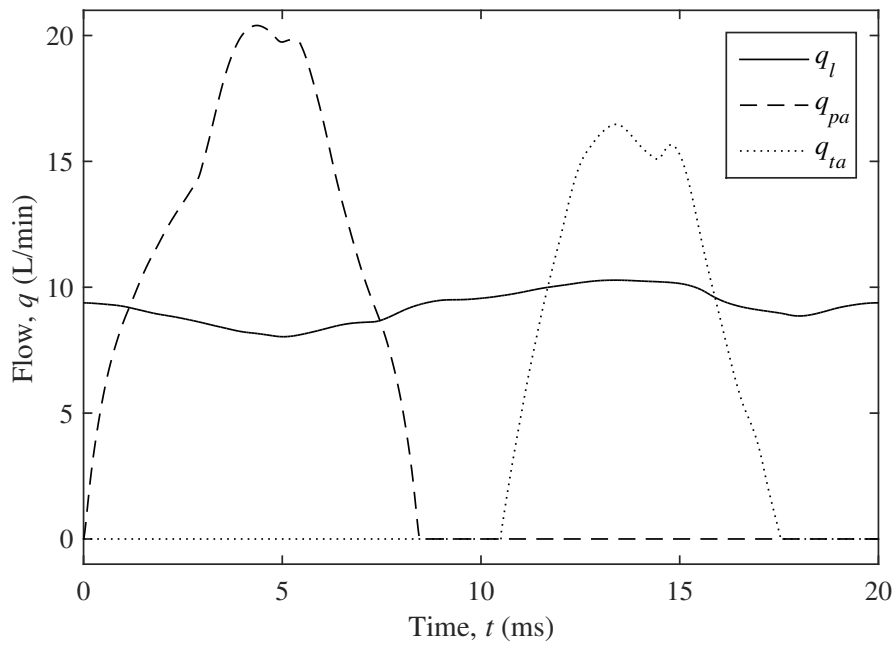
Figure 4.7: Flow responses over one cycle for the optimized shaped inertance tube with two tapered segments.
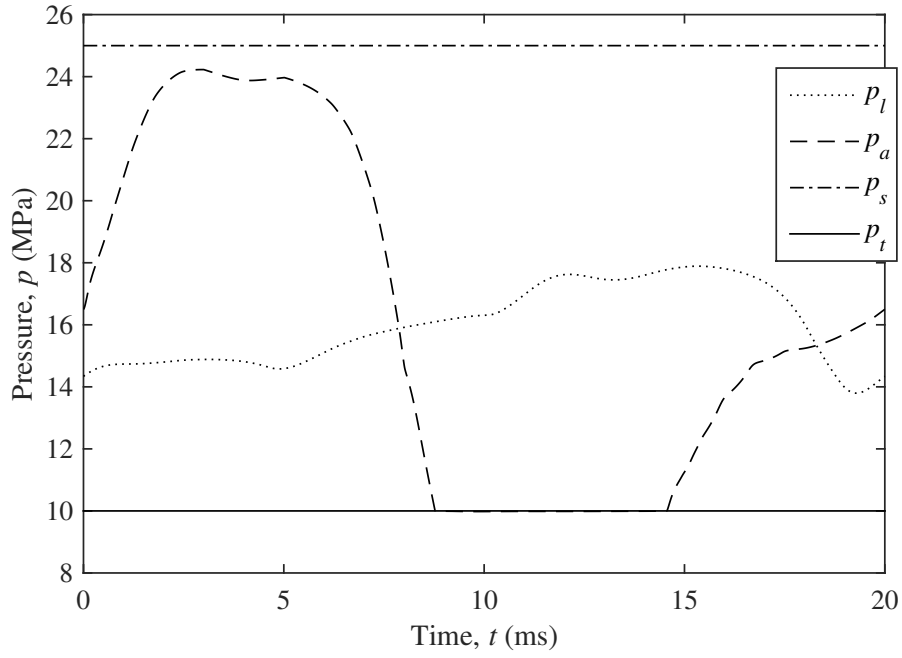
Figure 4.8: Pressure responses over one cycle for the optimized shaped inertance tube with three tapered segments.
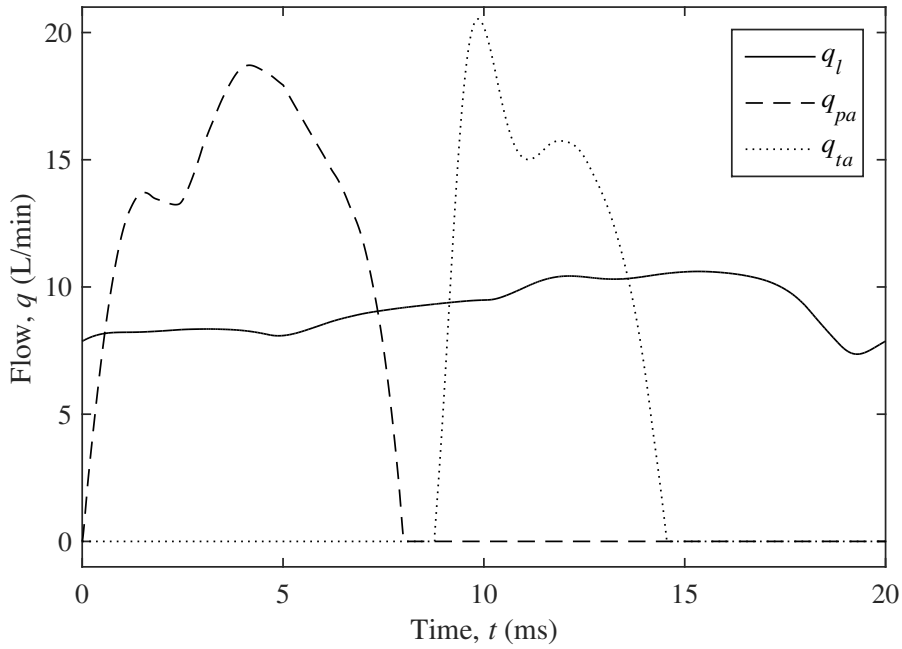
Figure 4.9: Flow responses over one cycle for the optimized shaped inertance tube with three tapered segments.

again provided in Tables 4.1 and 4.3 respectively. The performance of this inertance tube shows no improvement in system efficiency over the previous design using three sections. The line loss is greater in this case consuming 48% more power than the previous optimization. However, the valve loss has been reduced to the lowest value out of all optimizations. Similar to Optimizations 3 and 4, there is a near-uniform small diameter section of transmission line immediately after the switching valve, adding an area of high inertance. Following this near uniform section of line, there is also a diverging tapered section, however, leading to a slightly converging tapered section at the end of the pipe at significantly larger diameter. The dimensions up until the final tapered section are similar to that of Optimization 3 in both axial position and internal diameter. In general, this result does agree well with the previous optimizations having a very similar overall design to the shape. Initially it was expected that the results from this optimization have similar or improved efficiency than Optimization 4, however the final optimization had an efficiency 1.8% lower, and ended up with performance very similar to Optimization 3. It is believed that due to the limited random population size of 100 points used by the genetic algorithm caused it to find a local minimum rather than the solution of Optimization 4. An interesting result of this design is that it has the lowest valve loss, this can be seen in the pressure and flow traces of Figures 4.10 and 4.11. The same valve loss reducing phenomenon occur here as previously discussed, however in this case the valve flow is never high for a long period of time. The flow quickly rises to a maximum and then lowers immediately after, not having a period of high flow through the valve.

One of the major challenges with bringing switched inertance converter technology to market, besides limited valve performance, is the audible noise emitted from the system during operation. This noise is primarily caused by the vibration of the components due to the rapid fluctuation of pressures within the circuit. Comparing the pressure traces in Figures 4.2, 4.8, and 4.10 one can see that the magnitude of the load pressure oscillation is greatly reduced with the shaped inertance tube designs. This is largely due to the presence of increased hydraulic capacitance near the end of the shaped inertance tube smoothing out the response. To quantify this improvement, the root-mean-square error of the signal is
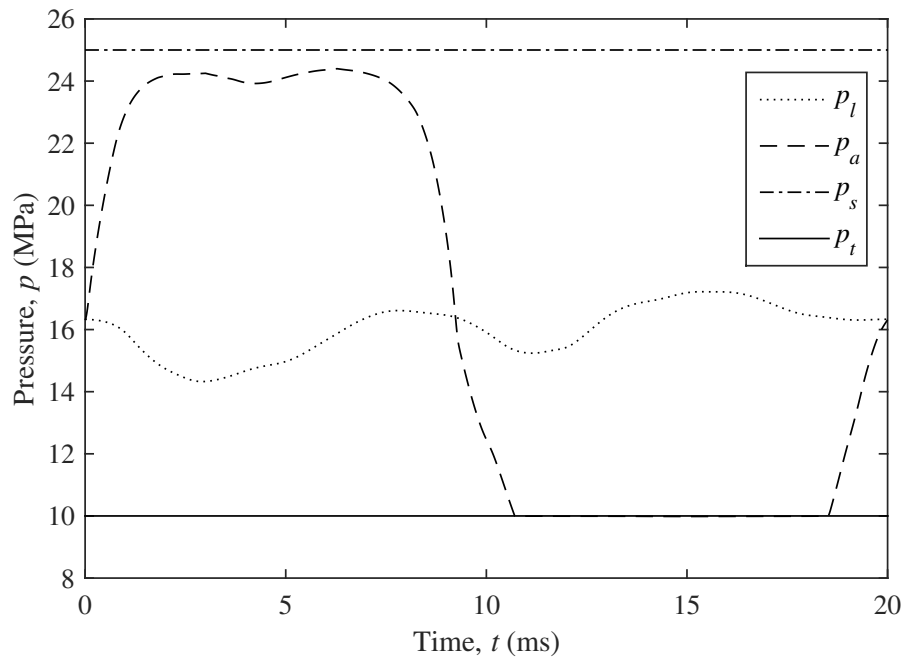
Figure 4.10: Pressure responses over one cycle for the optimized shaped inertance tube with four tapered segments.
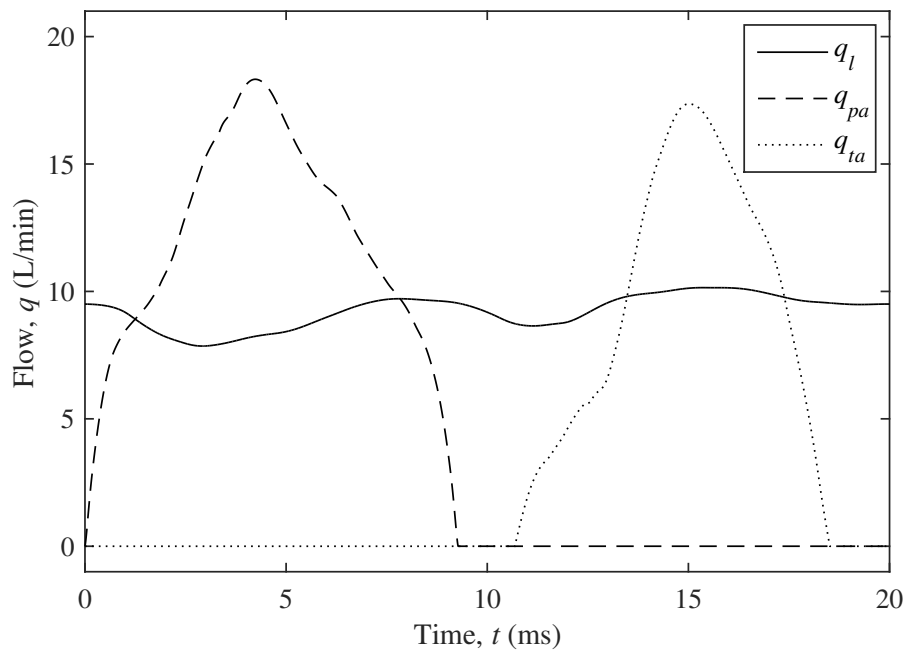
Figure 4.11: Flow responses over one cycle for the optimized shaped inertance tube with four tapered segments.

computed, defined as:

$$RMSE = \sqrt{\frac{1}{t_p} \int_{t_o}^{t_o+t_p} (p_l - \overline{p}_l)^2 dt} \tag{4.2}$$

where the mean load pressure, $\overline{p}_l$, is the desired 16 MPa. The $RMSE$ values are presented in Table 4.4. One can see that the uniform inertance tube design, Optimization 1, has the greatest $RMSE$ value indicating the most noise present. Improvements can be seen for all shaped designs, all having significantly smaller $RMSE$ values. Optimization 5 has the smallest value, likely due to large capacitance near the latter end of the tube. Even the best performing system, Optimization 4, has a reduction in $RSME$ of around 50%. Therefore, not only does the shaped inertance tube design improve system efficiency by reducing line and valve losses, it also provides the potential to reduce excessive noise emitted from the system.

Table 4.4: Root-mean-square error of the load pressure signals demonstrating reductions in audible noise.

Optimization	$RMSE$ (MPa)
1	2.49
2	1.79
3	0.847
4	1.28
5	0.834

4.3 Design Recommendation

The optimized results presented in this chapter all seem to point towards one general design involving a section of uniform, or near-uniform, transmission line followed by a diverging section. Further efficiency seems to be gained if another section of uniform, or near-uniform, line is connected after that. The results indicate that it is valuable to have a portion of high fluid inertance immediately after the valve, then the line can diverge to a larger diameter to

preserve wave propagation effects, but reduce line resistance. A sketch of the optimal design can be seen in Figure 4.12, which resembles the result of Optimization 4.
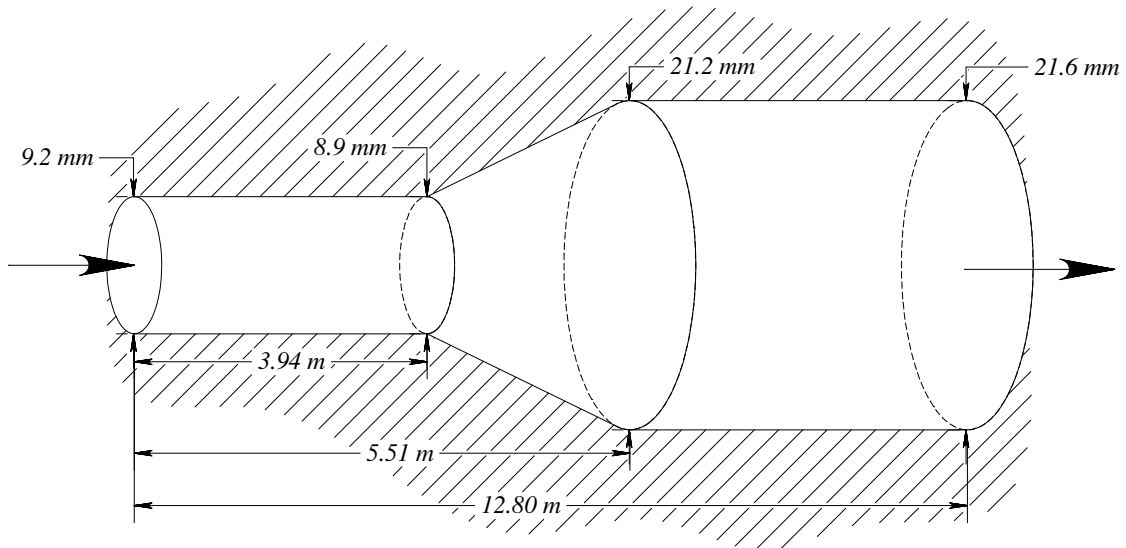
Figure 4.12: Sketch of the optimal inertance tube design. Note the schematic is not drawn to scale, the lengths are considerably larger in size than the diameter changes.

Chapter 5

Conclusions and Recommendations

This final chapter will briefly summarize this thesis with the some concluding remarks. A brief discussion about meeting the research objectives is also provided. Contributions to the research field are presented and the impact discussed. Finally, some recommendations and ideas for future research on the topic are also presented.

5.1   Conclusions

Section 1.3 of this thesis outlined the objectives of the research presented here. The main objective was to use simulation studies with numerical optimization to find the optimal shape of an inertance tube for use in hydraulic step-down (buck) switched inertance converters to maximize system efficiency. A secondary objective was to develop and experimentally validate a computer model for tapered transmission lines for use in modelling shaped inertance tubes.

Chapter 2 reviewed the most recent developments in modelling tapered transmission lines, and in turn indicated areas for improvements in model accuracy as well as solution symmetry. The TLM is a recently developed modelling technique that has shown to be very accurate and computationally efficient, and it was chosen as the candidate method for modelling tapered transmission lines. The tapered TLM approximation model was proposed, containing summations of weighted transfer functions. The weighting factors were found through an optimization in the frequency domain where the objective function compared a numerical solution of the Navier-Stokes equations to the proposed tapered TLM. The weighting factors were found, and can be calculated by using interpolation through a series of look-up tables.

71

Experimental validation of the numerical ODE solution, of which the TLM is optimized from, was desired in order to have confidence in the proposed model. The manufacturing of a rigid tapered transmission line proved to be challenging and expensive, and as a result a prototype made out of polymer was constructed using three-dimensional printing technology. This required the tapered TLM and numerical ODE solution to account for elastic pipe walls. The experimental result, in the frequency domain, showed good agreement for higher order harmonics, however the effects of line vibration was not accounted for. Simulations using MATLAB® SIMULINK® demonstrated the model's ability to be solved in the time domain. Subsequently connecting tapered TLM segments together in order to create transmission lines of arbitrarily changing diameter was proposed. This chapter met the second objective, as an accurate and validated model capable of modelling shaped inertance tubes was successfully completed.

The subsequent chapters looked to fulfil the main objective of finding the optimal shape of the inertance tube in order to maximize system efficiency. Chapter 3 first reviewed the configuration of the converter analyzed in this thesis. This was then followed by defining the dynamic models of each component in the simulation. Finally, the performance of the converter was quantified by defining system and volumetric efficiencies, and by identifying the power losses though the components in the system. Initial simulations of the converter using parameters from previous research showed poor performance. Chapter 4 initially presented the algorithms used to optimize the inertance tube dimensions. The results were then presented and discussed to determine the reasoning behind the different converters performance. The best design has an increase in efficiency of over 6% compared to the traditional design using uniform inertance tubes, due to significantly reduced line loss. Also, other optimizations had shown good performance in reducing the valve loss as well. In general, it appears that a design containing a near-uniform section of smaller diameter and high inertance followed by a diverging section to large diameter with low line resistance can realize efficiency gains. The optimal design maintains the proper dynamics required in the converter to boost flow and convert pressure. The research presented in these chapters met the main objective of this thesis.

The research presented in this thesis has made some important contributions to the field

of hydraulics and fluid power. While the idea that using shaped inertance tubes to increase the efficiency of hydraulic switched inertance converters has been discussed before (Wiens, 2015), the design was not yet fully optimized to determine what shape gives the best overall performance. The results of the optimizations presented here introduce a novel design which has not been introduced in the literature thus far, and due to its simplicity, it should be simpler to manufacture. The proposed design also introduces a potential for noise reduction within realistic implementations. Noise can be reduced by limiting pressure fluctuations at the load due to the increase capacitance near the end of the inertance tube. This could perhaps make the technology more commercially viable than before. The research also shows that not only is the switching valve loss significant, but the inertance tube line loss can also be significant if not designed properly. The proposed tapered TLM model will allow other researchers in the field, and other fields, to simulate flows in tapered channels all while including the effects of frequency-dependent friction. Rigid and elastic walls can be simulated with the models currently available online and ready for download (Wiens and ven der Buhs, 2017).

5.2   Recommendations for Future Work

There are a number of topics and ideas that arose from this research that could be areas where future work can be performed. First, the presented research into shaped inertance tubes was purely theoretical, using simulation studies as proof of concept. Future work on this topic would be to perform experiments, involving several areas of testing. Experimental work would involve characterizing a high speed switching valve and check valve, followed by optimizing the dimensions of the inertance tube using the predetermined recommended shape. Manufacturing a prototype inertance tube with internal taper has proven to be difficult. A design by Beitel and Wiens (2015) looked at machining a rectangular groove of fixed width and varying depth into a piece of round bar stock surrounded by a cylinder. The groove was in the shape of a coiled helix. The research presented here only assumed a straight intertance tube. Future research could look into modelling coiled tubes, with some research already performed by Kogler (2012) in this area. Future research into manufacturing

methods of shaped inertance tubes should also be performed. Then, the converter should be tested and have the results analyzed, comparing the shaped inertance tube to the traditional design that uses a uniform transmission line. Also, the potential reductions in audible noise using the optimized design should also be analyzed and compared with the traditional design. Noise has shown to be one of the major barriers to commercialization with switched inertance converters.

Research by Wiens (2015, 2016) looked at remotely positioning the reservoir check valve at some location along the tube length away from the switching valve as a method of improving performance. This idea has been analyzed for lines of uniform and variable cross section, but the combination of inertance tube shape and check valve location has not yet been optimized together. Future research should optimize both of these power loss mitigation methods simultaneously. The tapered TLM presented here to model shaped inertance tubes could be applied to this research.

The optimizations presented here only considered a maximum of four tapered sections. Future research could look at increasing the number of optimization parameters to perhaps find a more optimal shape. As noted, as more parameters are added to the optimization, the computation time increases significantly. For future optimizations it is recommended that research be performed in reducing computation times. Perhaps simplifying the dynamic model, modifying solver settings, or using a different optimization algorithm will provide areas of improvement with this problem.

Lastly, the tapered TLM proposed in this thesis was able to account for elastic pipe wall effects. Preliminary research on using the TLM to model uniform and tapered viscoelastic transmission lines using a similar method to what was proposed in this thesis has been performed. The ordinary differential equation describing this flow is derived in Appendix F from the partial differential equations available in the literature. The ordinary differential equation is then solved to generate the transmission matrix, and then plotted. Some discussion is also added on potential for integration with the TLM. The further development of this model could have important applications not only in the field of mechanical engineering, but also in biomedical engineering and medicine. A tapered viscoelastic TLM may be able model and simulate blood flow in veins and arteries of variable shape. This model could also be applied

to the modelling and fast simulation of hydraulic hoses constructed with rubber and braided steel reinforcement.

References

Adam Beitel and Travis Wiens. Design of an inertance tube for a new hydraulic system, 2015.

Forbes T. Brown. The transient response of fluid lines. *Journal of Basic Engineering*, 84(4): 547–553, 1962.

Forbes T. Brown. Switched reactance hydraulics: A new way to the control of fluid power. In *Proceedings of the National Conference on Fluid Power*, pages 25–33, 1987.

Dídia Covas, Ivan Stoianov, Joao Mano, Helena Ramos, Nigel Graham, and Cedo Maksimovic. The dynamic effect of pipe-wall viscoelasticity in hydraulic transients. part ii - model development, calibration and verification. *Journal of Hydraulic Research*, 43(1): 56–70, 2005.

A. Frank D'Souza and Rufus Oldenburger. Dynamic response of fluid lines. *Journal of Basic Engineering*, 86(3):589, 1964. doi: 10.1115/1.3653180.

William Durfee, Zongxuan Sun, and James Van de Ven. *Fluid Power System Dynamics*. Center for Compact and Efficient Fluid Power, University of Minnesota, 2015.

Asko Ellman and Robert Piché. A two regime orifice flow formula for numerical simulation. *ASME Journal of Dynamic Systems, Measurement, and Control*, 121(4):721–724, 1999.

Mohamed S. Ghidaoui, Ming Zhao, Duncan A. McInnis, and David H. Axworthy. A review of water hammer theory and practice. *Applied Mechanics Reviews*, 58(1):49, 2005. doi: 10.1115/1.1828050.

Green Line® Hose and Fittings Ltd. Hydraulic fittings > adapters, n.d. URL https://www.greenlinehose.com/index.jsp?ID=,Hydraulic.Fittings,Adapters, dept-36F&path=to&ds=dept.

D. Nigel Johnston. Efficient methods for numerical modeling of laminar friction in fluid lines. *Journal of Dynamic Systems, Measurement, and Control*, 128(4):829–834, 2006. doi: 10.1115/1.2361320.

D. Nigel Johnston. A switched inertance device for efficient control of pressure and flow. In *Proceedings of the ASME 2009 Dynamic Systems and Control Conference*, volume 1, pages 589–596, 2009.

Nigel Johnston. The transmission line method for modelling laminar flow of liquid in pipelines. *Journal of Systems and Control Engineering*, 226(5):586–597, 2012.

Nigel Johnston. Simulink models, 2014. URL http://people.bath.ac.uk/ensdnj/models/newtlm.html.

Nigel Johnston, Min Pan, and Sylwester Kudzma. An enhanced transmission line method for modelling laminar flow of liquid in pipelines. *Journal of Systems and Control Engineering*, 228(4):193–206, 2014.

Helmut Kogler. The hydraulic buck converter - conceptual study and experiments, 2012.

Helmut Kogler and Rudolf Scheidl. Two basic concepts of hydraulic switching converters. In *Proceedings of The First Workshop on Digital Fluid Power*, 2008.

Helmut Kogler, Rudolf Scheidl, and Bernd Hans Schmidt. Analysis of wave propagation effects in transmission lines due to digital valve switching. In *Proceedings of the ASME/-BATH 2015 Symposium on Fluid Power and Motion Control*, 2015.

Philip Koopman. Maximal length lfsr feedback terms, n.d. URL https://users.ece.cmu.edu/~koopman/lfsr/index.html.

Petter Krus, Arne Jansson, Jan-Ove Palmberg, and Kenneth Weddfelt. Distributed simulation of hydromechanical systems. In *Third Bath International Fluid Power Workshop*, 1990.

Petter Krus, Kenneth Weddfelt, and Jan-Ove Palmberg. Fast pipeline models for simulation of hydraulic systems. *Journal of Dynamic Systems Measurement and Control*, 116(1): 132–136, 1994.

MathWorks. Documentation: Check valve, a hydraulic valve that allows flow in one direction only, 2006a. URL https://www.mathworks.com/help/physmod/hydro/ref/checkvalve.html.

MathWorks. Documentation: Segmented pipeline, hydraulic pipeline with resistive, fluid inertia, and fluid compressibility properties, 2006b. URL http://www.mathworks.com/help/physmod/hydro/ref/segmentedpipeline.html.

Melanie Mitchell. *An Introduction to Genetic Algorithms*. The MIT Press, 1998.

Joseph Michel Montgolfier. Note sur le bólier hydraulique et sur la manière d'en calculer les effets [tr. a note on the hydraulic ram, and how to calculate its effects]. *Journal des Mines*, pages 42–51, 1803.

Takayoshi Muto and Hirotaka Kayukawa. Dynamic response of tapered fluid lines (2nd report, trasient response). *Bulletin of JSME*, 29(257), 1986.

Takayoshi Muto, Yoshifumi Kinoshita, and Ryuichi Yoneda. Dynamic response of tapered fluid lines (1st report, transfer matrix and frequency response). *Bulletin of the JSME*, 24 (191):809–815, 1981.

Min Pan. A global optimisation of a switched inertance hydraulic system based on genetic algorithm. In *Proceedings of The 15th Scandinavian International Conference on Fluid Power*, 2017.

Min Pan, Nigel Johnston, Andrew Plummer, Sylwester Kudzma, and Andrew Hillis. Theoretical and experimental studies of a switched inertance hydraulic system including switching transition dynamics, non-linearity and leakage. *Proceedings of the Institution of Mechanical Engineers, Part I: Journal of Systems and Control Engineering*, 228, 2014a.

Min Pan, Nigel Johnston, Andrew Plummer, Sylwester Kudzma, and Andrew Hillis. Theoretical and experimental studies of a switched inertance hydraulic system. *Journal of Systems and Control Engineering*, 2014b.

Michael B. Rannow and Perry Y. Li. Soft switching approach to reducing transition losses in an on/off hydraulic valve. *Journal of Dynamic Systems, Measurement, and Control*, 134 (6), 2012.

Rudolf Scheidl and Gudrun Hametner. The role of resonance in elementary hydraulic switching control. *Journal of Systems and Control Engineering*, 217, 2003.

Alexandre Soares, Dídia Covas, and Luisa Reis. Analysis of pvc pipe-wall viscoelasticity during water hammer. *Journal of Hydraulic Engineering*, 134(9), 2008.

Michail I. Soumelidis, D.Nigel Johnston, Kevin A. Edge, and Derek G. Tilley. A comparative study of modelling techniques for laminar flow transients in hydraulic pipelines. *Proceedings of the JFPS International Symposium on Fluid Power*, 2005(6):100–105, 2005. doi: 10. 5739/isfp.2005.100.

Lisheng Suo and Benjamin Wylie. Complex wavespeed and hydraulic transients in viscoelatic pipes. *Journal of Fluids Engineering*, 112:496–500, 1990.

Mazeda Tahmeen, Takayoshi Muto, and Hironao Yamada. Simulation of dynamic responses of tapered fluid lines. *JSME International Journal, Series B*, 44(2):247–254, 2001.

Jeremy ven der Buhs and Travis Wiens. Modelling dynamic response of hydraulic fluid within tapered transmission lines. In *Proceedings of the 15th Scandinavian International Conference on Fluid Power, SICFP'17*. Linköpings Universitet, Linköping, Sweden, 2017a.

Jeremy W. ven der Buhs and Travis K. Wiens. Modelling dynamic response of hydraulic fluid within tapered transmission lines [submitted]. *Journal of Dynamic Systems, Measurement, and Control*, 2017b.

Jeremy W. ven der Buhs and Travis K. Wiens. Detection of pipeline weakening and defects via analysis of fluid pressure dynamic response. In *Proceedings of the 2017 Maintenance, Engineering and Reliability / Mine Operators Conference*. Canadian Institute of Mining, Metallurgy and Petroleum, Saskatoon, Canada, 2017c.

Taco J. Viersma. Analysis, synthesis and design of hydraulic servosystems and pipelines. *Studies in Mechanical Engineering - Volume 1*, 1980.

Pengfei Wang, Sylwester Kudzma, Nigel Johnston, Andrew Plummer, and Andrew Hillis. The influence of wave effects on digital switching valve performance. In *Proceedings of the Fourth Workshop on Digital Fluid Power*, 2011.

Seiichi Washio, Tadataka Konishi, and Kenjiro Okamura. Research on wave phenomena in hydraulic lines : 2nd report, unsteady liquid flow in a tapered pipe. *Bulletin of JSME*, 17 (111):1165–1171, 1974. doi: 10.1299/jsme1958.17.1165.

John Whitehurst. Account of a machine for raising water, executed at oulton, in cheshire, in 1772. in a letter from mr. john whitehurst to dr. franklin. *Philosophical Transactions of the Royal Society of London*, 65(0):277–279, jan 1775. doi: 10.1098/rstl.1775.0026.

Travis Wiens. Kasami sequences, m-sequences, linear feedback shift registers, 2009. URL https://www.mathworks.com/matlabcentral/fileexchange/22716.

Travis Wiens. Analysis and mitigation of valve switching losses in switched inertance converters. In *Proceedings of the ASME/BATH 2015 Symposium on Fluid Power & Motion Control*, 2015.

Travis Wiens. Improving performance of a switched inertance buck converter via positiong of reservior flow valve. *Journal of Dynamic Systems, Measurement, and Control*, 138(12), 2016.

Travis Wiens and Jeremy ven der Buhs. Transmission line models, 2017. URL https://github.com/tkw954/usask_tlm.

Alexander C. Yudell and James D. Van de Ven. Soft switching in switched inertance hydraulic circuits. In *Proceedings of the BATH/ASME 2016 Symposium on Fluid Power and Motion Control*, 2016.

Werner Zielke. Frequency-dependent friction in transient pipe flow. *Journal of Basic Engineering*, 90(1):109–115, 1968.

Appendix A

Tabulation of Tapered TLM Parameters

The weighting factors that make up the Tapered TLM are tabulated in the following Appendix. In total there are 13 tables: 6 tables for the individual m_{Ei} factors, 6 tables for the individual m_{Gi} factors, and 1 table of the transmission time modifier τ. Two-dimensional linear interpolation is required to find the parameters for any given tapered transmission line. The top row of the table contains values of taper ratio λ. The first column of the tables contain values of dissipation number β. These two parameters must be determined for a given transmission line, then they are passed to the interpolation function which determines the appropriate weighting factors given by these tables. Performing this interpolation saves significant computation time as compared to calculating the numerical ODE solution each time and subsequently performing the optimization.

A.1 Parameters for m_{Ei}

This section contains the parameters for the $E(s)$ transfer function used within the TLM structure.

Table A.1: Weighting factors for m_{E1}

β \ λ	1	0.944	0.889	0.833	0.778	0.722	0.667	0.611	0.556	0.5
0.0001	0.007958	0.007948	0.007858	0.007687	0.007434	0.00707	0.006475	0.005649	0.004198	0.001837
0.0001334	0.009203	0.009183	0.009074	0.008912	0.008632	0.008273	0.007693	0.006863	0.005412	0.003054
0.0001778	0.01062	0.01061	0.01051	0.01032	0.01005	0.009652	0.009053	0.008199	0.006815	0.004456
0.0002371	0.01228	0.01225	0.01213	0.01195	0.01161	0.01124	0.01062	0.009794	0.008422	0.006057
0.0003162	0.01416	0.01413	0.01396	0.01382	0.01346	0.01306	0.01242	0.01162	0.01016	0.007896
0.0004217	0.01634	0.0163	0.01618	0.01595	0.01561	0.01509	0.01452	0.01364	0.01234	0.009854
0.0005623	0.01882	0.01877	0.01865	0.01842	0.01803	0.01754	0.01683	0.01595	0.0146	0.01238
0.0007499	0.02156	0.02158	0.02146	0.0212	0.0208	0.02025	0.01953	0.01856	0.01716	0.01493
0.001	0.02485	0.02485	0.02465	0.02436	0.02392	0.02329	0.02251	0.02151	0.02012	0.01811
0.001334	0.02834	0.02828	0.02819	0.02791	0.02708	0.02671	0.02586	0.02478	0.02336	0.02127
0.001778	0.03198	0.03188	0.03178	0.03146	0.03102	0.03038	0.0296	0.02853	0.02697	0.0248
0.002371	0.0356	0.0356	0.03555	0.03525	0.03476	0.03404	0.03322	0.03215	0.03073	0.02873
0.003162	0.03928	0.03932	0.03947	0.03918	0.03864	0.03791	0.03699	0.03585	0.03437	0.0325
0.004217	0.0426	0.04261	0.04281	0.04312	0.04279	0.04205	0.04102	0.0397	0.03807	0.03604
0.005623	0.04518	0.04517	0.04539	0.04596	0.04641	0.04647	0.04532	0.04389	0.042	0.03974
0.007499	0.0471	0.04704	0.04668	0.04605	0.04636	0.04829	0.05003	0.04836	0.04631	0.04383
0.01	0.04356	0.04346	0.04316	0.04303	0.04476	0.04712	0.05018	0.05369	0.05132	0.04859
0.01334	0.03776	0.0377	0.03777	0.0394	0.04171	0.04476	0.04856	0.05319	0.05792	0.05484
0.01778	0.03156	0.03159	0.03296	0.03527	0.03849	0.04251	0.04731	0.0529	0.05939	0.06393
0.02371	0.03362	0.0337	0.03395	0.03598	0.03971	0.04439	0.04993	0.05627	0.06343	0.07158
0.03162	0.0481	0.04813	0.04835	0.04874	0.0508	0.05538	0.06092	0.06734	0.07461	0.08277
0.04217	0.07012	0.07019	0.07043	0.07087	0.07157	0.07603	0.08142	0.08764	0.09462	0.1024
0.05623	0.09495	0.09507	0.09545	0.09638	0.09987	0.1044	0.1097	0.1159	0.1228	0.1303
0.07499	0.1234	0.1239	0.1253	0.1278	0.1314	0.136	0.1416	0.1481	0.1552	0.163
0.1	0.1531	0.1535	0.155	0.1575	0.1612	0.1661	0.1721	0.1791	0.1869	0.1955
0.1334	0.1793	0.1798	0.1813	0.1838	0.1876	0.1925	0.1987	0.206	0.2143	0.2236
0.1778	0.2034	0.204	0.2053	0.2077	0.2114	0.2162	0.2223	0.2294	0.2376	0.2468
0.2371	0.23	0.2303	0.2314	0.2334	0.2362	0.2399	0.2445	0.2478	0.2508	0.2547
0.3162	0.2432	0.2432	0.2434	0.2434	0.2442	0.2449	0.2459	0.2474	0.2498	0.2535
0.4217	0.2694	0.2695	0.2678	0.2639	0.2603	0.2587	0.2568	0.2549	0.2534	0.2549
0.5623	0.2855	0.2853	0.2848	0.2839	0.2855	0.2832	0.2848	0.2785	0.2708	0.2688
0.7499	0.2765	0.2766	0.2773	0.2785	0.2804	0.2807	0.2743	0.2708	0.2755	0.2905
1	0.3075	0.3067	0.3041	0.2994	0.2923	0.2825	0.2751	0.2634	0.242	0.2437

Table A.2: Weighting factors for m_{E2}

β \ λ	0.5	0.556	0.611	0.667	0.722	0.778	0.833	0.889	0.944	1
0.0001	2.646e-06	3.098e-06	3.705e-06	0.0001056	5.345e-06	6.16e-06	8.625e-06	7.356e-06	9.49e-06	3.662e-05
0.0001334	1.235e-05	1.445e-05	2.153e-05	2.125e-05	4.97e-06	5.848e-06	6.215e-06	4.093e-05	8.708e-06	6.843e-06
0.0001778	2.329e-06	2.732e-06	3.286e-06	2.027e-05	4.694e-06	5.321e-06	5.798e-06	6.293e-06	8.091e-06	3.961e-05
0.0002371	1.098e-05	2.592e-06	1.586e-05	3.935e-06	4.487e-06	0.000118	5.638e-06	5.792e-06	7.647e-06	6.18e-06
0.0003162	2.099e-06	1.242e-05	3.021e-06	3.845e-06	2.164e-05	0.0001151	5.466e-06	0.0001284	7.403e-06	2.934e-05
0.0004217	2.038e-06	2.443e-06	3.021e-06	3.716e-06	0.0001069	4.93e-06	5.351e-06	5.784e-06	7.294e-06	5.902e-06
0.0005623	2.007e-06	2.511e-06	3.116e-06	4.002e-06	4.58e-06	5.205e-06	5.818e-06	6.052e-06	7.939e-06	3.117e-05
0.0007499	2.035e-06	2.692e-06	3.387e-06	4.287e-06	5.199e-06	3.023e-05	6.703e-06	3.548e-05	9.505e-06	0.0001676
0.001	2.213e-06	2.949e-06	4.053e-06	5.639e-06	7.241e-06	8.516e-06	1.008e-05	1.152e-05	1.279e-05	1.279e-05
0.001334	2.719e-06	3.884e-06	6.329e-06	0.0001999	7.535e-05	0.0009208	4.929e-05	7.952e-05	0.0001017	0.0002354
0.001778	4.124e-06	7.542e-06	2.262e-05	0.0002528	0.000633	0.0008733	0.001041	0.001165	0.001196	0.001242
0.002371	1.59e-05	0.0006182	0.001367	0.001988	0.002431	0.002653	0.002813	0.002932	0.003114	0.003114
0.003162	0.001857	0.003052	0.003895	0.004512	0.004884	0.005119	0.005278	0.00545	0.005849	0.005969
0.004217	0.005392	0.006505	0.007296	0.007792	0.008139	0.00842	0.008939	0.009733	0.01027	0.01038
0.005623	0.01004	0.01093	0.01144	0.01204	0.01236	0.01533	0.01587	0.01752	0.01815	0.01813
0.007499	0.01566	0.01641	0.01695	0.01731	0.02643	0.03501	0.03563	0.03174	0.02955	0.02914
0.01	0.02241	0.02293	0.0232	0.03855	0.05133	0.06104	0.06809	0.06656	0.06459	0.06398
0.01334	0.02989	0.02999	0.04979	0.06782	0.08228	0.09355	0.1019	0.1076	0.1071	0.1066
0.01778	0.03729	0.05742	0.08109	0.1009	0.1174	0.1306	0.1407	0.1477	0.1518	0.1516
0.02371	0.05892	0.08724	0.1118	0.1329	0.1506	0.1649	0.1759	0.1812	0.1809	0.1807
0.03162	0.08568	0.1132	0.1375	0.1585	0.1761	0.1901	0.1951	0.1946	0.1943	0.1941
0.04217	0.111	0.1369	0.1602	0.1805	0.1977	0.2116	0.2117	0.2117	0.2117	0.2117
0.05623	0.1395	0.164	0.1867	0.2067	0.2238	0.2377	0.2482	0.25	0.2505	0.2506
0.07499	0.182	0.2062	0.2288	0.2489	0.2661	0.2801	0.2907	0.298	0.3021	0.3034
0.1	0.2506	0.2749	0.2976	0.3178	0.3351	0.349	0.3594	0.3665	0.3707	0.3718
0.1334	0.3519	0.3753	0.3971	0.4163	0.4325	0.4455	0.4553	0.462	0.4657	0.4669
0.1778	0.4825	0.5025	0.5211	0.5375	0.5514	0.5626	0.5711	0.5767	0.5797	0.5811
0.2371	0.6528	0.6594	0.6652	0.6716	0.68	0.6868	0.6921	0.6957	0.6978	0.6984
0.3162	0.8418	0.8417	0.8405	0.8392	0.8379	0.8368	0.8355	0.8356	0.8353	0.8352
0.4217	1.016	1.007	0.9933	0.9809	0.9706	0.9625	0.9497	0.9369	0.9313	0.9315
0.5623	1.157	1.141	1.113	1.089	1.072	1.045	1.043	1.031	1.025	1.023
0.7499	1.275	1.285	1.258	1.209	1.157	1.142	1.138	1.136	1.134	1.134
1	1.479	1.423	1.348	1.311	1.286	1.262	1.246	1.237	1.232	1.23

Table A.3: Weighting factors for m_{E3}

β \ λ	0.5	0.556	0.611	0.667	0.722	0.778	0.833	0.889	0.944	1
0.0001	0.05312	0.03714	0.02586	0.01786	0.01213	0.00808	0.005287	0.003503	0.002538	0.00227
0.0001334	0.05353	0.03756	0.02628	0.0183	0.01255	0.0085	0.005694	0.003907	0.002931	0.002646
0.0001778	0.05403	0.03806	0.02683	0.01883	0.01306	0.00898	0.00618	0.004375	0.003402	0.003113
0.0002371	0.05464	0.03866	0.02745	0.01946	0.01367	0.009586	0.006747	0.004964	0.003967	0.003667
0.0003162	0.05538	0.03948	0.0282	0.02023	0.01441	0.01031	0.007442	0.005669	0.004649	0.004352
0.0004217	0.05639	0.04033	0.02916	0.02112	0.01533	0.01117	0.008316	0.006464	0.005481	0.005175
0.0005623	0.05739	0.04155	0.03032	0.02228	0.0164	0.01224	0.009313	0.007488	0.006487	0.006178
0.0007499	0.05887	0.04303	0.03175	0.02362	0.01774	0.01349	0.0106	0.008729	0.00773	0.007433
0.001	0.0605	0.04477	0.03349	0.02533	0.01939	0.0151	0.01214	0.01026	0.008924	0.008924
0.001334	0.0628	0.04699	0.03566	0.02738	0.0214	0.01704	0.01406	0.01217	0.01117	0.01082
0.001778	0.06559	0.04971	0.03827	0.02993	0.02388	0.01944	0.01642	0.01449	0.01348	0.01313
0.002371	0.069	0.05301	0.04141	0.03299	0.02686	0.02238	0.01933	0.01738	0.01721	0.01721
0.003162	0.07303	0.05695	0.04527	0.03675	0.03055	0.02608	0.02297	0.02151	0.02312	0.02361
0.004217	0.07793	0.06175	0.04996	0.04132	0.03503	0.03055	0.02932	0.0323	0.03442	0.03482
0.005623	0.08384	0.06752	0.05552	0.04686	0.04049	0.03496	0.04846	0.05417	0.05636	0.05631
0.007499	0.09079	0.07439	0.06235	0.05349	0.04398	0.0365	0.04762	0.06764	0.07882	0.08148
0.01	0.09887	0.08241	0.07022	0.05626	0.04565	0.03793	0.03254	0.04657	0.05751	0.06091
0.01334	0.1079	0.09134	0.07286	0.05835	0.04748	0.03951	0.03392	0.03025	0.03772	0.04097
0.01778	0.1173	0.0948	0.07561	0.06098	0.04993	0.04174	0.03592	0.0321	0.02998	0.03293
0.02371	0.1226	0.09811	0.07922	0.06471	0.05368	0.04548	0.03965	0.04126	0.05008	0.05283
0.03162	0.1255	0.1019	0.08364	0.06952	0.05876	0.05076	0.05858	0.07314	0.08135	0.08398
0.04217	0.1273	0.105	0.08762	0.07407	0.06368	0.05593	0.0743	0.08698	0.09416	0.09642
0.05623	0.1266	0.1058	0.08946	0.07661	0.0667	0.05927	0.05396	0.06244	0.06842	0.07029
0.07499	0.1212	0.1022	0.08711	0.07521	0.06599	0.05907	0.0541	0.05083	0.04902	0.04846
0.1	0.1092	0.0925	0.07918	0.06868	0.06056	0.05446	0.05011	0.04728	0.04564	0.0452
0.1334	0.08999	0.07641	0.06575	0.05746	0.05112	0.0464	0.04305	0.04085	0.03965	0.03927
0.1778	0.06437	0.0553	0.04859	0.04366	0.04007	0.03748	0.03569	0.0346	0.03419	0.03373
0.2371	0.03476	0.03177	0.03067	0.03048	0.03153	0.03259	0.03351	0.03418	0.03458	0.0347
0.3162	0.006958	0.0147	0.02294	0.03079	0.03771	0.0434	0.05067	0.05066	0.05234	0.05286
0.4217	3.723e-05	0.01209	0.03159	0.04916	0.06414	0.07622	0.09535	0.1144	0.1206	0.1171
0.5623	1.288e-07	0.01134	0.03957	0.06557	0.1099	0.164	0.1473	0.1614	0.1692	0.1717
0.7499	1.514e-07	0.005247	0.0687	0.1683	0.2675	0.2732	0.2575	0.2476	0.2423	0.2416
1	6.807e-07	0.106	0.1787	0.1882	0.1687	0.1587	0.1469	0.137	0.1309	0.1289

Table A.4: Weighting factors for m_{E4}

β \ λ	1	0.944	0.889	0.833	0.778	0.722	0.667	0.611	0.556	0.5
0.0001	0.00815	0.009263	0.01318	0.02041	0.03173	0.04805	0.07089	0.1027	0.1466	0.2077
0.0001334	0.009522	0.01063	0.01455	0.02188	0.03313	0.04951	0.07246	0.1041	0.1481	0.2092
0.0001778	0.01102	0.01224	0.01619	0.02355	0.03485	0.05127	0.07427	0.1061	0.1499	0.211
0.0002371	0.01294	0.01415	0.01825	0.0254	0.03682	0.05335	0.07643	0.1082	0.152	0.2132
0.0003162	0.0152	0.01643	0.0205	0.02773	0.03923	0.05582	0.07897	0.1107	0.1548	0.2157
0.0004217	0.01802	0.01925	0.02315	0.03067	0.04217	0.05868	0.082	0.1139	0.1577	0.2191
0.0005623	0.02124	0.02241	0.02654	0.03382	0.04561	0.06231	0.08564	0.1177	0.1616	0.2224
0.0007499	0.02501	0.02633	0.03045	0.03796	0.04948	0.06655	0.09002	0.1222	0.1663	0.2272
0.001	0.02982	0.02982	0.03518	0.04275	0.05458	0.07154	0.0952	0.1277	0.1718	0.2323
0.001334	0.03541	0.03677	0.04091	0.04851	0.05979	0.07761	0.1014	0.1341	0.1786	0.2392
0.001778	0.04167	0.04297	0.04718	0.05488	0.06699	0.08474	0.1089	0.142	0.1867	0.2475
0.002371	0.05308	0.05308	0.05453	0.06236	0.07457	0.09236	0.1169	0.1503	0.1958	0.2574
0.003162	0.0716	0.07008	0.06512	0.07128	0.08365	0.1015	0.1262	0.16	0.2058	0.268
0.004217	0.1047	0.1035	0.097	0.0801	0.09428	0.1122	0.1372	0.1712	0.2173	0.2796
0.005623	0.07518	0.0663	0.06396	0.07936	0.1049	0.1249	0.1501	0.1843	0.2307	0.2931
0.007499	0.05036	0.05356	0.06516	0.08621	0.1101	0.134	0.1653	0.1998	0.2463	0.3087
0.01	0.06384	0.06744	0.07908	0.09778	0.115	0.1395	0.1732	0.2176	0.2641	0.3263
0.01334	0.0769	0.08048	0.09082	0.1025	0.1203	0.1455	0.1799	0.2255	0.284	0.3458
0.01778	0.08642	0.08993	0.09663	0.1087	0.1271	0.153	0.1878	0.2337	0.2934	0.3659
0.02371	0.09064	0.09407	0.1051	0.1194	0.1379	0.1638	0.1985	0.244	0.3027	0.3781
0.03162	0.09645	0.0997	0.1103	0.1294	0.1528	0.1781	0.2121	0.2564	0.3132	0.3856
0.04217	0.1102	0.1132	0.1231	0.141	0.1678	0.1924	0.2252	0.2677	0.3218	0.39
0.05623	0.1344	0.1372	0.1463	0.162	0.1789	0.2026	0.2339	0.2742	0.325	0.3884
0.07499	0.1485	0.1503	0.1562	0.1667	0.1827	0.2048	0.2341	0.2714	0.3182	0.3758
0.1	0.1481	0.1496	0.155	0.1643	0.1786	0.1985	0.2246	0.2579	0.2993	0.3498
0.1334	0.1465	0.1478	0.1522	0.16	0.1718	0.1882	0.2097	0.2371	0.271	0.3123
0.1778	0.1519	0.153	0.156	0.1616	0.1701	0.1818	0.1972	0.2167	0.2408	0.2702
0.2371	0.1707	0.1712	0.1728	0.1756	0.1799	0.1858	0.1935	0.2025	0.2132	0.2267
0.3162	0.2016	0.2014	0.2009	0.2009	0.1986	0.1968	0.1945	0.1918	0.1891	0.187
0.4217	0.2721	0.2546	0.2429	0.2421	0.2377	0.2268	0.2128	0.1956	0.1755	0.1532
0.5623	0.536	0.5268	0.4972	0.4443	0.3081	0.2738	0.2517	0.2156	0.173	0.1239
0.7499	0.7255	0.7116	0.6627	0.5743	0.4393	0.2991	0.2759	0.2395	0.1736	0.08969
1	1.041	1.029	0.9886	0.9161	0.8063	0.6552	0.4431	0.2697	0.1416	0.0424

Table A.5: Weighting factors for m_{E5}

β \ λ	1	0.944	0.889	0.833	0.778	0.722	0.667	0.611	0.556	0.5
0.0001	0.02476	0.02824	0.04041	0.06281	0.09791	0.1485	0.2193	0.3176	0.4533	0.6415
0.0001334	0.02894	0.03237	0.04454	0.06727	0.1022	0.1529	0.2241	0.3221	0.4578	0.6461
0.0001778	0.03347	0.03725	0.04949	0.07233	0.1074	0.1583	0.2295	0.3278	0.4632	0.6515
0.0002371	0.03926	0.04304	0.05574	0.07794	0.1133	0.1646	0.236	0.3342	0.4697	0.658
0.0003162	0.0461	0.04991	0.06253	0.08496	0.1206	0.172	0.2437	0.342	0.4779	0.6657
0.0004217	0.05463	0.05845	0.07052	0.09385	0.1295	0.1807	0.2529	0.3516	0.4867	0.6759
0.0005623	0.06433	0.06792	0.08076	0.1033	0.1398	0.1916	0.2638	0.363	0.4985	0.6861
0.0007499	0.07561	0.07971	0.0925	0.1158	0.1515	0.2043	0.277	0.3766	0.5126	0.7004
0.001	0.09009	0.09009	0.1067	0.1302	0.1668	0.2193	0.2925	0.3929	0.5293	0.7157
0.001334	0.1068	0.1109	0.1238	0.1474	0.1823	0.2374	0.3112	0.4122	0.5495	0.7364
0.001778	0.1254	0.1293	0.1424	0.1663	0.2038	0.2587	0.3334	0.4358	0.5737	0.7612
0.002371	0.1594	0.1594	0.1641	0.1884	0.2262	0.2812	0.3573	0.4605	0.6009	0.7906
0.003162	0.2148	0.2103	0.1954	0.2145	0.2529	0.308	0.3845	0.489	0.6304	0.822
0.004217	0.1092	0.119	0.1605	0.2404	0.284	0.3395	0.4167	0.5218	0.664	0.8561
0.005623	0.1365	0.1557	0.1919	0.2383	0.3151	0.3766	0.4545	0.5602	0.7032	0.8953
0.007499	0.1512	0.1608	0.1957	0.2589	0.3309	0.4034	0.4988	0.6055	0.7487	0.9407
0.01	0.1916	0.2024	0.2374	0.2936	0.3459	0.4204	0.5225	0.6572	0.8006	0.9919
0.01334	0.2308	0.2415	0.2727	0.3081	0.362	0.4387	0.5428	0.681	0.8585	1.048
0.01778	0.2594	0.27	0.2903	0.327	0.3829	0.4613	0.5669	0.7058	0.8865	1.107
0.02371	0.2723	0.2826	0.3158	0.359	0.4151	0.4937	0.599	0.7368	0.9145	1.143
0.03162	0.2899	0.2997	0.3316	0.389	0.4597	0.5367	0.6398	0.7741	0.9463	1.165
0.04217	0.3313	0.3406	0.3704	0.4241	0.5048	0.5796	0.6794	0.8085	0.9726	1.179
0.05623	0.4041	0.4127	0.4402	0.4874	0.5391	0.6112	0.7066	0.8293	0.9837	1.176
0.07499	0.4484	0.454	0.4719	0.5041	0.553	0.6208	0.7102	0.8244	0.9668	1.142
0.1	0.4523	0.4572	0.4736	0.5027	0.5468	0.6081	0.6886	0.7909	0.9175	1.072
0.1334	0.4575	0.4618	0.4755	0.5003	0.5376	0.5891	0.6567	0.7422	0.8475	0.9747
0.1778	0.4894	0.493	0.5033	0.5222	0.5506	0.5898	0.6408	0.7048	0.7829	0.8765
0.2371	0.5597	0.562	0.5693	0.5825	0.602	0.6284	0.6622	0.6995	0.742	0.7923
0.3162	0.6444	0.6456	0.6493	0.6494	0.6652	0.6772	0.6915	0.7077	0.7254	0.7445
0.4217	0.7112	0.7222	0.7338	0.7431	0.752	0.7561	0.7586	0.7577	0.7513	0.734
0.5623	0.6604	0.6675	0.6902	0.731	0.8094	0.8513	0.8665	0.858	0.8365	0.7915
0.7499	0.7154	0.7223	0.7455	0.7873	0.8507	0.9193	0.9429	0.9607	0.9578	0.9121
1	0.9411	0.9433	0.9502	0.9635	0.9851	1.018	1.072	1.078	1.051	1.026

Table A.6: Weighting factors for m_{E6}

β \ λ	1	0.944	0.889	0.833	0.778	0.722	0.667	0.611	0.556	0.5
0.0001	0.07432	0.08478	0.1214	0.1888	0.2943	0.4464	0.6592	0.9548	1.363	1.928
0.0001334	0.08687	0.09719	0.1338	0.2021	0.3071	0.4597	0.6735	0.9682	1.376	1.942
0.0001778	0.1005	0.1118	0.1487	0.2173	0.3228	0.4757	0.69	0.9855	1.393	1.958
0.0002371	0.1179	0.1292	0.1674	0.2342	0.3406	0.4947	0.7096	1.005	1.412	1.978
0.0003162	0.1384	0.1498	0.1878	0.2552	0.3624	0.517	0.7326	1.028	1.437	2.001
0.0004217	0.164	0.1755	0.2117	0.2819	0.3891	0.5429	0.7601	1.057	1.463	2.031
0.0005623	0.1931	0.2039	0.2425	0.3103	0.4201	0.5758	0.7929	1.091	1.498	2.062
0.0007499	0.2269	0.2393	0.2777	0.3477	0.455	0.614	0.8324	1.132	1.541	2.105
0.001	0.2704	0.2704	0.3204	0.3908	0.501	0.6588	0.879	1.181	1.591	2.151
0.001334	0.3205	0.3329	0.3717	0.4426	0.5474	0.7133	0.9351	1.239	1.651	2.213
0.001778	0.3761	0.388	0.4274	0.4991	0.6118	0.7771	1.002	1.31	1.724	2.287
0.002371	0.34	0.34	0.4924	0.5654	0.6791	0.8445	1.073	1.383	1.805	2.376
0.003162	0.1809	0.262	0.5267	0.6438	0.759	0.9249	1.155	1.469	1.894	2.47
0.004217	0.3275	0.3569	0.4816	0.7212	0.8522	1.019	1.251	1.567	1.995	2.572
0.005623	0.4094	0.4672	0.5758	0.7149	0.9455	1.13	1.364	1.682	2.112	2.689
0.007499	0.4536	0.4825	0.5871	0.7768	0.9928	1.211	1.497	1.818	2.248	2.825
0.01	0.5749	0.6073	0.7122	0.881	1.038	1.262	1.568	1.973	2.404	2.979
0.01334	0.6924	0.7246	0.818	0.9244	1.086	1.317	1.629	2.044	2.577	3.148
0.01778	0.7783	0.8099	0.871	0.9812	1.149	1.385	1.702	2.119	2.661	3.322
0.02371	0.8169	0.8478	0.9475	1.077	1.246	1.482	1.798	2.212	2.745	3.43
0.03162	0.87	0.8994	0.995	1.167	1.379	1.611	1.921	2.324	2.841	3.498
0.04217	0.9942	1.022	1.111	1.273	1.515	1.74	2.039	2.427	2.92	3.54
0.05623	1.213	1.238	1.321	1.463	1.618	1.835	2.122	2.49	2.954	3.53
0.07499	1.346	1.363	1.416	1.514	1.66	1.864	2.133	2.476	2.904	3.43
0.1	1.359	1.373	1.423	1.511	1.643	1.828	2.07	2.378	2.759	3.222
0.1334	1.377	1.39	1.431	1.506	1.619	1.774	1.978	2.236	2.553	2.936
0.1778	1.477	1.488	1.519	1.576	1.663	1.782	1.936	2.13	2.367	2.65
0.2371	1.693	1.7	1.723	1.764	1.824	1.906	2.011	2.127	2.258	2.412
0.3162	1.951	1.955	1.968	1.968	2.023	2.065	2.114	2.171	2.231	2.297
0.4217	2.156	2.189	2.225	2.258	2.292	2.317	2.338	2.351	2.348	2.311
0.5623	2.047	2.068	2.136	2.258	2.49	2.625	2.694	2.701	2.67	2.567
0.7499	2.298	2.318	2.385	2.505	2.687	2.892	2.993	3.085	3.131	3.056
1	2.827	2.839	2.876	2.944	3.045	3.182	3.369	3.508	3.579	3.589

A.2 Parameters for m_{Gi}

This section contains the parameters for the $G(s)$ transfer function used within the TLM structure.

Table A.7: Weighting factors for m_{G1}

β \ λ	1	0.944	0.889	0.833	0.778	0.722	0.667	0.611	0.556	0.5
0.0001	0.007988	0.007567	0.007384	0.007332	0.004772	0.00219	5.429e-05	1.305e-06	4.044e-07	2.089e-07
0.0001334	0.009372	0.008728	0.008543	0.007386	0.00838	0.003211	0.003206	1.811e-05	2.431e-06	1.141e-06
0.0001778	0.0101	0.01006	0.009867	0.00915	0.007447	0.005007	0.004854	1.24e-06	6.317e-07	2.547e-07
0.0002371	0.01164	0.01158	0.01206	0.01119	0.009506	0.007042	0.006697	0.002399	9.551e-07	1.466e-06
0.0003162	0.01336	0.01331	0.01354	0.01286	0.01181	0.009333	0.008714	0.001282	3.615e-06	3.537e-07
0.0004217	0.01527	0.01528	0.01508	0.01544	0.01442	0.01398	0.008413	0.003735	0.0007823	3.232e-07
0.0005623	0.01723	0.0175	0.0173	0.01694	0.01728	0.01471	0.0134	0.006441	0.003206	6.845e-07
0.0007499	0.02002	0.01998	0.0195	0.0196	0.01928	0.01779	0.0142	0.009383	0.005826	6.199e-07
0.001	0.02196	0.02196	0.02195	0.02204	0.02221	0.02193	0.01882	0.01252	0.006002	0.0002755
0.001334	0.02512	0.02576	0.02495	0.02474	0.02482	0.02483	0.02079	0.01714	0.009162	0.002983
0.001778	0.02855	0.02902	0.02837	0.02843	0.02815	0.02801	0.02449	0.01914	0.01237	0.005454
0.002371	0.03257	0.03257	0.03206	0.03183	0.03147	0.03118	0.02763	0.02243	0.01612	0.007693
0.003162	0.03615	0.03611	0.036	0.03576	0.03539	0.03401	0.03084	0.02552	0.01845	0.009071
0.004217	0.0402	0.03993	0.03976	0.03897	0.03744	0.03527	0.03232	0.02799	0.02103	0.01144
0.005623	0.04116	0.04098	0.04045	0.03951	0.03796	0.0359	0.03309	0.0277	0.02234	0.01323
0.007499	0.04074	0.04052	0.0399	0.03879	0.03739	0.03567	0.0331	0.02909	0.02267	0.0133
0.01	0.03837	0.03818	0.03755	0.03653	0.03553	0.03399	0.0317	0.02828	0.02246	0.01274
0.01334	0.034	0.03381	0.03329	0.03293	0.03222	0.03103	0.02909	0.02606	0.02128	0.01199
0.01778	0.02807	0.02791	0.02803	0.02812	0.02799	0.0274	0.02605	0.02353	0.01931	0.01066
0.02371	0.02587	0.02572	0.02525	0.02531	0.02565	0.02559	0.02476	0.02268	0.01878	0.01219
0.03162	0.03287	0.03267	0.03209	0.03104	0.0303	0.03014	0.02922	0.02705	0.02299	0.01611
0.04217	0.04794	0.04773	0.04708	0.04588	0.04403	0.04349	0.04212	0.03942	0.03473	0.02711
0.05623	0.06807	0.06787	0.06723	0.0662	0.06586	0.06498	0.0632	0.06001	0.05474	0.04643
0.07499	0.09282	0.09281	0.09278	0.09264	0.09222	0.09128	0.08945	0.08623	0.08096	0.07264
0.1	0.1191	0.119	0.1191	0.119	0.1188	0.1181	0.1167	0.1141	0.1096	0.1023
0.1334	0.1421	0.1422	0.1423	0.1425	0.1426	0.1424	0.1418	0.1402	0.137	0.1316
0.1778	0.1613	0.1615	0.1617	0.162	0.1625	0.1629	0.1629	0.1624	0.1608	0.1574
0.2371	0.1776	0.1777	0.178	0.1785	0.1791	0.1798	0.1804	0.1804	0.1797	0.178
0.3162	0.1899	0.19	0.1902	0.1899	0.1909	0.1913	0.1918	0.1921	0.1921	0.1916
0.4217	0.2079	0.2079	0.2072	0.2055	0.204	0.2038	0.2034	0.2029	0.2021	0.2022
0.5623	0.227	0.2268	0.2258	0.2241	0.2241	0.2202	0.219	0.2171	0.2144	0.2143
0.7499	0.237	0.2369	0.2369	0.237	0.2371	0.2354	0.2277	0.2213	0.2202	0.2268
1	0.2495	0.2492	0.2484	0.2467	0.2436	0.2387	0.2343	0.2279	0.2136	0.2091

Table A.8: Weighting factors for m_{G2}

β \ λ	1	0.944	0.889	0.833	0.778	0.722	0.667	0.611	0.556	0.5
0.0001	2.956e-05	6.074e-06	5.027e-06	1.099e-05	0.01256	0.02195	0.03194	0.02944	0.03761	0.04912
0.0001334	0.000215	5.386e-06	2.783e-05	0.007336	0.0002101	0.02235	0.01826	0.03139	0.03963	0.0512
0.0001778	2.35e-05	4.793e-06	3.934e-06	0.005463	0.01154	0.0203	0.01688	0.04218	0.04195	0.0536
0.0002371	3.406e-06	4.287e-06	3.06e-05	4.296e-06	0.009189	0.01802	0.01546	0.03087	0.04461	0.05634
0.0003162	1.525e-05	3.86e-06	0.0001845	3.593e-06	0.006672	0.01553	0.01422	0.04481	0.056	0.05948
0.0004217	2.989e-06	4.025e-06	2.868e-06	1.141e-05	0.003843	0.00257	0.02538	0.04244	0.04949	0.07121
0.0005623	1.116e-05	3.228e-06	2.91e-06	2.763e-06	0.0009482	0.01005	0.01192	0.03997	0.04824	0.06716
0.0007499	5.944e-05	3.03e-06	1.088e-05	3.231e-06	2.047e-05	0.007209	0.02004	0.03751	0.04717	0.08004
0.001	1.515e-06	1.515e-06	1.741e-06	2.373e-06	5.49e-06	5.116e-05	0.01067	0.0352	0.05916	0.07724
0.001334	7.954e-06	2.931e-06	1.697e-06	1.906e-06	0.0004474	0.0002237	0.01529	0.02662	0.05755	0.07754
0.001778	1.773e-06	3.123e-06	1.912e-06	2.743e-06	4.043e-06	0.0002319	0.01225	0.03186	0.05657	0.07979
0.002371	2.912e-06	2.912e-06	1.216e-05	2.862e-06	3.962e-06	0.0001222	0.01272	0.03111	0.05327	0.08371
0.003162	1.748e-05	2.273e-05	4.214e-06	5.814e-06	1.439e-05	0.003287	0.01306	0.03201	0.05764	0.09243
0.004217	2.38e-05	2.005e-05	2.377e-05	0.003366	0.007663	0.01379	0.02216	0.03563	0.06038	0.09584
0.005623	0.01147	0.01197	0.01358	0.01653	0.02127	0.027	0.03423	0.05182	0.06886	0.1015
0.007499	0.02746	0.02819	0.0298	0.03271	0.03667	0.042	0.04969	0.06055	0.08147	0.1147
0.01	0.04621	0.04674	0.04847	0.0514	0.05496	0.06034	0.06823	0.07973	0.09657	0.1306
0.01334	0.06826	0.06883	0.0705	0.0726	0.07611	0.08145	0.08941	0.1011	0.1184	0.1486
0.01778	0.09244	0.09303	0.09395	0.09579	0.09897	0.1041	0.112	0.1238	0.1415	0.1731
0.02371	0.1124	0.1131	0.1151	0.1174	0.1204	0.1255	0.1335	0.1457	0.164	0.1914
0.03162	0.1227	0.1235	0.1258	0.13	0.1351	0.1408	0.1497	0.1629	0.1825	0.2114
0.04217	0.1268	0.1276	0.1301	0.1348	0.1419	0.1487	0.1587	0.1734	0.1946	0.2253
0.05623	0.1324	0.1332	0.1359	0.1404	0.1454	0.1529	0.164	0.1797	0.2021	0.2339
0.07499	0.1438	0.1443	0.146	0.1492	0.1544	0.1621	0.1732	0.1889	0.2109	0.2421
0.1	0.1685	0.169	0.1705	0.1734	0.1781	0.1851	0.1951	0.2093	0.2292	0.2572
0.1334	0.2148	0.2151	0.2164	0.2187	0.2224	0.2279	0.2359	0.2473	0.2634	0.2863
0.1778	0.2815	0.2817	0.2826	0.2842	0.2868	0.2907	0.2964	0.3046	0.3163	0.333
0.2371	0.3669	0.3669	0.3671	0.3674	0.368	0.3692	0.3711	0.3727	0.3758	0.3817
0.3162	0.4462	0.446	0.4453	0.444	0.4425	0.4406	0.4387	0.4373	0.4371	0.4392
0.4217	0.5164	0.5162	0.5162	0.5167	0.5161	0.5134	0.5105	0.5075	0.5052	0.5029
0.5623	0.563	0.5635	0.5652	0.5683	0.568	0.5757	0.5791	0.5758	0.5724	0.5664
0.7499	0.6015	0.6015	0.6011	0.6004	0.5993	0.6014	0.6156	0.6285	0.633	0.6247
1	0.6694	0.669	0.6678	0.6662	0.6648	0.6649	0.6643	0.6652	0.6784	0.6888

Table A.9: Weighting factors for m_{G3}

β \ λ	1	0.944	0.889	0.833	0.778	0.722	0.667	0.611	0.556	0.5
0.0001	1.789e-05	0.004732	0.01073	0.01686	9.025e-06	1.189e-05	0.001859	0.0366	0.04798	0.0622
0.0001334	3.009e-05	0.005283	0.01113	8.929e-05	0.02635	0.001265	0.03346	0.03762	0.04888	0.06294
0.0001778	0.004205	0.005992	0.01205	0.004624	0.005201	0.006009	0.0368	0.01363	0.04994	0.0638
0.0002371	0.005041	0.00691	0.009016	0.02147	0.01072	0.01142	0.0404	0.04368	0.05118	0.06481
0.0003162	0.006279	0.008098	0.01266	0.02361	0.01693	0.01757	0.04389	0.01914	0.02879	0.06602
0.0004217	0.01437	0.01507	0.01571	0.02144	0.0241	0.04341	0.02503	0.02559	0.05522	0.04514
0.0005623	0.01961	0.01172	0.02257	0.02873	0.03206	0.03232	0.05194	0.03285	0.06002	0.06909
0.0007499	0.01265	0.01445	0.02869	0.03277	0.04124	0.04105	0.04105	0.04094	0.06533	0.04902
0.001	0.03207	0.03207	0.03595	0.03997	0.04616	0.05739	0.06122	0.04988	0.04888	0.07163
0.001334	0.03449	0.02289	0.04047	0.04841	0.04998	0.06256	0.06061	0.06959	0.05804	0.07707
0.001778	0.03798	0.02928	0.0439	0.04604	0.05796	0.07284	0.0711	0.07032	0.06797	0.08042
0.002371	0.03584	0.03584	0.04862	0.05683	0.0695	0.08448	0.08402	0.07841	0.08093	0.08296
0.003162	0.04928	0.05061	0.055	0.06309	0.0756	0.08855	0.09706	0.09417	0.09001	0.08378
0.004217	0.05807	0.06237	0.06792	0.06634	0.07223	0.08064	0.09307	0.1045	0.1021	0.09439
0.005623	0.05268	0.05323	0.05492	0.05795	0.06253	0.07228	0.08862	0.09014	0.1072	0.1049
0.007499	0.04514	0.04498	0.04721	0.05138	0.05835	0.06829	0.08208	0.1013	0.1091	0.1055
0.01	0.04405	0.04461	0.04643	0.04997	0.05622	0.06501	0.07667	0.09157	0.1112	0.1058
0.01334	0.04618	0.04658	0.04803	0.05143	0.0565	0.06374	0.07338	0.08555	0.1004	0.1063
0.01778	0.05307	0.05329	0.05462	0.05707	0.06088	0.06631	0.0736	0.08284	0.09367	0.09166
0.02371	0.06687	0.06688	0.06693	0.06804	0.07033	0.07363	0.07809	0.08374	0.09021	0.09623
0.03162	0.08808	0.08787	0.08726	0.08623	0.08586	0.08683	0.08818	0.08988	0.09151	0.09181
0.04217	0.113	0.1126	0.1114	0.1093	0.1063	0.1048	0.103	0.1007	0.0977	0.09271
0.05623	0.1334	0.1329	0.1312	0.1284	0.1255	0.1218	0.117	0.1112	0.104	0.09447
0.07499	0.1437	0.1432	0.1417	0.1389	0.1348	0.1294	0.1225	0.1142	0.1042	0.09183
0.1	0.1375	0.1369	0.1351	0.1319	0.1271	0.1208	0.1128	0.1033	0.09204	0.07884
0.1334	0.1114	0.1108	0.1088	0.1054	0.1003	0.09359	0.0852	0.07531	0.06413	0.05176
0.1778	0.0723	0.07144	0.06954	0.06588	0.06047	0.05331	0.04449	0.0343	0.02326	0.01204
0.2371	0.01698	0.01662	0.01545	0.01342	0.0105	0.006813	0.002545	0.001092	8.691e-05	1.054e-05
0.3162	3.852e-07	3.751e-07	6.923e-08	6.927e-08	6.498e-06	1.093e-06	9.21e-07	3.187e-08	1.392e-07	2.574e-06
0.4217	2.187e-06	4.271e-07	1.595e-06	1.039e-06	3.636e-08	5.543e-07	4.302e-07	3.438e-09	5.715e-08	1.263e-06
0.5623	0.03779	0.03694	0.03419	0.02925	0.02603	0.01374	0.001255	5.333e-07	2.458e-07	8.593e-09
0.7499	0.09059	0.09007	0.08876	0.08641	0.08294	0.07543	0.05604	0.03434	0.01488	0.0006762
1	0.06342	0.06377	0.06484	0.06642	0.06799	0.06855	0.06735	0.06445	0.05394	0.0289

Table A.10: Weighting factors for m_{G4}

β \ λ	1	0.944	0.889	0.833	0.778	0.722	0.667	0.611	0.556	0.5
0.0001	7.211e-06	0.01314	0.002403	4.168e-05	1.355e-06	1.241e-06	2.777e-05	2.33e-06	1.265e-06	7.795e-07
0.0001334	1.902e-06	0.01581	0.005574	1.734e-06	1.285e-05	1.392e-06	2.488e-05	1.661e-05	6.786e-06	4.065e-06
0.0001778	0.02179	0.01876	0.007779	1.838e-06	1.652e-06	1.44e-06	2.564e-05	9.645e-07	1.483e-06	8.559e-07
0.0002371	0.02536	0.02196	2.145e-06	6.321e-05	4.32e-05	1.501e-06	5.261e-06	1.627e-05	1.661e-06	4.556e-06
0.0003162	0.02859	0.02541	6.201e-05	9.974e-05	4.593e-05	7.898e-06	5.227e-06	1.078e-06	4.02e-06	9.861e-07
0.0004217	3.691e-06	4.388e-06	0.01804	2.41e-06	1.985e-06	0.0001949	1.393e-06	1.126e-06	2.217e-06	6.142e-07
0.0005623	2.675e-05	0.03269	4.047e-06	0.001982	2.198e-06	1.835e-06	5.164e-06	1.189e-06	2.303e-06	1.24e-06
0.0007499	0.03929	0.03631	3.291e-05	4.203e-06	0.0001067	2.057e-06	1.636e-06	1.278e-06	2.425e-06	6.979e-07
0.001	0.002014	0.002014	2.342e-05	7.682e-06	3.743e-06	8.005e-06	5.176e-06	1.406e-06	1.059e-06	1.616e-06
0.001334	0.01419	0.0423	0.00799	0.000119	0.003154	4.122e-05	5.538e-05	3.562e-06	1.169e-06	1.724e-06
0.001778	0.02735	0.04399	0.02115	0.01359	2.982e-05	4.69e-06	5.405e-06	1.952e-06	1.341e-06	1.755e-06
0.002371	0.04765	0.04765	0.03535	0.02669	0.01331	7.761e-05	4.931e-06	3.739e-06	1.274e-06	1.777e-06
0.003162	0.0569	0.05541	0.05054	0.04185	0.02847	0.01296	3.307e-05	4.922e-06	1.144e-06	1.328e-06
0.004217	0.07296	0.03957	0.0292	0.06149	0.05247	0.04021	0.02037	2.277e-05	4.497e-06	1.853e-06
0.005623	0.1015	0.1005	0.09742	0.09204	0.08374	0.06661	0.03618	0.0001275	8.064e-06	1.758e-05
0.007499	0.1314	0.1318	0.1267	0.1171	0.1025	0.08291	0.05551	0.01798	6.764e-05	4.323e-06
0.01	0.1459	0.1444	0.1397	0.1311	0.1181	0.09969	0.07479	0.04219	0.0001506	6.127e-06
0.01334	0.1573	0.156	0.1518	0.144	0.1323	0.1155	0.0927	0.06292	0.02484	1.194e-05
0.01778	0.1663	0.1652	0.1615	0.1547	0.1442	0.1291	0.1085	0.08145	0.04704	3.782e-06
0.02371	0.1724	0.1714	0.1684	0.1626	0.1537	0.1408	0.1232	0.09981	0.06977	0.0326
0.03162	0.1749	0.1742	0.1717	0.1672	0.1599	0.1493	0.1346	0.115	0.08965	0.05805
0.04217	0.1758	0.1752	0.1733	0.1696	0.1639	0.1552	0.1431	0.1268	0.1052	0.0779
0.05623	0.1801	0.1796	0.1781	0.1752	0.1705	0.1635	0.1536	0.1399	0.1217	0.09803
0.07499	0.1921	0.1917	0.1904	0.188	0.1842	0.1783	0.1699	0.1581	0.142	0.1205
0.1	0.2127	0.2123	0.2112	0.2091	0.2058	0.2007	0.1932	0.1824	0.1674	0.1468
0.1334	0.2364	0.2362	0.2353	0.2335	0.2307	0.2263	0.2197	0.2099	0.1957	0.1757
0.1778	0.2518	0.2521	0.2511	0.25	0.248	0.2448	0.2397	0.2317	0.2193	0.2008
0.2371	0.2729	0.2724	0.2707	0.2675	0.2623	0.2544	0.243	0.2275	0.2086	0.1832
0.3162	0.2469	0.2464	0.2445	0.2443	0.2355	0.2273	0.2157	0.1996	0.1776	0.1482
0.4217	0.1915	0.1909	0.1894	0.1866	0.1826	0.1771	0.1688	0.1567	0.1393	0.1153
0.5623	0.1086	0.1087	0.109	0.1094	0.1076	0.1097	0.1116	0.1051	0.09329	0.07616
0.7499	0.025	0.02516	0.0255	0.026	0.02643	0.02799	0.03457	0.04069	0.04378	0.04197
1	1.419e-07	5.799e-09	6.239e-09	7.135e-09	1.766e-09	2.424e-09	8.952e-08	1.755e-07	8.768e-08	0.00423

Table A.11: Weighting factors for m_{G5}

β \ λ	1	0.944	0.889	0.833	0.778	0.722	0.667	0.611	0.556	0.5
0.0001	8.831e-06	0.01572	0.03119	0.02548	1.669e-06	1.587e-06	3.695e-05	8.119e-06	3.22e-06	1.773e-06
0.0001334	1.963e-06	0.01625	0.03043	1.876e-06	0.01571	1.684e-06	0.0005658	7.773e-05	1.875e-05	9.624e-06
0.0001778	0.01285	0.017	0.03284	1.956e-06	1.861e-06	1.74e-06	0.001169	1.393e-06	4.649e-06	2.137e-06
0.0002371	0.01319	0.01817	2.134e-06	0.04485	4.851e-05	1.81e-06	0.003117	0.0002671	6.439e-06	1.225e-05
0.0003162	0.01546	0.01985	5.793e-05	0.05301	5.115e-05	9.505e-06	0.008644	1.537e-06	6.401e-06	2.963e-06
0.0004217	2.74e-06	3.375e-06	0.03802	2.374e-06	2.187e-06	0.02758	1.827e-06	1.615e-06	3.255e-05	1.082e-06
0.0005623	1.59e-05	0.02605	2.959e-06	0.0691	2.383e-06	2.186e-06	0.02342	1.719e-06	5.166e-05	6.226e-06
0.0007499	0.02724	0.03103	1.788e-05	3.193e-06	0.06805	2.425e-06	2.151e-06	1.864e-06	0.000192	1.242e-06
0.001	5.06e-06	5.06e-06	4.726e-06	4.071e-06	3.342e-06	0.05808	0.04483	2.075e-06	1.727e-06	3.505e-05
0.001334	2.738e-05	0.04738	5.732e-06	5.973e-06	0.0878	0.07211	7.261e-05	0.04295	1.953e-06	0.000197
0.001778	6.116e-06	0.05981	6.443e-06	0.1005	0.1096	4.773e-06	0.07561	2.998e-06	2.326e-06	0.01405
0.002371	0.0716	0.0716	3.835e-05	8.467e-06	1.008e-05	4.746e-05	6.176e-06	0.07925	0.05877	0.03345
0.003162	4.667e-05	5.952e-05	1.021e-05	1.173e-05	1.525e-05	2.322e-05	2.682e-05	9.182e-06	2.438e-05	3.001e-06
0.004217	1.523e-05	0.1214	0.1342	0.0001019	0.0006579	5.12e-05	0.005046	0.01134	1.945e-05	5.528e-06
0.005623	2.978e-05	3.108e-05	3.577e-05	4.867e-05	0.0001135	0.00793	0.02993	0.1559	0.03065	0.002083
0.007499	0.006245	0.004175	0.007681	0.01443	0.02455	0.03688	0.05485	0.07989	0.07651	0.04649
0.01	0.04122	0.04214	0.04516	0.05052	0.05796	0.06857	0.08305	0.1023	0.1264	0.09585
0.01334	0.08238	0.08318	0.08567	0.08983	0.09588	0.1048	0.117	0.1332	0.1542	0.1535
0.01778	0.1259	0.1266	0.1283	0.1317	0.1369	0.1443	0.1547	0.1686	0.1866	0.265
0.02371	0.1696	0.17	0.1715	0.1737	0.177	0.1817	0.1884	0.1977	0.21	0.2259
0.03162	0.2117	0.2119	0.2127	0.2142	0.2161	0.2183	0.2215	0.2263	0.2328	0.2416
0.04217	0.2487	0.2488	0.2492	0.2499	0.2511	0.2518	0.2529	0.2549	0.2582	0.263
0.05623	0.2752	0.2752	0.2753	0.2754	0.275	0.2745	0.274	0.2739	0.2744	0.2757
0.07499	0.2846	0.2845	0.2842	0.2838	0.2831	0.2822	0.2813	0.2803	0.2795	0.2791
0.1	0.2755	0.2755	0.2753	0.2751	0.2748	0.2744	0.2738	0.2733	0.2729	0.2728
0.1334	0.2533	0.2533	0.2534	0.2535	0.2537	0.254	0.2544	0.255	0.2558	0.257
0.1778	0.2263	0.2258	0.2265	0.2271	0.2278	0.2288	0.23	0.2316	0.2336	0.2362
0.2371	0.1656	0.1664	0.1688	0.1732	0.1801	0.1898	0.2029	0.2147	0.224	0.2345
0.3162	0.1169	0.1177	0.12	0.1201	0.1312	0.1408	0.1538	0.171	0.1932	0.221
0.4217	0.08422	0.085	0.08726	0.09125	0.09729	0.1057	0.1173	0.1329	0.1534	0.1796
0.5623	0.06355	0.06406	0.06575	0.06887	0.07436	0.08065	0.08902	0.102	0.1199	0.1431
0.7499	0.04596	0.04635	0.0477	0.05021	0.05421	0.05973	0.06606	0.07517	0.08814	0.1059
1	0.01773	0.01802	0.01897	0.02073	0.02357	0.02784	0.03403	0.04243	0.05406	0.06896

Table A.12: Weighting factors for m_{G6}

β \ λ	0.5	0.556	0.611	0.667	0.722	0.778	0.833	0.889	0.944	1
0.0001	6.54e-06	1.202e-05	3.216e-05	0.9661	0.9758	0.9827	0.01976	0.01529	0.03932	0.9919
0.0001334	3.584e-05	7.142e-05	0.0003395	0.01937	0.9732	0.03693	0.9852	0.02608	0.04766	0.9904
0.0001778	8.073e-06	1.835e-05	0.9442	0.03422	0.9687	0.9758	0.9808	0.03249	0.05713	0.06369
0.0002371	4.73e-05	2.736e-05	0.01391	0.04809	0.9635	0.9705	0.02391	0.9789	0.06745	0.0752
0.0003162	1.185e-05	0.9152	0.9348	0.05564	0.9575	0.9645	0.02584	0.9735	0.07867	0.08564
0.0004217	0.8836	0.009171	0.9282	0.9412	0.06396	0.9576	0.9631	0.0662	0.9696	0.9703
0.0005623	3.261e-05	0.0381	0.9207	0.07103	0.9429	0.9497	0.03601	0.9601	0.103	0.9631
0.0007499	0.8709	0.07113	0.9122	0.9247	0.934	0.05296	0.9476	0.9517	0.1159	0.122
0.001	0.04762	0.886	0.9024	0.08568	0.08308	0.9316	0.938	0.9421	0.944	0.9439
0.001334	0.09119	0.8752	0.09313	0.9032	0.08882	0.07684	0.9267	0.9266	0.1402	0.9262
0.001778	0.1055	0.8631	0.8787	0.09622	0.8989	0.06998	0.08722	0.9066	0.1507	0.9061
0.002371	0.1111	0.1056	0.1016	0.8756	0.8841	0.8857	0.8846	0.8839	0.1659	0.1659
0.003162	0.8147	0.8339	0.8483	0.859	0.8612	0.8605	0.8593	0.8584	0.8578	0.8576
0.004217	0.7983	0.8165	0.8205	0.827	0.83	0.8295	0.8297	0.1454	0.1654	0.8287
0.005623	0.7782	0.771	0.09793	0.7779	0.7903	0.7944	0.7939	0.7936	0.7933	0.7932
0.007499	0.72	0.7102	0.7112	0.7248	0.7343	0.7405	0.7455	0.7487	0.7504	0.7491
0.01	0.655	0.6432	0.656	0.6656	0.6724	0.6772	0.6805	0.6827	0.6839	0.6843
0.01334	0.5797	0.5809	0.5912	0.5984	0.6035	0.607	0.6092	0.6107	0.6116	0.6118
0.01778	0.04258	0.5119	0.5197	0.5251	0.5288	0.5312	0.5327	0.5336	0.534	0.5342
0.02371	0.4417	0.4472	0.4504	0.4521	0.4528	0.453	0.4529	0.4529	0.4529	0.4529
0.03162	0.381	0.3806	0.3789	0.3768	0.3747	0.3727	0.3714	0.3705	0.37	0.3698
0.04217	0.314	0.3096	0.3047	0.3001	0.296	0.2927	0.2905	0.2889	0.2881	0.2878
0.05623	0.2515	0.2431	0.2352	0.2282	0.2224	0.2178	0.2144	0.2123	0.2111	0.2108
0.07499	0.1939	0.1824	0.1723	0.1637	0.1567	0.1514	0.1475	0.1449	0.1434	0.143
0.1	0.142	0.1289	0.1176	0.1084	0.101	0.09543	0.09142	0.08878	0.0873	0.08686
0.1334	0.0977	0.08388	0.07232	0.06301	0.05575	0.0503	0.04642	0.04388	0.04248	0.04204
0.1778	0.06061	0.04672	0.03539	0.02642	0.01955	0.01444	0.01084	0.008556	0.007527	0.006814
0.2371	0.02259	0.01184	0.003684	3.085e-06	5.364e-06	6.936e-07	5.444e-07	4.732e-07	2.202e-08	4.309e-07
0.3162	3.302e-06	7.271e-08	9.309e-09	1.716e-07	1.39e-07	5.993e-07	4.092e-09	4.055e-09	1.956e-08	1.935e-08
0.4217	5.714e-07	1.495e-08	5.48e-10	4.327e-08	3.618e-08	1.584e-09	2.898e-08	2.74e-08	5.314e-09	2.632e-08
0.5623	1.927e-09	2.548e-08	1.861e-08	7.235e-08	2.91e-09	2.492e-09	9.032e-11	2.109e-10	2.032e-09	4.017e-08
0.7499	4.363e-09	2.385e-09	3.888e-10	2.815e-10	1.104e-10	9.404e-10	8.437e-10	1.572e-08	1.512e-10	5.976e-10
1	6.591e-09	2.112e-09	3.98e-08	3.395e-08	1.368e-09	1.62e-09	1.067e-08	1.475e-08	2.013e-08	5.609e-07

A.3 Parameters for τ

This section contains the parameters for the τ parameter used within the TLM structure. This is the wave propagation time modifier.

Table A.13: Weighting factors for τ

β \ λ	0.5	0.556	0.611	0.667	0.722	0.778	0.833	0.889	0.944	1
0.0001	1.001	1.001	1.001	0.989	0.989	0.9889	1.001	1	1	0.9889
0.0001334	1.001	1.001	1.001	1.001	0.9891	1.001	0.9891	1.001	1	0.9891
0.0001778	1.001	1.001	0.9894	1.001	0.9893	0.9893	0.9893	1.001	1	1
0.0002371	1.002	1.002	1.002	1.001	0.9896	0.9895	1.001	0.9895	1.001	1
0.0003162	1.002	0.9898	0.9898	1.001	0.9898	0.9898	1.001	0.9898	1.001	1.001
0.0004217	0.99	1.002	0.9901	0.9901	1.001	0.9901	0.9901	1.001	0.9901	0.9902
0.0005623	1.002	1.002	0.9904	1.001	0.9904	0.9904	1.001	0.9905	1.001	0.9905
0.0007499	0.9907	1.002	0.9908	0.9908	0.9908	1.001	0.9909	0.9909	1.001	1.001
0.001	1.003	0.9912	0.9912	1.002	1.002	0.9913	0.9914	0.9914	0.9914	0.9914
0.001334	1.003	0.9916	0.9912	0.9918	1.002	1.002	0.9919	0.9919	1.001	0.9919
0.001778	1.003	0.9922	0.9923	1.002	0.9924	1.002	1.002	0.9924	1.002	0.9924
0.002371	1.003	1.003	1.003	0.993	0.9931	0.9931	0.993	0.993	1.002	1.002
0.003162	0.9934	0.9936	0.9937	0.9938	0.9938	0.9937	0.9937	0.9937	0.9937	0.9937
0.004217	0.9942	0.9944	0.9945	0.9945	0.9945	0.9945	0.9945	1.003	1.003	0.9944
0.005623	0.9952	0.9951	1.004	0.9952	0.9953	0.9953	0.9953	0.9953	0.9953	0.9953
0.007499	0.9958	0.9958	0.9958	0.9959	0.996	0.9961	0.9962	0.9962	0.9962	0.9962
0.01	0.9965	0.9965	0.9966	0.9968	0.9969	0.997	0.997	0.9971	0.9971	0.9971
0.01334	0.997	0.9972	0.9974	0.9976	0.9978	0.9979	0.998	0.998	0.9981	0.9981
0.01778	1.006	0.9979	0.9983	0.9985	0.9988	0.9989	0.999	0.9991	0.9992	0.9992
0.02371	0.9986	0.9991	0.9994	0.9997	1	1	1	1	1	1
0.03162	0.9999	1	1.001	1.001	1.001	1.002	1.002	1.002	1.002	1.002
0.04217	1.001	1.002	1.002	1.003	1.003	1.003	1.003	1.003	1.003	1.003
0.05623	1.003	1.003	1.004	1.004	1.005	1.005	1.005	1.005	1.005	1.005
0.07499	1.004	1.005	1.006	1.006	1.007	1.007	1.007	1.007	1.007	1.007
0.1	1.007	1.007	1.008	1.009	1.009	1.009	1.009	1.009	1.01	1.01
0.1334	1.009	1.01	1.011	1.011	1.012	1.012	1.012	1.012	1.012	1.012
0.1778	1.012	1.013	1.014	1.014	1.015	1.015	1.015	1.016	1.016	1.016
0.2371	1.015	1.016	1.017	1.018	1.019	1.02	1.021	1.021	1.021	1.021
0.3162	1.02	1.022	1.024	1.026	1.027	1.028	1.029	1.029	1.029	1.029
0.4217	1.028	1.03	1.033	1.035	1.036	1.037	1.038	1.038	1.038	1.039
0.5623	1.037	1.041	1.044	1.046	1.048	1.049	1.05	1.05	1.051	1.051
0.7499	1.048	1.053	1.056	1.059	1.061	1.063	1.064	1.065	1.065	1.065
1	1.06	1.065	1.069	1.072	1.074	1.075	1.076	1.077	1.077	1.077

Appendix B

Tapered TLM Matlab Code

The code presented in this appendix is used to generate the TLM parameters that are collected in Appendix A. `TableGenerate.m` is the main m-file that generates and organizes the look-up tables, it calls `OptimizationsForTable.m` to perform the parameter optmizations. This script calls `ExactSolutionforOpt.m` which computes the numerical solution to the ODE, then performs the optimization using `fmincon()` of the objective function `TaperedObjectiveFunction.m`. `ExactSolutionforOpt.m` computes the transmission matrix terms in parallel calling `t11t21venderBuhsExact.m` and `t12t23venderBuhsExact.m`. Inside these scripts the differential equation `Q_odefun.m` is solved according to the boundary conditions `Q_bcfun.m` and `PQ_bcfun.m` depending on which transmission matrix terms are being solved. Back to the optimization, the objective function `TaperedObjectiveFunction.m` calls `TaperedTLMFunction.m` that computes the TLM transfer functions, then `TaperedTLM TransferMatrix.m` which takes the TLM transfer functions and computes the transmission matrix terms for comparison to the numerical ODE solution. Once the TLM parameters are fully computed, `interpolateTLMparams.m` is a look-up function that returns the TLM weighting factors for any specified tapered transmission line.

B.1   TableGenerate.m

```matlab
1  % This code will generate a 3D lookup table of wighting factors for the
2  % Tapered Transmission Line method as developed in ven der Buhs et. al
3  % (2017).
4
5  % References:
6
7  % J ven der Buhs and T Wiens. Modelling Dynamic Response of Hydraulic Fluid
        Within Tapered Transmission Lines.
8  % Proceedings of the 15th Scandinavian International Conference on Fluid
        Power, 2017
9
10
11 % Number of weighing factors used
```

```matlab
k = 6;

% Initilize counters
opt_failed = 0;
h = 1;

% Range of dissipation number (beta) (dimensionless)
beta = logspace(-4,0,33);

% Range of taper ratio (lambda) (dimensionless)
lambda = linspace(1,0.5,10);

% Preallocate parameters
mE = NaN(numel(lambda),k,numel(beta));
mG = NaN(numel(lambda),k,numel(beta));
tau = NaN(numel(lambda),numel(beta));

% Loop through the range of dissipation number
for i=1:numel(beta)
    % Loop through the range of taper ratio. Always starting at no taper
    % (i.e. lambda = 1) and moving towards larger taper.
    for j=1:numel(lambda)
            if j==1
             % Initial guess of paramters found from reference:
             % N Johnston. Simulink models, http://people.bath.ac.uk/ensdnj/
                 models/newtlm.html, 2014.
             [ni, k2, mgi, mei, deltai] = gettlmcoeffs(beta(i), 6);

             % Assign initial parameters to vector params
              params = [mei mgi deltai];
            elseif opt_failed==1
             % If optimization failed on previos iteration, select initial
             % paramters again from Johnston et al. solution.
                 [ni, k2, mgi, mei, deltai] = gettlmcoeffs(beta(i), 6);
              params = [mei mgi deltai];
            else
             % If optimization was successful on previous iteration, use
             % paramters from previous iteration as initial guess.
              params = [mE(j-1,:,i) mG(j-1,:,i) tau(j-1,i)];

            end

            % The numerical solver will not arrive at a solution for small
            % values of dissipation number (beta) and will return an error.
            % As a result try the optimization, if an error occurs assign NaN
```

```
56              % to the paramters and try again for the next value.
57              try
58              [mE(j,:,i), mG(j,:,i), tau(j,i)] = OptimizationsForTable(lambda(j),
                    beta(i),params);
59
60              % opt_failed = 0 if the optimization/solution was successful.
61              opt_failed = 0;
62
63              catch
64              mE(j,:,i) = NaN(1,k);
65              mG(j,:,i) = NaN(1,k);
66              tau(j,i) = NaN;
67              warning(['Optimization for beta = ' num2str(beta(i)) ' and lambda =
                    ' num2str(lambda(j)) ' failed since the exact numerical
                    solution could not be found.'])
68              % opt_failed = 1 if the optimization/solution failed.
69              opt_failed = 1;
70              end
71
72              % Displays progress to the user (i.e. how many optimizations
73              % completed vs. how many in total)
74              disp([num2str(h) ' of ' num2str(numel(beta)*numel(lambda))]);
75
76              % Number of optimizations counter
77              h = h+1;
78          end
79  end
80
81  mE_lookup = permute(mE,[1 3 2]);
82  mG_lookup = permute(mG,[1 3 2]);
83  tau_lookup = tau;
```

B.2   OptimizationsForTable.m

```
1  function [ mE,mG,tau ] = OptimizationsForTable(lambda, beta, params0)
2  %[ mE, mG, tau ] = OptimizationsForTable(lambda, beta, params0)
3  % Inputs: lambda  = Taper ratio (dimensionless)
4  %         beta    = dissipation number (dimensionless)
5  %         params0 = Initial guess parameter vector of the form [ mE0, mG0,
        tau0 ]
6  %
7  % Outputs: Optimized weighting factors
8  %
```

```matlab
 9 % Note: Optimized parameters are not sensitive to the assumed radii and
10 % fluid properties since this model is linear. The optimal weighting
11 % factors only depend on dissipation number (beta) and taper ratio
12 % (lambda).
13 %
14 % Reference:
15 % J ven der Buhs and T Wiens. Modelling Dynamic Response of Hydraulic Fluid
      Within Tapered Transmission Lines.
16 % Proceedings of the 15th Scandinavian International Conference on Fluid
      Power, 2017
17
18 r1 = 20e-3; %Assume some fixed radius value (m)
19 r2 = r1*lambda; %(m)
20 nu=100e-6;%(m^2/s) kinematic viscosity
21 K=1.5e9;%(Pa) bulk modulus
22 rho=890;%(kg/m^3) density
23 c=sqrt(K/rho);%(m/s) sonic speed
24 lambda = min(r1,r2)/max(r1,r2); % Taper ratio (dimensionless)
25
26 % Assign length, L (m), based off of given dissipation number
27 L = (beta*c*max(r1,r2)^2/nu)*((9*lambda^3)/((lambda^2+lambda+1)^2));
28
29 T=L/c;% Wave propagation time (s)
30
31 k=6; %number of weighting function terms
32 n=nan(1,k);%weighting function coefficient
33 n(1)=0.3/(1+3*beta);% Equation (19)
34 for i=2:k
35     n(i)=n(i-1)*3;% Equation (19)
36 end
37 N_per_decade=50;% Number of frequency points per decade
38 omegaT_min=0.01;% Minimum omega*T for frequency points
39
40 %Log space between omegaT_min and n(end)
41 omegaT=logspace(log10(omegaT_min),log10(n(end)),round(N_per_decade*(log10(n(
      end)/T)-log10(omegaT_min/T)))));
42
43 omega=omegaT/T;%(rad/s) frequency
44
45 % Calculate exact transmission matrix using boundary value solver.
46 [ t11, t21, t12, t22 ] = ExactSolutionforOpt( omega, L, r1, r2, nu, rho, K );
47
48 fcn_min=@(params) TaperedObjectiveFunction( params, omega, L, r1, r2, nu, rho
      , K,t11,t21,t12,t22);%objective function to minimize
49 options = optimset('MaxFunEvals',500000,'MaxIter',500000);
```

```
50
51  % Ensure parameters are positive or 0 (i.e. set lower bound to 0)
52  lb = zeros(1,numel(params0));
53
54  % Perform optimization
55  params=fmincon(fcn_min,params0,[],[],[],[],lb,[],[],options);%optimize
56
57  mE = params(1:k);
58  mG = params((k+1):(2*k));
59  tau = params(end);
```

B.3   ExactSolutionforOpt.m

```
1   function [ t11, t21, t12, t22 ] = ExactSolutionforOpt( omega, L, r1, r2, nu,
        rho, K )
2   %[ t11, t21, t12, t22 ] = ExactSolutionforOpt( omega, L, r1, r2, nu, rho, K )
3   % Calculates the exact transmission matrix for a tapered pipeline using a
4   % numerical boundary value solver. NOTE: The Parallel Computing Toolbox
5   % required.
6   %
7   % Inputs: omega = freqeuncy (rad/s)
8   %              L = pipeline length (m)
9   %             r1 = inlet radius (m)
10  %             r2 = outlet radius (m)
11  %             nu = kinematic viscosity (m^2/s)
12  %            rho = density (kg/m^3)
13  %              K = bulk modulus (Pa)
14  %
15  % Outputs = Four terms of the tranmission matrix [t11, t21, t12, t22] in eq
16  % (7).
17  %
18  % Reference:
19  % J ven der Buhs and T Wiens. Modelling Dynamic Response of Hydraulic Fluid
        Within Tapered Transmission Lines.
20  % Proceedings of the 15th Scandinavian International Conference on Fluid
        Power, 2017
21
22
23
24  A = nan(numel(omega),2);
25  B = nan(numel(omega),2);
26
27  % Loop can be computed in parallel for significant time savings.
```

```matlab
if license('test', 'distrib_computing_toolbox')
    parfor i=1:2
        if i==1
        % Calculate first 2 terms of the transmission matrix
        [A(:,i), B(:,i) ] = t11t21venderBuhsExact( omega, L, r1, r2, nu, rho,
            K );

        else
        % Calculate last 2 terms of the transmission matrix
        [ A(:,i), B(:,i) ] = t12t22venderBuhsExact( omega, L, r1, r2, nu, rho
            , K );
        end
    end

else
    for i=1:2
        if i==1
        % Calculate first 2 terms of the transmission matrix
        [A(:,i), B(:,i) ] = t11t21venderBuhsExact( omega, L, r1, r2, nu, rho,
            K );

        else
        % Calculate last 2 terms of the transmission matrix
        [ A(:,i), B(:,i) ] = t12t22venderBuhsExact( omega, L, r1, r2, nu, rho
            , K );
        end
    end
end

% Outputs
t11(1,1:numel(omega)) = A(:,1);
t21(1,1:numel(omega)) = B(:,1);
t12(1,1:numel(omega)) = A(:,2);
t22(1,1:numel(omega)) = B(:,2);

end
```

B.4   t11t21venderBuhsExact.m

```matlab
function [ t11, t21 ] = t11t21venderBuhsExact( omega, L, r1, r2, nu, rho, K )
%[ t11, t21 ] = t11t21venderBuhsExact( omega, L, r1, r2, nu, rho, K )
%    Solves the boundary value problem for flow in tapered pipe and returns
%    t11 and t21 of the transmission matrix. This solver assumes a blocked
```

```matlab
 5 %   outlet with inlet flow excitation.
 6 % Inputs: omega = freqeuncy (rad/s)
 7 %            L = pipeline length (m)
 8 %           r1 = inlet radius (m)
 9 %           r2 = outlet radius (m)
10 %           nu = kinematic viscosity (m^2/s)
11 %          rho = density (kg/m^3)
12 %            K = bulk modulus (Pa)
13 %
14 % Outputs = Terms of the tranmission matrix [t11, t21 ] in eq (7).
15 %
16 % Reference:
17 % J ven der Buhs and T Wiens. Modelling Dynamic Response of Hydraulic Fluid
        Within Tapered Transmission Lines.
18 % Proceedings of the 15th Scandinavian International Conference on Fluid
        Power, 2017
19
20 %% Boundary conditions
21 Q0=1;% Flow frequency component at X=0 (Unit Input)
22 Q1=0;% Flow frequency component at X=1 (Blocked Outlet)
23
24 %% Initial guess
25 N_grid=100; % 100 points over the pipe length
26 X0=0;
27 X1=L;
28 X=linspace(X0,X1,N_grid);
29
30 y_bv0=[(Q1-Q0)/(X1-X0)*[1 1];
31      Q0 Q1];%initial guess for y at boundaries
32
33 %% Set up loop
34 P0_sol=nan(1,numel(omega));
35 P1_sol=nan(1,numel(omega));
36 Q0_sol=nan(1,numel(omega));
37 Q1_sol=nan(1,numel(omega));
38
39 for i=1:numel(omega)
40     s=1j.*omega(i);
41
42     %% set up BVP
43     odefcn=@(x,y) Q_odefun(x,y,K,nu,rho,r1,r2,L,s);
44     bcfun=@(ya,yb) Q_bcfun(ya,yb,Q0,Q1);
45     bvpinitfun=@(X) [(X-X0)/(X1-X0)*(y_bv0(1,2)-y_bv0(1,1))+y_bv0(1,1);
46         (X-X0)/(X1-X0)*(y_bv0(2,2)-y_bv0(2,1))+y_bv0(2,1)];
47     if i==1
```

```matlab
48        solinit = bvpinit(X,bvpinitfun);
49        end
50        options = bvpset('RelTol',1e-3);
51        %% solve
52        sol = bvp4c(odefcn,bcfun,solinit,options);
53
54        y=deval(sol,X);
55        dQ_dX=y(1,:);
56        Q=y(2,:);
57        solinit.x = X;
58        solinit.y = [dQ_dX;
59                        Q];
60        y_bv0=[y(:,1) y(:,end)];%update initial guess
61
62        A = pi*(r1+(r2-r1)*X/L).^2;
63        P = -dQ_dX.*K./s./A;
64
65        Q0_sol(i)=Q(1);
66        Q1_sol(i)=Q(end);
67        P0_sol(i)=P(1);
68        P1_sol(i)=P(end);
69    end
70
71    t11 = P0_sol./P1_sol;
72
73    t21 = Q0_sol./P1_sol;
```

B.5 t12t22venderBuhsExact.m

```matlab
1  function [ t12, t22 ] = t12t22venderBuhsExact( omega, L, r1, r2, nu, rho, K )
2  %[ t12, t22 ] = t12t22venderBuhsExact( omega, L, r1, r2, nu, rho, K )
3  %   Solves the boundary value problem for flow in tapered pipe and returns
4  %   t12 and t22 of the transmission matrix. This solver assumes a blocked
5  %   outlet with inlet flow excitation.
6  % Inputs: omega = freqeuncy (rad/s)
7  %             L = pipeline length (m)
8  %            r1 = inlet radius (m)
9  %            r2 = outlet radius (m)
10 %            nu = kinematic viscosity (m^2/s)
11 %           rho = density (kg/m^3)
12 %             K = bulk modulus (Pa)
13 %
14 % Outputs = Terms of the tranmission matrix [t12, t22 ] in eq (7).
```

```matlab
%
% Reference:
% J ven der Buhs and T Wiens. Modelling Dynamic Response of Hydraulic Fluid
%     Within Tapered Transmission Lines.
% Proceedings of the 15th Scandinavian International Conference on Fluid
%     Power, 2017

%% Boundary conditions
Q0=1;% Flow frequency component at X=0 (Unit Input)
P1=0;% Pressure frequency component at X=1 (Constant 0 Pressure Outlet)

%% Initial guess
N_grid=100;
X0=0;
X1=L;
X=linspace(X0,X1,N_grid);
Q1=0.5;
y_bv0=[(Q1-Q0)/(X1-X0)*[1 1];
    Q0 Q1];%initial guess for y at boundaries

%% set up loop
P0_sol=nan(1,numel(omega));
P1_sol=nan(1,numel(omega));
Q0_sol=nan(1,numel(omega));
Q1_sol=nan(1,numel(omega));
dQ_dX0_sol= nan(1,numel(omega));
dQ_dX1_sol = nan(1,numel(omega));

for i=1:numel(omega)
    s=1j.*omega(i);

    %% set up BVP
    odefcn=@(x,y) Q_odefun(x,y,K,nu,rho,r1,r2,L,s);
    bcfun=@(ya,yb) PQ_bcfun(ya,yb,Q0,P1,r1,r2,L,K,s);
    bvpinitfun=@(X) [(X-X0)/(X1-X0)*(y_bv0(1,2)-y_bv0(1,1))+y_bv0(1,1);
        (X-X0)/(X1-X0)*(y_bv0(2,2)-y_bv0(2,1))+y_bv0(2,1)];
    if i==1
    solinit = bvpinit(X,bvpinitfun);
    end
    options = bvpset('RelTol',1e-3);
    %% solve
    sol = bvp4c(odefcn,bcfun,solinit,options);

    y=deval(sol,X);
    dQ_dX=y(1,:);
```

```
58 |     Q=y(2,:);
59 |     solinit.x = X;
60 |     solinit.y = [dQ_dX;
61 |                    Q];
62 |     y_bv0=[y(:,1) y(:,end)];%update initial guess
63 |
64 |
65 |     A = pi*(r1+(r2-r1)*X/L).^2;
66 |
67 |     P = -dQ_dX.*K./s./A;
68 |
69 |     dQ_dX0_sol(i)=dQ_dX(1);
70 |     dQ_dX1_sol(i)=dQ_dX(end);
71 |     Q0_sol(i)=Q(1);
72 |     Q1_sol(i)=Q(end);
73 |     P0_sol(i)=P(1);
74 |     P1_sol(i)=P(end);
75 | end
76 |
77 | t12 = P0_sol./Q1_sol;
78 | t22 = -Q0_sol./Q1_sol;
```

B.6   ODE and Boundary Functions

```
1  | function dydx=Q_odefun(x,y,K,nu,rho,r1,r2,L,s)
2  | %dydx=Q_odefun(x,y,K,nu,rho,r1,r2,L,s)
3  | % ODE for flow in tapered pipe.
4  | %
5  | % Inputs:    x = X;
6  | %            y = [dQdx;Q]
7  | %            K = bulk modulus (Pa)
8  | %           nu = kinematic viscosity (m^2/s)
9  | %          rho = density (kg/m^3)
10 | %           r1 = inlet radius (m)
11 | %           r2 = outlet radius (m)
12 | %            L = pipeline length (m)
13 | %            s = Laplace frequency, j*omega
14 | %
15 | % Output: dydx = [d2Qdx2;dQdx]
16 | %
17 | % Reference:
18 | % J ven der Buhs and T Wiens. Modelling Dynamic Response of Hydraulic Fluid
   |     Within Tapered Transmission Lines.
```

```matlab
% Proceedings of the 15th Scandinavian International Conference on Fluid
    Power, 2017

dQdx=y(1);
Q=y(2);

r = r1+(r2-r1).*x/L;
N = -besselj(0,1j.*r.*sqrt(s./nu),1)./besselj(2,1j.*r.*sqrt(s./nu),1);

A = pi*(r1+(r2-r1)*x/L).^2;
dAdx = 2*pi*(r1+(r2-r1)*x/L)*(r2-r1)/L;
d2Qdx2 = dAdx./A.*dQdx+N.*rho.*s.^2.*Q./K;

dydx=[d2Qdx2;dQdx];
```

```matlab
function res=Q_bcfun(ya,yb,Qa,Qb)
%res=Q_bcfun(ya,yb,Qa,Qb)
% Flow boundary conditions for ODE solver
%
% Inputs: ya,yb = States at inlet and outlet
%         Qa,Qb = boundary conditions
%
% Output: res = residual
% Reference:
% J ven der Buhs and T Wiens. Modelling Dynamic Response of Hydraulic Fluid
    Within Tapered Transmission Lines.
% Proceedings of the 15th Scandinavian International Conference on Fluid
    Power, 2017

% Calculate residual, NOTE: y(2) is Q and y(1) is dQ/dx.
res=[ya(2)-Qa;
     yb(2)-Qb];
```

```matlab
function res=PQ_bcfun(ya,yb,Q0,P1,r1,r2,L,K,s)
%res=PQ_bcfun(ya,yb,Q0,P1,r1,r2,L,K,s)
% Pressure/Flow boundary conditions for ODE solver
%
% Inputs: ya,yb = States at inlet and outlet
%         Q0,P1 = boundary conditions
%          r1 = inlet radius (m)
%          r2 = outlet radius (m)
%           L = pipeline length (m)
%           K = bulk modulus (Pa)
%           s = Laplace frequency, j*omega
%
```

```
13  % Output: res = residual
14  %
15  % Reference:
16  % J ven der Buhs and T Wiens. Modelling Dynamic Response of Hydraulic Fluid
        Within Tapered Transmission Lines.
17  % Proceedings of the 15th Scandinavian International Conference on Fluid
        Power, 2017
18
19  %Outlet Pressure
20  A1 = pi*r2^2;
21  dAdx1 = 2*pi*r2*(r2-r1)/L;
22  %P_1 = -dAdx1.*K.*yb(2)./A1.^2./s-yb(1).*K./s./A1;
23  P_1 = -yb(1).*K./s./A1;
24
25  res=[ya(2)-Q0;
26      P_1-P1];
```

B.7   TaperedObjectiveFunction.m

```
1     function [ epsilon ] = ...
2       TaperedObjectiveFunction(params, omega, L, r1, r2, nu, rho, K, t11, t21,
          t12, t22)
3   %[ epsilon, t11_star, t12_star, t21_star, t22_star] =
        TaperedObjectiveFunctionErrors(params, omega, L, r1, r2, nu, rho, K, t11,
        t21, t12, t22)
4   %  Objective function for parameter optimization.
5   %
6   % Inputs: params = optmization parameters
7   %          omega = freqeuncy (rad/s)
8   %              L = pipeline length (m)
9   %             r1 = inlet radius (m)
10  %             r2 = outlet radius (m)
11  %             nu = kinematic viscosity (m^2/s)
12  %            rho = density (kg/m^3)
13  %              K = bulk modulus (Pa)
14  %t11,t21,t12,t22 = transmission matrix terms
15  %
16  % Reference:
17  % J ven der Buhs and T Wiens. Modelling Dynamic Response of Hydraulic Fluid
        Within Tapered Transmission Lines.
18  % Proceedings of the 15th Scandinavian International Conference on Fluid
        Power, 2017
19
```

```
20
21  %Extract optimization parameters from parameter vector
22  k = (numel(params)−1)/2;%number of weighting functions
23  mE = params(1:k);%coefficients for transfer function G_1
24
25  mG = params((k+1):(2*k));%coefficients for transfer function G
26
27  tau = params(end);
28
29  [ E_1, E_2, F_1, F_2, G_1, G_2, Zc_1, Zc_2, T_1, T_2 ] = TaperedTLMFunctions(
        omega, L, r1, r2, nu, rho, K, mG, mE, tau);
30
31  [ t11_star, t12_star, t21_star, t22_star ] = TaperedTLMTransferMatrix( omega,
        E_1, E_2, F_1, F_2, G_1, G_2, Zc_1, Zc_2, T_1, T_2);
32
33  c=sqrt(K/rho);%(m/s) sonic speed
34  T=L/c;%(s) transmission time
35
36  eps_12=sum((abs((t12−t12_star)/Zc_1)).^2./(omega*T));%error in T12
37  eps_21=sum((abs((t21−t21_star)*Zc_1)).^2./(omega*T));%error in T21
38  eps_11=sum(abs(t11−t11_star).^2./(omega*T));%error in T12
39  eps_22=sum(abs(t22−t22_star).^2./(omega*T));%error in T21
40
41
42  eps_E=sum(max(0, mE(3:end)−3*mE(2:(end−1))).^2);%constraint on mE. eq(26)
43  eps_G=10*max(0,sum(mG)−1).^2;%constraint on mG. eq (25)
44
45  epsilon=eps_11+eps_22+eps_12+eps_21+eps_E+eps_G;%total objective function. eq
        (24)
46
47  end
```

B.8   TaperedTLMFunctions.m

```
1  function [ E_1, E_2, F_1, F_2, G_1, G_2, Zc_1, Zc_2, T_1, T_2 ] =
        TaperedTLMFunctions( omega, L, r1, r2, nu, rho, K, mG, mE, tau)
2  %[ E_1, E_2, F_1, F_2, G_1, G_2, Zc_1, Zc_2, T_1, T_2 ] = TaperedTLMFunctions
        ( omega, L, r1, r2, nu, rho, K, mG, mE, tau)
3  %Calculates the E, F, and G transfer functions for the tapered TLM
4  %
5  % Inputs:  omega = freqeuncy (rad/s)
6  %              L = pipeline length (m)
7  %             r1 = inlet radius (m)
```

```matlab
 8  %              r2 = outlet radius (m)
 9  %              nu = kinematic viscosity (m^2/s)
10  %             rho = density (kg/m^3)
11  %               K = bulk modulus (Pa)
12  %      mG,mE,tau = parameters
13  %
14  % Outputs: Transfer functions, characteristic impedance, and wave
15  %          propagation times.
16  % NOTE: Outputs are separated to allow investigation into using separate
17  % weighiting factors, propagation times, and impedance values.
18  %
19  % Reference:
20  % J ven der Buhs and T Wiens. Modelling Dynamic Response of Hydraulic Fluid
21  %     Within Tapered Transmission Lines.
21  % Proceedings of the 15th Scandinavian International Conference on Fluid
        Power, 2017
22
23
24  c = sqrt(K/rho);
25  lambda = min(r1,r2)/max(r1,r2); % Taper ratio (dimensionless). eq(11)
26  beta = ((nu*L)/(c*max(r1,r2)^2))*((lambda^2+lambda+1)^2/(9*lambda^3)); %
        Dimensonless dissipation number. eq(13)
27  Zc = ((3*c*rho)/(pi*max(r1,r2)^2))/(lambda^2+lambda+1); % Characteristic
        impedance. eq(10)
28
29  T=L/c;%(s) Nominal propagation time
30  T_1=T*tau;%(s) adjusted transmission time forward propagation. eq(18)
31  T_2=T_1;%(s) adjusted transmission time reverse propagation
32  Zc_1 = Zc;
33  Zc_2 = Zc;
34
35  k = max([numel(mG), numel(mE)]);
36
37  n=nan(1,k);%weighting function coefficient
38  n(1)=0.3/(1+3*beta);% eq(19)
39  for i=2:k
40      n(i)=n(i-1)*3;% eq(19)
41  end
42
43  %calculate transfer function E. eq(14)
44  tmpsum=zeros(size(omega));
45  for i=1:numel(mE)
46      tmpsum=tmpsum+mE(i)./(n(i)+1j.*omega*T);
47  end
48  E_1=tmpsum*Zc_1;
```

```
49  E_2=E_1;
50
51  %calculate transfer function F, eq (15)
52  tmpsum=0;
53  for i=1:numel(mE)
54      tmpsum=tmpsum+mE(i)/(n(i));
55  end
56  b=1-8*beta/tmpsum; % eq (16)
57  F_1=Zc_2+b*E_1;
58  F_2=F_1;
59
60  %calculate transfer function G, eq (17)
61  tmpsum=zeros(size(omega));
62  for i=1:numel(mG)
63      tmpsum=tmpsum+mG(i)*1j*omega*T./(n(i)+1j.*omega*T);
64  end
65  G_1=1-tmpsum;
66  G_2=G_1;
67
68  end
```

B.9   TaperedTLMTransferMatrix.m

```
1   function [ t11, t12, t21, t22 ] = TaperedTLMTransferMatrix( omega, E_1, E_2,
        F_1, F_2, G_1, G_2, Zc_1, Zc_2, T_1, T_2 )
2   %[ t11, t12, t21, t22 ] = TaperedTLMTransferMatrix( omega, E_1, E_2, F_1, F_2
        , G_1, G_2, Zc_1, Zc_2, T_1, T_2 )
3   % Calculates the transmission matrix from the TLM transfer functions,
4   % characteristic impedance, and wave propagation times.
5   %
6   % Inputs: Transfer functions, characteristic impedance, and wave
7   %          propagation times.
8   %
9   % Outputs: t11,t21,t12,t22 = TLM transmission matrix terms
10  %
11  % NOTE: E, F, G, T, and Z_c are separated by _1 and _2 to allow investigation
        into
12  % separate transfer functions as discussed in ven der Buhs and Wiens [2017].
13  %
14  % References:
15  % J ven der Buhs and T Wiens. Modelling Dynamic Response of Hydraulic Fluid
        Within Tapered Transmission Lines.
```

```matlab
% Proceedings of the 15th Scandinavian International Conference on Fluid
    Power, 2017
%
% N Johnston, M Pan, and S Kudzma. An enhanced transmission line method for
    modelling laminar flow of liquid
% in pipelines. Journal of Systems and Control Engineering, 228(4):193Ű206,
    2014.

t11 = ((E_1+Zc_1).*G_1.^(-1).*exp(1j*omega*T_1)+F_1.*G_2.*exp(-1j*omega*T_2)
    )./(E_1+Zc_1+F_1); %eq (20)

t21 = ((-G_2.*exp(-1j.*omega.*T_2)+G_1.^(-1).*exp(1j*omega*T_1)))./(E_1+
    Zc_1+F_1); %eq (22)

t12 = ((E_1+Zc_1).*(E_2+Zc_2).*G_1.^(-1).*exp(1j*omega*T_1)-F_1.*F_2.*G_2.*
    exp(-1j*omega*T_2))./((E_1+Zc_1+F_1)); %eq (21)

t22 = -((E_2+Zc_2).*G_1.^(-1).*exp(1j*omega*T_1)+F_2.*G_2.*exp(-1j*omega*
    T_2))./(E_1+Zc_1+F_1); %eq (23)

end
```

B.10   interpolateTLMparams.m

```matlab
function [ mE_interp, mG_interp, tau_interp ] = interpolateTLMparams(
    request_beta, request_lambda, k_request )
%[ mE_interp, mG_interp, tau_interp ] = interpolateTLMparams( request_beta,
    request_lambda, k )
%   This interpolates TLM transfer function parameters based on beta
%   (dissipation number), lambda (taper ratio), and number of parameters k.
%   Refer to ven der Buhs and Wiens, 2017 for details.
%
%   References
%   J ven der Buhs and T Wiens. Modelling Dynamic Response of Hydraulic Fluid
%    Within Tapered Transmission Lines. Proceedings of the 15th Scandinavian
    International Conference on Fluid Power, 2017

    load TaperedTLMLookupTable.mat

if k_request ~= 6
    error('Currenly only 6 weighting factors are available, k must be 6 for
        this version of the model')
end
```

```matlab
mE_interp=nan(1,k_request);
mG_interp=nan(1,k_request);

for i=1:k_request
    mE_interp(i) = interp2(beta_lookup,lambda_lookup,mE_lookup(:,:,i),
        request_beta,request_lambda,'linear');
    mG_interp(i) = interp2(beta_lookup,lambda_lookup,mG_lookup(:,:,i),
        request_beta,request_lambda,'linear');
end

tau_interp = interp2(beta_lookup,lambda_lookup,tau_lookup,request_beta,
    request_lambda,'linear');
end
```

Appendix C

CAD Drawings For Experimental Apparatus

This Appendix contains the detailed CAD drawings for the prototype tapered transmission line used for the validation experiments presented in Chapter 2. The drawings presented here contain all dimensions and manufacturing instructions required for reproduction. Assembly drawings contain bills of material, tabulating manufactured and purchased parts. Hydraulic fittings have part numbers provided by Green Line® Hose and Fittings Ltd. (n.d.), a Canadian supplier.
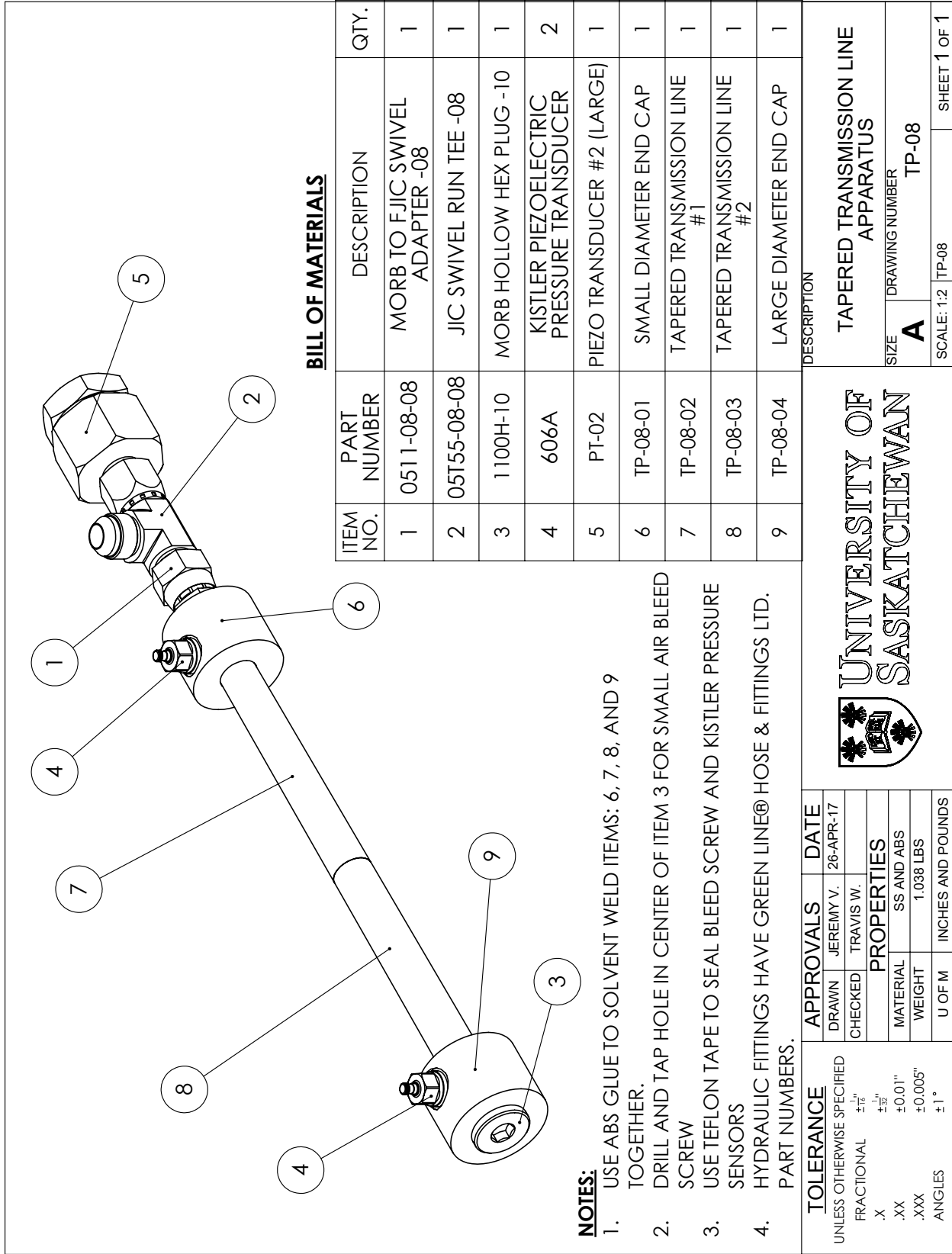
BILL OF MATERIALS

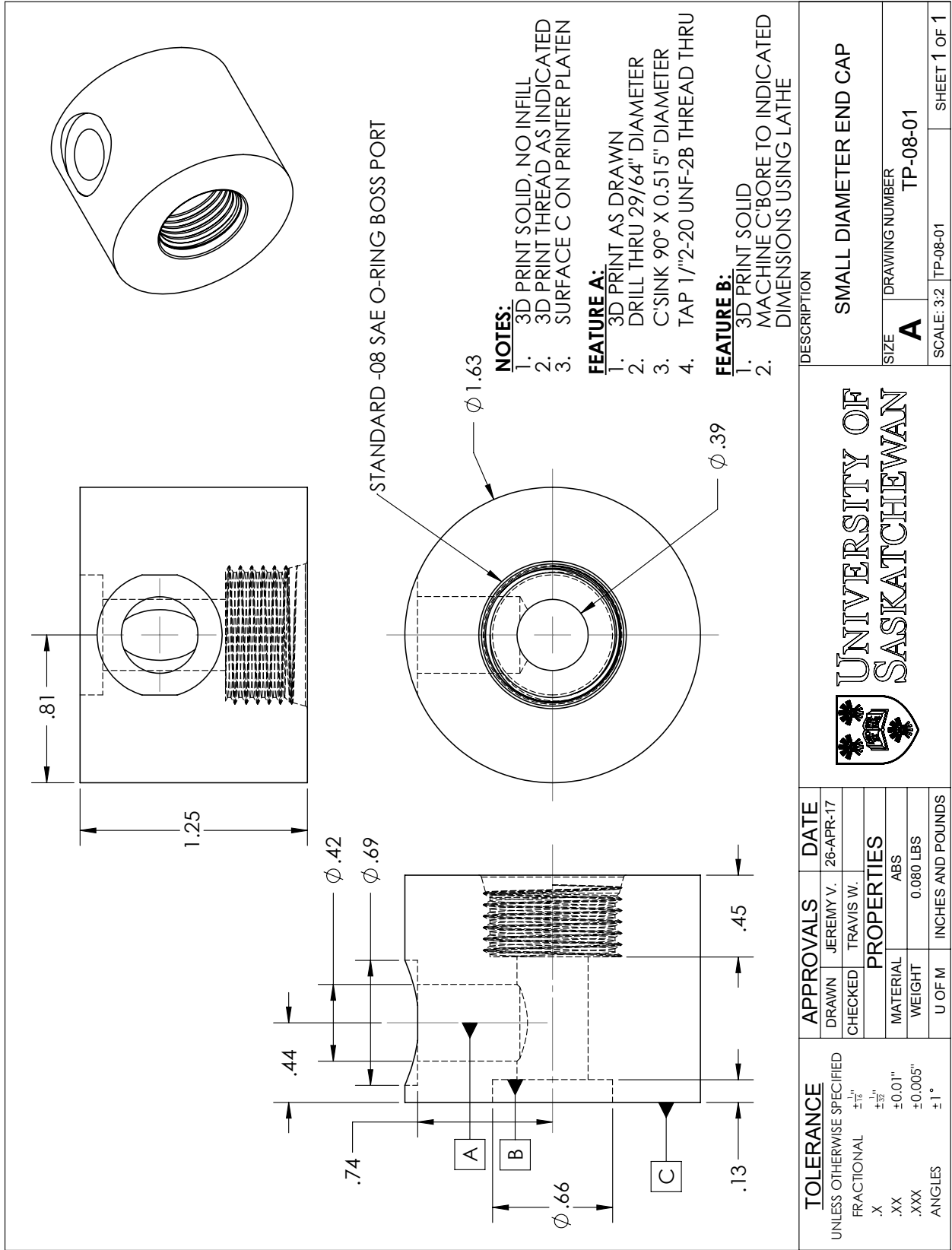| ITEM NO.	PART NUMBER	DESCRIPTION	QTY.
1	0511-08-08	MORB TO FJIC SWIVEL ADAPTER -08	1
2	05T55-08-08	JIC SWIVEL RUN TEE -08	1
3	1100H-10	MORB HOLLOW HEX PLUG -10	1
4	606A	KISTLER PIEZOELECTRIC PRESSURE TRANSDUCER	2
5	PT-02	PIEZO TRANSDUCER #2 (LARGE)	1
6	TP-08-01	SMALL DIAMETER END CAP	1
7	TP-08-02	TAPERED TRANSMISSION LINE #1	1
8	TP-08-03	TAPERED TRANSMISSION LINE #2	1
9	TP-08-04	LARGE DIAMETER END CAP	1

NOTES:

1. USE ABS GLUE TO SOLVENT WELD ITEMS: 6, 7, 8, AND 9 TOGETHER.
2. DRILL AND TAP HOLE IN CENTER OF ITEM 3 FOR SMALL AIR BLEED SCREW
3. USE TEFLON TAPE TO SEAL BLEED SCREW AND KISTLER PRESSURE SENSORS
4. HYDRAULIC FITTINGS HAVE GREEN LINE® HOSE & FITTINGS LTD. PART NUMBERS.
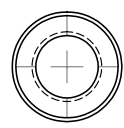
UNIVERSITY OF SASKATCHEWAN

TOLERANCE			APPROVALS	DATE
UNLESS OTHERWISE SPECIFIED			DRAWN	JEREMY V.	26-APR-17
FRACTIONAL	$\pm\frac{1}{16}$		CHECKED	TRAVIS W.	
.X	$\pm\frac{1}{32}$		**PROPERTIES**	
.XX	±0.01"		MATERIAL	SS AND ABS
.XXX	±0.005"		WEIGHT	1.038 LBS
ANGLES	±1°		U OF M	INCHES AND POUNDS

DESCRIPTION

TAPERED TRANSMISSION LINE APPARATUS

SIZE **A**

DRAWING NUMBER TP-08

SCALE: 1:2 | TP-08 | SHEET 1 OF 1

STANDARD -08 SAE O-RING BOSS PORT

∅ 1.63

∅ .39

NOTES:
1. 3D PRINT SOLID, NO INFILL
2. 3D PRINT THREAD AS INDICATED
3. SURFACE C ON PRINTER PLATEN

FEATURE A:
1. 3D PRINT AS DRAWN
2. DRILL THRU 29/64" DIAMETER
3. C'SINK 90° X 0.515" DIAMETER
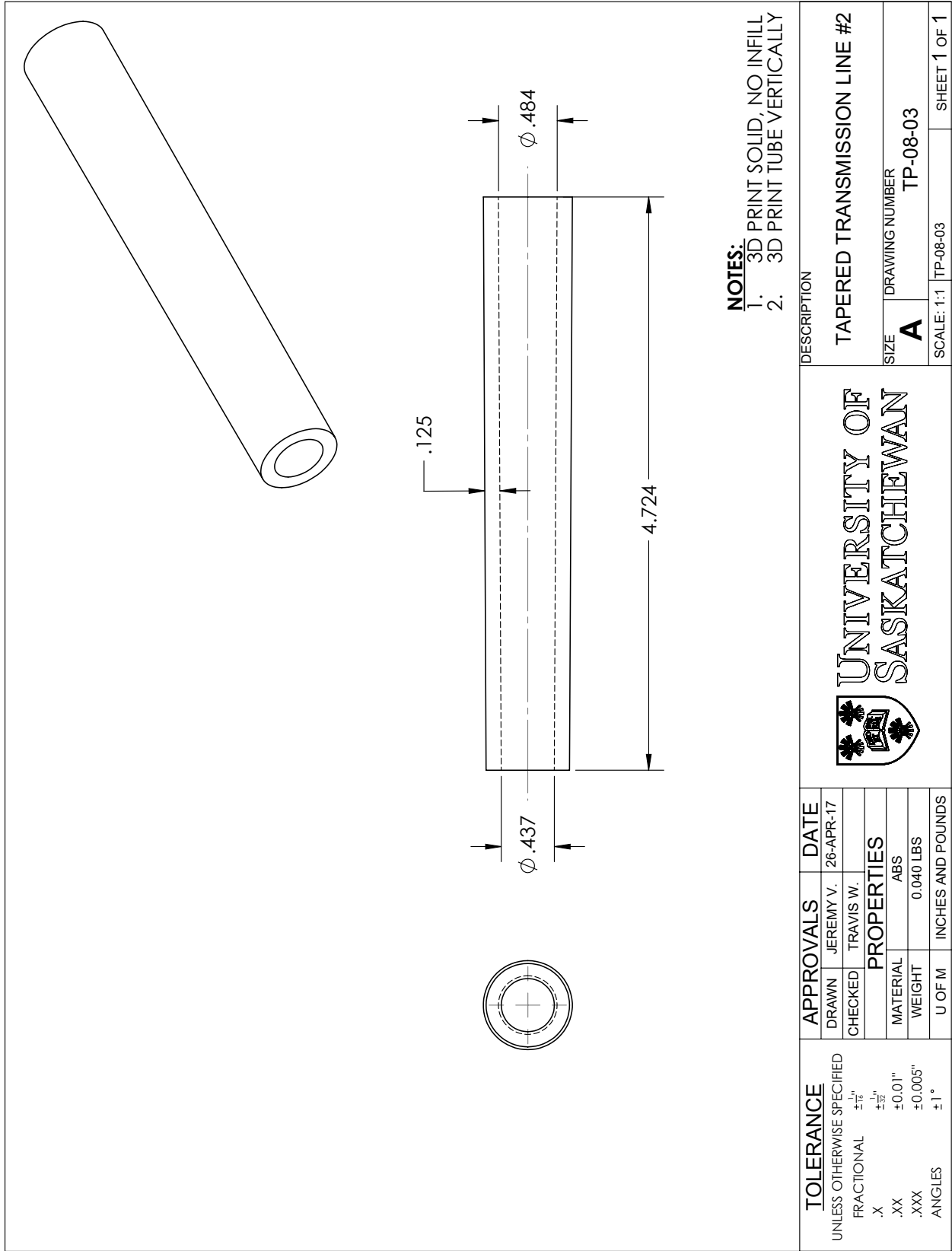4. TAP 1/"2-20 UNF-2B THREAD THRU

FEATURE B:
1. 3D PRINT SOLID
2. MACHINE C'BORE TO INDICATED
   DIMENSIONS USING LATHE

.81

1.25

∅ .42

∅ .69

.44

.74

∅ .66

.45

.13

A

B

C

TOLERANCE			APPROVALS	DATE
UNLESS OTHERWISE SPECIFIED			DRAWN	JEREMY V.	26-APR-17
FRACTIONAL	±$\frac{1}{16}$"		CHECKED	TRAVIS W.	

.X	±$\frac{1}{32}$"
.XX	±0.01"
.XXX	±0.005"
ANGLES	±1°

PROPERTIES

MATERIAL	ABS
WEIGHT	0.080 LBS
U OF M	INCHES AND POUNDS

UNIVERSITY OF SASKATCHEWAN

DESCRIPTION

SMALL DIAMETER END CAP

DRAWING NUMBER

TP-08-01

SIZE **A**

SCALE: 3:2 | TP-08-01 | SHEET 1 OF 1

Ø .437

.125

4.724

Ø .391
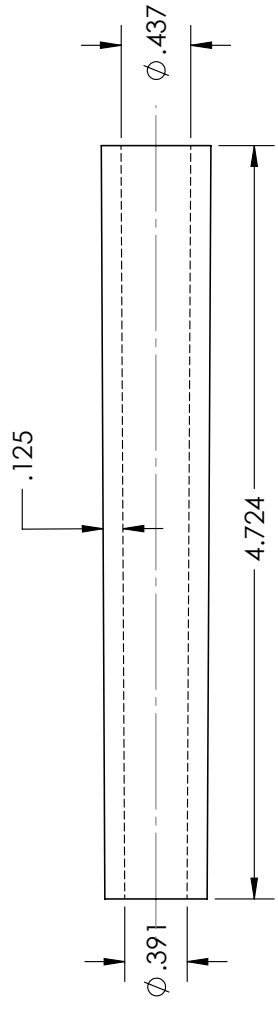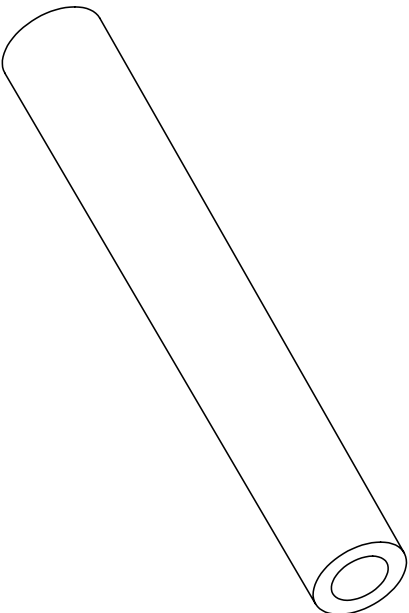
NOTES:
1. 3D PRINT SOLID, NO INFILL
2. 3D PRINT TUBE VERTICALLY

DESCRIPTION

TAPERED TRANSMISSION LINE #1

DRAWING NUMBER
TP-08-02

SIZE
A

SCALE: 1:1 | TP-08-02 | SHEET 1 OF 1

APPROVALS		DATE
DRAWN	JEREMY V.	26-APR-17
CHECKED	TRAVIS W.	

PROPERTIES

MATERIAL	ABS
WEIGHT	0.037 LBS
U OF M	INCHES AND POUNDS

UNIVERSITY OF
SASKATCHEWAN

TOLERANCE
UNLESS OTHERWISE SPECIFIED

FRACTIONAL	$\pm\frac{1}{16}$"
.X	$\pm\frac{1}{32}$"
.XX	± 0.01"
.XXX	± 0.005"
ANGLES	$\pm 1°$

∅.484

.125

4.724

∅.437

DESCRIPTION

TAPERED TRANSMISSION LINE #2

DRAWING NUMBER

TP-08-03

SIZE **A**

SCALE: 1:1 | TP-08-03 | SHEET 1 OF 1
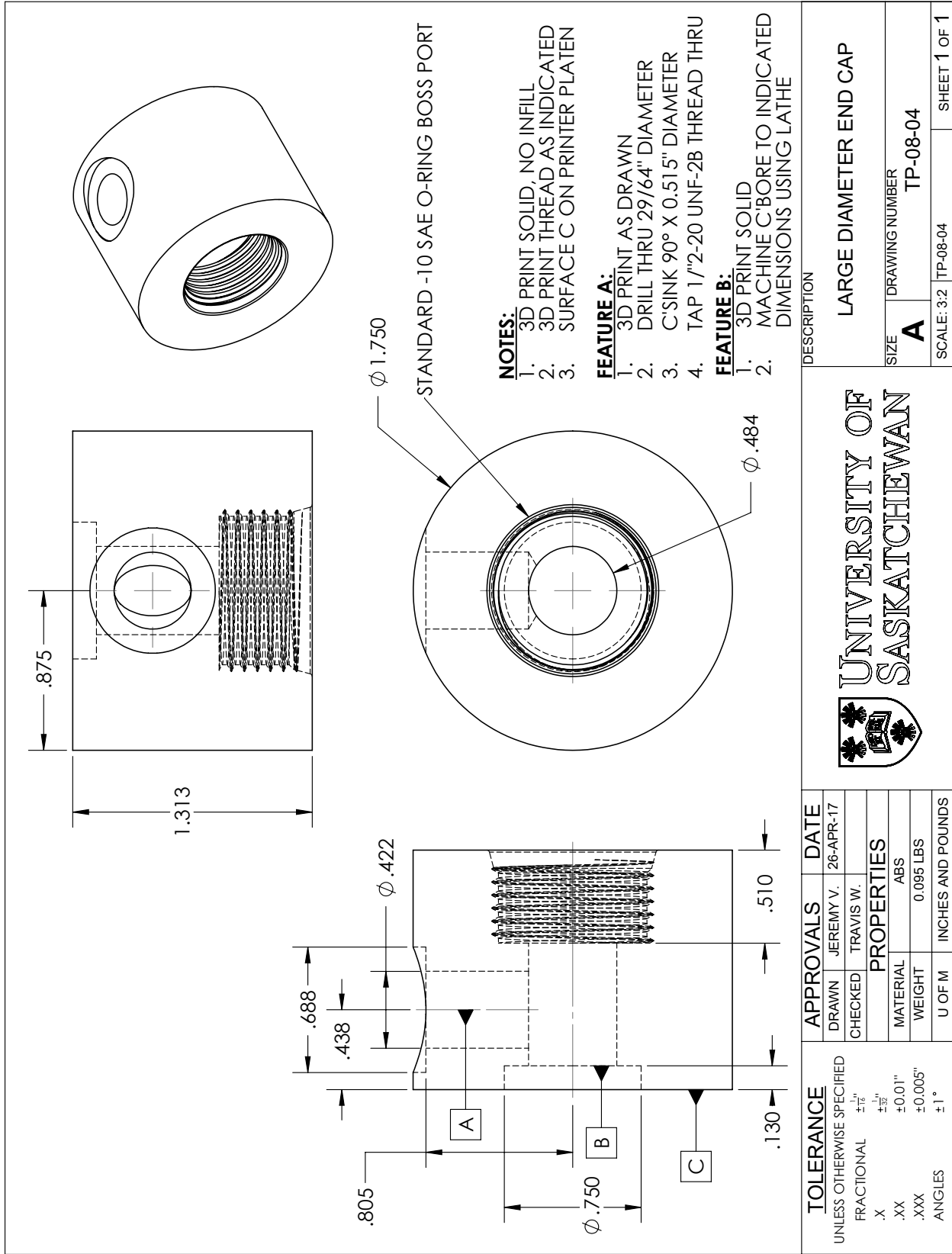
UNIVERSITY OF
SASKATCHEWAN

APPROVALS		DATE
DRAWN	JEREMY V.	26-APR-17
CHECKED	TRAVIS W.	

PROPERTIES

MATERIAL	ABS
WEIGHT	0.040 LBS
U OF M	INCHES AND POUNDS

TOLERANCE

UNLESS OTHERWISE SPECIFIED

FRACTIONAL	±$\frac{1}{16}$"
.X	±$\frac{1}{32}$"
.XX	±0.01"
.XXX	±0.005"
ANGLES	±1°

STANDARD -10 SAE O-RING BOSS PORT

⌀ 1.750

⌀ .484

NOTES:
1. 3D PRINT SOLID, NO INFILL
2. 3D PRINT THREAD AS INDICATED
3. SURFACE C ON PRINTER PLATEN

FEATURE A:
1. 3D PRINT AS DRAWN
2. DRILL THRU 29/64" DIAMETER
3. C'SINK 90° X 0.515" DIAMETER
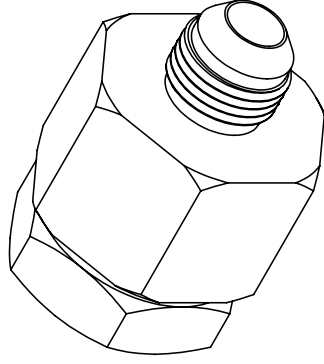4. TAP 1/2"-20 UNF-2B THREAD THRU

FEATURE B:
1. 3D PRINT SOLID
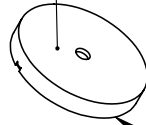2. MACHINE C'BORE TO INDICATED DIMENSIONS USING LATHE

.875

1.313

⌀ .422

.688

.438

.805

⌀ .750

.510

.130

A

B

C

TOLERANCE		APPROVALS		DATE
UNLESS OTHERWISE SPECIFIED		DRAWN	JEREMY V.	26-APR-17
FRACTIONAL	$\pm\frac{1}{16}$"	CHECKED	TRAVIS W.	
.X	$\pm\frac{1}{32}$"	**PROPERTIES**		
.XX	±0.01"	MATERIAL	ABS	
.XXX	±0.005"	WEIGHT	0.095 LBS	
ANGLES	±1°	U OF M	INCHES AND POUNDS	

UNIVERSITY OF SASKATCHEWAN

DESCRIPTION

LARGE DIAMETER END CAP

SIZE **A**

DRAWING NUMBER

TP-08-04
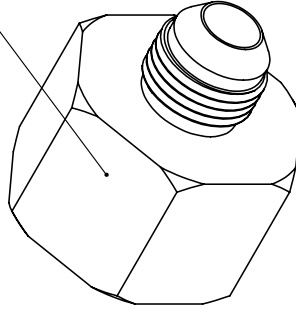
SCALE: 3:2 | TP-08-04 | SHEET 1 OF 1

MACHINING NOTE:
BORE INSIDE OF PLUG TO FIT PIEZO ELEMENT.
BORE APPROX 1/2" TO 5/8" DEEP.
BORE LARGE ENOUGH DIAMETER TO HOUSE
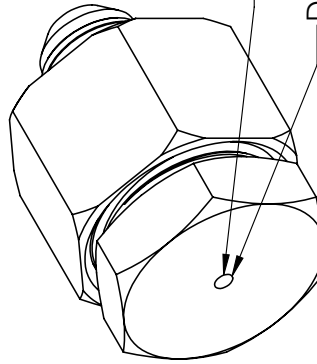PIEZO AND WIRE LEADS

①

③

②

EPOXY PIEZO TRANSDUCER INTO DRILLED PLUG

FILE EDGE SMOOTH FOR PROPER FLARE SEAL

ENSURE EPOXY FILLS DRILLED HOLE

DRILL 1/8" HOLE THRU FOR WIRE LEADS

NOTES:
1. USE APPROPRIATE STRENGTH EPOXY TO PREVENT LEAKAGE
2. HYDRAULIC FITTINGS HAVE GREEN LINE® HOSE & FITTINGS LTD. PART NUMBERS.

BILL OF MATERIALS

ITEM NO.	PART NUMBER	DESCRIPTION	QTY.
1	0515-06-08	FJIC-16 TO MJIC-08 REDUCER	1
2	1500-16	MJIC PLUG -16	1
3	AT-2310-T-LW100-R1	PIEZO SPEAKER ELEMENT	1

UNIVERSITY OF SASKATCHEWAN

TOLERANCE		APPROVALS	DATE
UNLESS OTHERWISE SPECIFIED		DRAWN	JEREMY V.	04-AUG-16
FRACTIONAL	$\pm\frac{1}{16}$"	CHECKED	TRAVIS W.	
.X	$\pm\frac{1}{32}$"	**PROPERTIES**	
.XX	±0.01"	MATERIAL	STAINLESS STEEL
.XXX	±0.005"	WEIGHT	0.60 LBS
ANGLES	±1°	U OF M	INCHES AND POUNDS

DESCRIPTION

PIEZO TRANSDUCER #2 (LARGE)

SIZE	DRAWING NUMBER
A	PT-02
SCALE: 1:1 PT-02	SHEET 1 OF 1

Appendix D

Inertance Tube Optimization Matlab Code

The MATLAB® code provided here corresponds to the simulation and optmization of the hydraulic buck converter analyzed in this thesis. `ShapedInertanceSegmenting.m` is a function called in the shaped inertance tube SIMULINK® block mask that ensures tapered segments meet a minimum taper ratio. If the minimum taper ratio is not met, the line is segmented maintaining the same taper ratio throughout until the minimum is met. The function then outputs the individual lengths and diameters for the individual tapered TLM blocks making up the shaped inertance tube. `Tapered3TubeOptimization.m` is the main m-file used for Optimization 4 in Chapter 4. This function calls the algorithm `patternsearch()` or genetic algorithm `ga()`, optimizing the objective function `optEffFcn.m`. The objective function simulates the model, but also calls `DesiredLoadPerformance.m` to find the correct duty cycle to maintain desired load pressure.

D.1   ShapedInertanceSegmenting.m

```
1  function [ blockDiameters, blockLengths, N ] = ShapedInertanceSegmenting( d,
       x, lambda_min )
2  % [ blockDiameters, blockLengths, N ] = ShapedInertanceSegmenting( d, x,
       lambda_min )
3  %
4  % This script allowes for the specification of arbitrary tube shapes with
5  % linear tapered connections between points in the look-up table. This
6  % script will segment tapered sections that have excessive taper, by
7  % maintaining a minimum taper ratio specified by the user.
8  %
9  % Inputs:  d = User specified diameter look-up table
10 %          x = User specified axial position look-up table
11 % lambda_min = User specified minimum taper ratio
12 %
```

```
13  % Outputs: blockDiameters = Look-up table of diameters of all segments
14  %              including those segmented due to excessive taper.
15  %              blockLengths = Look-up table of the lengths of each tapered
16  %              TLM block, including those segmented due to excessive taper.
17
18  %%
19  % First find any uniform sections in the given shape
20  for i = 2:numel(d);
21      uniform(i-1) = d(i) - d(i-1);
22  end
23  uniformIndex = find(~uniform);
24  numUniform = numel(uniformIndex);
25
26  % Compute the taper ratios for all sections in the look-up table
27  for i = 2:numel(d);
28      taperRatios(i-1) = min(d(i),d(i-1))/max(d(i),d(i-1));
29  end
30
31  taperedIndex = find(abs(taperRatios - 1));
32  numTapered = numel(taperedIndex);
33
34  % We want to be within acceptable error, i.e. lower the amount of taper per
35  % section. So excessivly tapered sections need to be split up.
36
37  % Preallocate size for diameters.
38  % This ensures matrix diameters is preallocated to the maximum size of
39  % the number of segments required to avoid matrix dimension errors later on.
40  [~,index] = min(taperRatios);
41      taperRatio = taperRatios(index);
42      j = 2;
43      d_mids = 0;
44  if taperRatio <= lambda_min
45      while taperRatio <= lambda_min
46          SectionDiameters = [d(index)];
47          d_mids = (d(index)^(j-1)*d(index+1))^(1/j);
48          taperRatio = min(d(index),d_mids)/max(d(index),d_mids);
49
50          if d(index) < d(index+1)
51              for n = 1:j
52              SectionDiameters  = [SectionDiameters SectionDiameters(n)/
                     taperRatio];
53              end
54          else
55              for n = 1:j
```

```matlab
                SectionDiameters  = [SectionDiameters SectionDiameters(n)*
                    taperRatio];
            end
        end

        j = j+1;

    end
    diameters = zeros(1,numel(SectionDiameters));
end

% Segment the largely tapered sections
for i = taperedIndex
    taperRatio = taperRatios(i);
    j = 2;
    d_mids = 0;
    if taperRatio <= lambda_min
    while taperRatio <= lambda_min
        SectionDiameters = [d(i)];
        d_mids = (d(i)^(j-1)*d(i+1))^(1/j); % Equation (3.5)
        taperRatio = min(d(i),d_mids)/max(d(i),d_mids);

        if d(i) < d(i+1)
            for n = 1:j
            SectionDiameters  = [SectionDiameters SectionDiameters(n)/
                taperRatio]; % Equation (3.6)
            end
        else
            for n = 1:j
            SectionDiameters  = [SectionDiameters SectionDiameters(n)*
                taperRatio]; % Equation (3.6)
            end
        end

        j = j+1;

    end
    % Assigns the segmented diameters into 1 matrix
    diameters(i,1:numel(SectionDiameters)) = SectionDiameters;
    else
    % Assigns given diameters if taper ratio is OK.
    diameters(i,1:2) = [d(i) d(i+1)];
    end
end

```

```matlab
98
99  % Diameters selected, now interpolate the tube lengths.
100 for i = taperedIndex
101     for m = 1:nnz(diameters(i,:))
102     locations(i,m) = interp1([d(i) d(i+1)], [x(i) x(i+1)], diameters(i,m),'
            linear','extrap');
103     end
104
105     for m = 1:(numel(locations(i,:))−1)
106         lengths(i,m) = locations(i,m+1) − locations(i,m);
107     end
108
109 end
110
111 % Combine 2D lengths into a 1D blockLengths matrix in order from inlet to
112 % outlet.
113 % Creates look−up table of lengths.
114     blockLengths = [];
115 for i = 1:(numTapered+numUniform)
116     if ~isempty(find(~(taperedIndex−i)))
117         blockLengths = [blockLengths lengths(i,1:nnz(lengths(i,:)>0))];
118     else
119         blockLengths = [blockLengths, x(i+1)−x(i)];
120     end
121
122 end
123
124 % Combine 2D diameters into a 1D blockDiameters matrix in order from inlet
125 % to outlet.
126 % Creates look−up table of diameters
127     blockDiameters = [d(1)];
128 for i = 1:(numTapered+numUniform)
129     if ~isempty(find(~(taperedIndex−i)))
130         blockDiameters = [blockDiameters diameters(i,2:nnz(diameters(i,:)>0))
                ];
131
132     else
133         blockDiameters = [blockDiameters, d(i+1)];
134
135     end
136
137 end
138
139 % Compute the number of TLM segments required in total.
140 N = nnz(blockLengths > 0);
```

```
141
142  end
```

D.2   Tapered3TubeOptimization.m

```
1   % This script performs an optimization of the inertance tube within a
        switched inertance converter.
2
3   % This script optimized 3 tapered segments, resulting tin 7 prameters of
4   % diameters and lengths
5
6   % Copyright 2017, Jeremy ven der Buhs
7
8   % Initialize model parameters. I'm using a structure here as it can be easily
        passed to the objective function as a single input.
9   params.kappa_pa_0 = 24.5; % Inital guess for switching duty cycle
10  params.f_pa = 50; % Switching frequency (Hz)
11  params.P_HP = 25e6; % High pressure supply pressure (Pa)
12  params.P_LP = 10e6; % Low pressure reservoir pressure (Pa)
13  params.P_L_desired = 16e6; % Targer load pressure (Pa)
14  params.t_sw = 0.003; % Valve switching time (s)
15
16  warning off; % Suppress warning output from simulink. Warning is the buffer
        size of the TLM time delays.
17
18  open Tapered3InertanceTube.slx
19
20  % This is how MATLAB command window talks with the simulink model
21  WS = get_param('Tapered3InertanceTube','modelworkspace'); % Gets the simulink
        model's variable workspace
22  % Assign values from this workspace to the models workspace
23  assignin(WS,'P_HP',params.P_HP);
24  assignin(WS,'P_LP',params.P_LP);
25  assignin(WS,'f_pa',params.f_pa);
26  assignin(WS,'t_sw',params.t_sw);
27  assignin(WS,'P_L_desired',params.P_L_desired);
28
29  % Choose optimization algorithm using switch-case statements.
30  optAlgor = 'patternsearch';
31
32  switch optAlgor
33      % Pattern search alorigthm
34      case 'patternsearch'
```

```matlab
             % Define our optimization function
             fcn_min = @(dims) optEffFcn(dims, params);
             % Lower and upper bounds
             lb = [0.5, 0.5, 0.5, 4.5, 4.5, 4.5, 4.5];
             ub = [8, 8, 8, 40, 40, 40, 40];
             % Solver options
             optionsOpt = psoptimset('Cache','on');
             % Run patternsearch
             x = patternsearch(fcn_min
                 ,[3.9718,1.5419,7.2813,9.2136,8.8806,21.1802,21.8497],[],[],[],[],
                 lb,ub,[],optionsOpt);

     % Genetic algorithm (ga)
     case 'ga'
             % Define our optimization function
             fcn_min = @(dims) optEffFcn(dims, params);
             % Lower and upper bounds on parameters
             lb = [0.5, 0.5, 0.5, 4.5, 4.5, 4.5, 4.5];
             ub = [8, 8, 8, 40, 40, 40, 40];
             % Solver options
             options = optimoptions('ga','MaxStallGenerations', 5, '
                 FunctionTolerance', 1e-2,'PopulationSize', 100);
             % Run genetic algorithm
             x = ga(fcn_min,7,[],[],[],[],lb,ub,[],[],options);

end
```

D.3   optEffFcn.m

```matlab
function [ eta_sys, dims ] = optEffFcn(dims, params)
%[ eta_sys, dims ] = optEffFcn(dims, params)
%   Efficiency optimization objective function. Takes inputs of
%   inertabe tube parameters dims, and general model parameters params
%   in the form of a structure. Outputs eta_sys being the system
%   energetic efficiency, and dims being the dimensions of the inertance
%   tube.

% Extract section lengths from first 3 entries of the dims vector
l_1 = dims(1);
l_2 = dims(2);
l_3 = dims(3);
% Extract section diameters from final 4 entries of the dims vector
d_1 = dims(4);
```

```matlab
15  d_2 = dims(5);
16  d_3 = dims(6);
17  d_4 = dims(7);
18
19  % Provide some updates to the user such as the dimensions currently being
20  % simulated:
21  disp(['Length_1 = ' num2str(l_1) 'm']);
22  disp(['Length_2 = ' num2str(l_2) 'm']);
23  disp(['Length_3 = ' num2str(l_3) 'm']);
24  disp(['Diameter_1 = ' num2str(d_1) 'mm']);
25  disp(['Diameter_2 = ' num2str(d_2) 'mm']);
26  disp(['Diameter_3 = ' num2str(d_3) 'mm']);
27  disp(['Diameter_4 = ' num2str(d_4) 'mm']);
28
29  % This is how MATLAB command window talks with the simulink model.
30  WS = get_param('Tapered3InertanceTube','modelworkspace'); % Gets the simulink
        model's variable workspace
31  % Assign values from this workspace to the models workspace
32  assignin(WS,'l_1',l_1);
33  assignin(WS,'l_2',l_2);
34  assignin(WS,'l_3',l_3);
35  assignin(WS,'d_1',d_1);
36  assignin(WS,'d_2',d_2);
37  assignin(WS,'d_3',d_3);
38  assignin(WS,'d_4',d_4);
39
40  % What duty cycle is needed to ensure same performance regardless of tube
        dimensions?
41  options = optimset('tolX',0.01); % Set fzero tolerance
42  FUN = @(kappa_pa) DesiredLoadPerformance(kappa_pa, params.f_pa, params.
        P_L_desired); % Define function
43  % Run fzero to find the correct duty cycle of the valve to operate the load
44  % at an average of params.P_L_desired.
45  kappa_pa = fzero(FUN,params.kappa_pa_0,options); %
46  % Assign the correct duty cyle
47  assignin(WS,'kappa_pa',kappa_pa);
48
49  % Had to implement a try catch structure just incase an error was thrown by
50  % simulink. Errors typically would included invalid inertance tube
51  % dimensions.
52
53  try % Try a simulation
54      simOut = sim('Tapered3InertanceTube'); % Simulate the model, and put
            output data in simOut structure
55      %% Get workspace variables from the SIMULINK output
```

```matlab
56      % Get Load Pressure
57      P_L = simOut.get('P_L');
58      % Get Load Flow
59      Q_L = simOut.get('Q_L');
60      % Get Check Flow
61      Q_CV = simOut.get('Q_CV');
62      % Get Pressure at A
63      P_A = simOut.get('P_A');
64      % Get Switching valve Flow
65      Q_PA = simOut.get('Q_PA');
66      % Get Timeseries
67      t_sim = simOut.get('tout');
68
69      % Some code used to select the last cycle of the simulation
70      t_end = t_sim(end);
71      t_start = t_end   (1/params.f_pa);
72      [~,index] = min(abs(t_sim t_start));
73
74      %% Compute Power efficiency. Useful power divided by power input
75      % Load power
76      W_load = (P_L(index:end)-params.P_LP).*Q_L(index:end);
77      % Area under curve (integration)
78      A = trapz(t_sim(index:end),W_load);
79      % Average load power
80      W_load_ave = A/(t_sim(end)-t_sim(index));
81      % System Input Power
82      W_HP = (params.P_HP-params.P_LP).*Q_PA(index:end);
83      % Area under curve (integration)
84      B = trapz(t_sim(index:end),W_HP);
85      % Average load power
86      W_HP_ave = B/(t_sim(end)-t_sim(index));
87      % Average mechanical efficiency.
88      eta_sys = -W_load_ave/W_HP_ave; % Must be negative as MATLAB's
            optimization functions MINIMIZE problems.
89
90      %% Volumetric efficiency
91      % Average load flow (integration)
92      A = trapz(t_sim(index:end),Q_L(index:end));
93      Q_L_ave = A/(t_sim(end)-t_sim(index));
94      % Average switching valve flow (integration)
95      A = trapz(t_sim(index:end),Q_PA(index:end));
96      Q_PA_ave = A/(t_sim(end)-t_sim(index));
97
98      % Volumetric efficiency
99      eta_vol = Q_L_ave*(kappa_pa/100)/Q_PA_ave;
```

```matlab
100
101      % Update the user on the result of this objective function evaulation.
102      disp(['SysEff = ' num2str(-eta_sys*100) '%']);
103      disp(['VolEff = ' num2str(eta_vol*100) '%']);
104      disp('-----------------------'); % Visual seperator.
105
106  catch
107      % Catch the error and assign a very poor value of efficiency. In this
            case 40%.
108      eta_sys = -0.40;
109      % This allows the program to continue running if errors occur.
110  end
111
112  end
```

D.4   DesiredLoadPerformance.m

```matlab
1  function [ fitness ] = DesiredLoadPerformance( kappa_pa, f_pa, P_L_desired)
2  %[ fitness ] = DesiredLoadPerformance( kappa_pa, f_pa, P_L_desired)
3  %   Function used to find the correct valve switching duty cycle kappa_pa to
       achieve
4  %   a load pressure of P_L_desired. Also takes input of f_pa being the
5  %   valves operating frequency. Outputs fitness, being the the actual
6  %   load pressure minus P_L_desired.
7
8  % This is how MATLAB command window talks with the simulink model.
9  WS = get_param('Tapered3InertanceTube','modelworkspace'); % Gets the simulink
       model's variable workspace
10
11  % Assign duty cycle from this workspace to the models workspace
12  assignin(WS,'kappa_pa',kappa_pa);
13
14  % Had to implement a try-catch structure just incase an error was thrown by
15  % simulink. Errors typically would included invalid inertance tube
16  % dimensions.
17
18  try % Try a simulation
19      simOut = sim('Tapered3InertanceTube'); % Simulate the model, and put
            output data in simOut structure
20      % Get Load Pressure
21      P_L = simOut.get('P_L');
22      % Get Timeseries
23      t_sim = simOut.get('tout');
```

```matlab
24
25     % Some code used to select the last cycle of the simulation
26     t_end = t_sim(end);
27     t_start = t_end − (1/f_pa);
28     [~,index] = min(abs(t_sim−t_start));
29
30     % Integration to find average load pressure over last cycle
31     A = trapz(t_sim(index:end),P_L(index:end));
32     % Average load pressure
33     P_L_ave = A/(t_sim(end)−t_sim(index));
34
35     % Evaluate fitness, how close the actual load pressure it to the desired
           load pressure
36     fitness = P_L_ave − P_L_desired;
37
38     % Provide the user with some information
39     disp(['kappa_pa = ' num2str(kappa_pa)])
40     disp(['Load Pressure = ' num2str(P_L_ave)])
41
42 catch
43     % Catch error, if any, and make fitness 0. This way fzero will stop
           immediately and will be caught in optEffFcn and will be assigned a
           poor value of efficiency.
44     fitness = 0;
45 end
46
47 end
```

Appendix E

Tabulation of Parameters

This Appendix provides two tables of the physical parameters used for simulations and computations presented in this thesis. All parameters are reported using Système International (SI) units with imperial values and units reported in parenthesis where provided. Table E.1 contains the parameters of the experimental apparatus, and those used for theoretical calculations in Chapter 2.

Table E.1: Parameters of the experimental apparatus

Parameter	Value	Unit
l	270	mm
r_1	4.9	mm
r_2	6.15	mm
e	3.18 (1/8)	mm (in)
E	2	GPa
ν_p	0.3	-
p_s	1379 (200)	kPa (psi)
ρ	882 [a]	kg/m^3
T_p	23	°C
ν	180×10^{-6} [b]	m^2/s
K	1.5 [c]	GPa
V_p	± 15	V
f_s	10	kHz

[a] Fluid used was Mobil™ Nuto™ H 68 hydaulic oil.
[b] Determined using ASTM D341 - 09 (Reapproved 2015).
[c] Difficult to measure directly, therefore tuned to give satisfactory results.

Table E.2 contains the parameters used for the initial simulations in Chapter 3, as well as the optimizations performed in Chapter 4. The diameter and location look-up tables, $\boldsymbol{d}$ and $\boldsymbol{x}_d$, included here are only for the initial simulation, the optimized values in Table 4.1

are used for the simulations and calculations in Chapter 4.

Table E.2: Parameters used for simulation

Parameter	Value	Unit
p_s	25	MPa
p_t	10	MPa
t_{sw}	3	ms
f_{pa}	50	Hz
κ_{pa}	54%	-
$A_{pa,min}$	25	mm^2
$A_{pa,min}$	0.001	mm^2
$A_{pa,max}$	10	mm^2
$A_{ta,min}$	0.001	mm^2
$A_{ta,max}$	96.2	mm^2
p_{cr}	0	kPa
p_{or}	10	kPa
C_d	0.61	-
ρ	860	kg/m^3
μ/ν	39.6/46.0	cP/cSt
K	1.4	GPa
R_{cr}	1000	-
$\boldsymbol{d}$	[5 5]	mm
$\boldsymbol{x}_d$	[0 6.38]	m
V_l	0.32	L
A_l	2.14	mm^2
Solver	`ode23t`	-
relTol	1×10^{-6}	-

Appendix F

Transmission Line Modelling of Viscoelastic Pipes

This Appendix proposes the exact transmission matrix used for computing the fluid dynamics in long fluid-filled tapered viscoelastic transmission lines. The work presented here takes the partial differential equations given by Covas et al. (2005) for uniform lines and applies it to tapered lines. The main goal of the derivation is to get the partial differential equations into a single ordinary differential equation so it can be solved. The work presented here takes it further by providing the Laplace transform of the Navier-Stokes equations for application to the TLM weighing factor optimization for tapered lines. Selected equations are presented here, however if more information on the derivation is required, please refer to the paper by Covas et al.

F.1 Derivation of the Differential Equation

A tapered viscoelastic transmission line has a schematic given by Figure F.1.

The internal radius varies linearly over the length of the line given by the following equation:
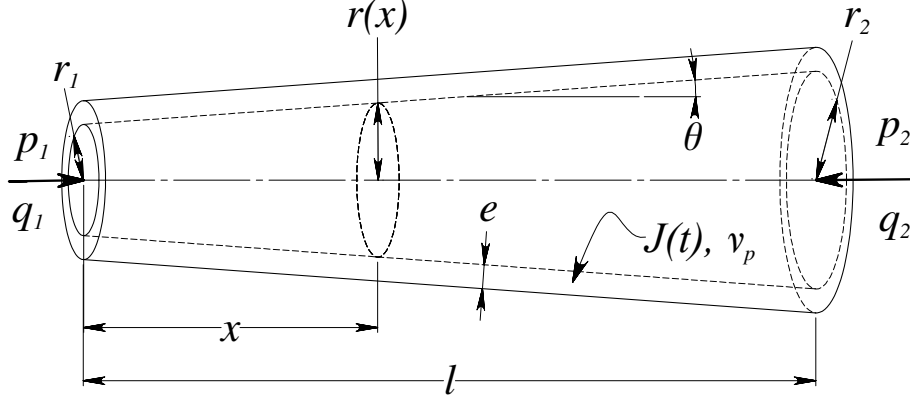
$$r(x) = r_1 + \frac{(r_2 - r_1)x}{l}, \tag{F.1}$$

with the internal cross sectional area given as:

$$A(x) = \pi \left[r_1 + \frac{(r_2 - r_1)x}{l} \right]^2. \tag{F.2}$$

The Navier-Stokes equation of motion is the same as presented in Chapter 2 (Viersma, 1980):

$$\frac{\partial P(x, s)}{\partial x} + \frac{\rho s}{A(x)} Q(x, s) N(x, s) = 0, \tag{F.3}$$

Figure F.1: Schematic of a tapered transmission line with viscoelastic wall effects. Note that constant wall thickness is maintained throughout the length of the pipe. Angle, θ, is assumed to be small.

however the continuity equation is modified to include the effects of wall viscoelasticity, represented in the time-domain here using pressure, p, instead of pressure head, H, as in Covas et al. (2005):

$$\frac{dp(x,t)}{dt} + \frac{\rho c_e(x)^2}{A(x)}\frac{\partial q(x,t)}{\partial x} + 2\rho c_e(x)^2\frac{d\epsilon_r(x,t)}{dt} = 0. \tag{F.4}$$

Here the elastic wavespeed is $c_e(x)$, and the retarded strain due to wall viscoelasticity is $\epsilon_r(x,t)$. Since the wavespeed is considerably larger than the fluid velocity, the convective terms when expanding the total time derivatives are neglected yielding the following differential equation:

$$\frac{\partial p(x,t)}{\partial t} + \frac{\rho c_e(x)^2}{A(x)}\frac{\partial q(x,t)}{\partial x} + 2\rho c_e(x)^2\frac{\partial\epsilon_r(x,t)}{\partial t} = 0. \tag{F.5}$$

Then taking the Laplace transform of continuity Equation (F.5) and dividing through by s:

$$P(x,s) + \frac{\rho c_e(x)^2}{A(x)s}\frac{\partial Q(x,s)}{\partial x} + 2\rho c_e(x)^2\hat{\epsilon}_r(x,s) = 0, \tag{F.6}$$

where the elastic wavespeed is defined as:

$$c_e(x) = \sqrt{\frac{\dfrac{K}{\rho}}{1+\alpha\dfrac{2Kr(x)}{eE_0}}}, \tag{F.7}$$

133

and the axial effects are calculated by:

$$\alpha = \begin{cases} 1 - \dfrac{\nu_p}{2} & \text{Anchored upstream,} \\ 1 - \nu_p^2 & \text{Anchored throughout,} \\ 1 & \text{Anchored with expansion joints.} \end{cases} \tag{F.8}$$

The Laplace transform of the retarded strain within the viscoelastic wall, $\hat{\epsilon}_r(x, s)$, requires further derivation. The wall material is assumed to be a generalized Kelvin-Voigt viscoelastic model shown schematically in Figure F.2. The model contains a combination of spring and dashpot elements connected in series and parallel to describe the overall dynamics.
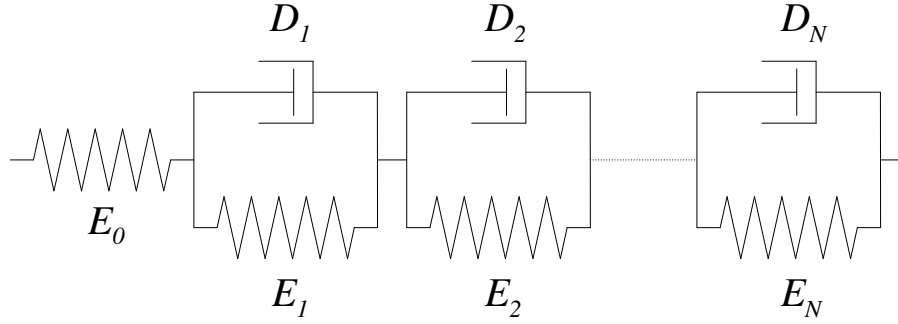
Figure F.2: Schematic representation of the generalized Kelvin-Voigt viscoelastic solid mechanical model. Here E_k is the elastic modulus for the kth element, and D_k is the dashpot viscosity of the kth element.

The dynamics of the viscoelastic wall is computed by the creep compliance function:

$$J(t) = J_0 + \sum_{k=1}^{N} J_k \left(1 - e^{\frac{-t}{\tau_k}} \right) \tag{F.9}$$

where $J_0 = \frac{1}{E_0}$ for the first spring element, and $J_k = \frac{1}{E_k}$ for subsequent elements. The retardation time of each element, τ_k, is defined as $\tau_k = \frac{D_k}{E_k}$. Typically these parameters are found from experimental creep compliance calibrations of the material (Covas et al., 2005). Therefore the total retarded strain, $\epsilon_r(x, t)$, is computed as a summation of the retarded strain of each Kelvin-Voigt element:

$$\epsilon_r(x, t) = \sum_{k=1}^{N} \epsilon_{rk}(x, t) \tag{F.10}$$

where each strain element, $\epsilon_{rk}(x, t)$, is defined by the integral:

$$\epsilon_{rk}(x, t) = \int_0^t f(x, t - t') \frac{J_k}{\tau_k} e^{\frac{-t'}{\tau_k}} \, dt'. \tag{F.11}$$

The last two terms of the integral come from taking the derivative of the creep-compliance function with respect to time. The function $f(x, t)$ relates to how the fluid pressure creates

circumferential stress on the pipe wall defined as:

$$f(x,t) = \frac{\alpha r(x)}{e}[p(x,t) - p_o(x)] \tag{F.12}$$

where $p_o(x)$ is the initial steady state pressure at location x, which will be assumed to be zero as the TLM assumes zero initial conditions. The next step is to take the Laplace transform of Equation (F.10) giving:

$$\hat{\epsilon}_r(x,s) = \sum_{k=1}^{N} \hat{\epsilon}_{rk}(x,s)$$
$$= \sum_{k=1}^{N} \mathscr{L}\left[\int_0^t f(x,t-t')\frac{J_k}{\tau_k}e^{\frac{-t'}{\tau_k}}dt'\right] \tag{F.13}$$

where Equation (F.13) is evaluated using the transform identify given by:

$$\mathscr{L}\left[\int_0^t g(t-t')h(t')dt'\right] = G(s)H(s). \tag{F.14}$$

The following relations to the identity are made:

$$g(t) = f(x,t) = \frac{\alpha r(x)}{e}p(x,t)$$
$$h(t) = \frac{J_k}{\tau_k}e^{\frac{-t}{\tau_k}} \tag{F.15}$$

then taking the corresponding Laplace transforms:

$$G(s) = F(x,s) = \frac{\alpha r(x)}{e}P(x,s)$$
$$H(s) = \frac{J_k}{\tau_k}\frac{1}{s+\frac{1}{\tau_k}} = \frac{J_k}{\tau_k}\frac{\tau_k}{\tau_k s+1} = \frac{J_k}{\tau_k s+1}. \tag{F.16}$$

By substituting these equations, the Laplace transform of the retarded strain is found to be:

$$\hat{\epsilon}_r(x,t) = \frac{\alpha r(x)}{e}P(x,s)\sum_{k=1}^{N}\frac{J_k}{\tau_k s+1}. \tag{F.17}$$

Then substituting Equation (F.17) into Equation (F.6) yields:

$$P(x,s) + \frac{\rho c_e(x)^2}{A(x)s}\frac{\partial Q(x,s)}{\partial x} + \frac{2\rho c_e(x)^2 \alpha r(x)}{e}\sum_{k=1}^{N}\frac{J_k}{\tau_k s+1}P(x,s) = 0. \tag{F.18}$$

Then combining the two pressure terms gives:

$$\left(1 + \frac{2\rho c_e(x)^2 \alpha r(x)}{e}\sum_{k=1}^{N}\frac{J_k}{\tau_k s+1}\right)P(x,s) + \frac{\rho c_e(x)^2}{A(x)s}\frac{\partial Q(x,s)}{\partial x} = 0. \tag{F.19}$$

135

Equation (F.19) is then rearranged as:

$$P(x, s) + \frac{\dfrac{\rho c_e(x)^2}{A(x)s}}{\left(1 + \dfrac{2\rho c_e(x)^2 \alpha r(x)}{e} \sum_{k=1}^{N} \dfrac{J_k}{\tau_k s + 1}\right)} \frac{\partial Q(x, s)}{\partial x} = 0. \tag{F.20}$$

Then simplifying to:

$$P(x, s) + \frac{1}{A(x)\psi(x, s)s} \frac{\partial Q(x, s)}{\partial x} = 0, \tag{F.21}$$

where $\psi(x, s)$ represents the compressibility of the fluid and pipe wall together:

$$\psi(x, s) = \frac{1}{K} + \frac{2\alpha r(x)}{e} W(s), \tag{F.22}$$

where the wall mechanical system is given as:

$$W(s) = J_0 + \sum_{k=1}^{N} \frac{J_k}{\tau_k s + 1}. \tag{F.23}$$

Taking the partial derivative of Equation (F.21) with respect to x and solving for the derivative of pressure yields:

$$\frac{\partial P(x, s)}{\partial x} = \left[\frac{1}{A(x)^2 \psi(x, s)s} \frac{dA(x)}{dx} + \frac{1}{A(x)\psi(x, s)^2 s} \frac{\partial \psi(x, s)}{\partial x} \right] \frac{\partial Q(x, s)}{\partial x} - \frac{1}{A(x)\psi(x, s)s} \frac{\partial^2 Q(x, s)}{\partial x^2} \tag{F.24}$$

then substituting Equation (F.24) into Equation F.3 and simplifying yields the final ordinary differential equation:

$$\frac{\partial^2 Q(x, s)}{\partial x^2} - \left[\frac{1}{A(x)} \frac{dA(x)}{dx} + \frac{1}{\psi(x, s)} \frac{\partial \psi(x, s)}{\partial x} \right] \frac{\partial Q(x, s)}{\partial x} - \rho\psi(x, s)s^2 Q(x, s)N(x, s) = 0, \tag{F.25}$$

where

$$\frac{dA(x)}{dx} = 2\pi \left[\frac{r_2 - r_1}{l} \right] \left[r_1 + \frac{(r_2 - r_1)x}{l} \right], \tag{F.26}$$

and

$$\frac{\partial \psi(x, s)}{\partial x} = \frac{2\alpha W(s)}{e} \left[\frac{r_2 - r_1}{l} \right]. \tag{F.27}$$

F.2 Results

Now with the ode derived, it is solved numerically, resulting in a transmission matrix given in Equation (F.28). They are solved using code similar to the MATLAB m-files ExactSolution

136

`forOpt.m`, `t11t21venderBuhsExact.m`, and `t12t22venderBuhsExact.m` in Appendix B.3, B.4 and B.5. It uses `bvp4c()` as the numerical solver to find the t_{xx} entries of the exact transmission matrix. Setting Q_2 to 0 allows for t_{11} and t_{21} to be found, and by setting P_2 to 0 allows for the solution of the other two entries, t_{12} and t_{22}. The boundary value problem is solved for every value of frequency.

$$\begin{pmatrix} P_1 \\ Q_1 Z_c \end{pmatrix} = \begin{pmatrix} t_{11} & t_{12} \\ t_{21} & t_{22} \end{pmatrix} \begin{pmatrix} P_2 \\ Q_2 Z_c \end{pmatrix}. \tag{F.28}$$

The parameters used for calculation are provided in Table F.1 below, and the computed transmission matrix terms of Equation (F.28) are provided in the following Figures F.3 - F.6. In the Figures, results of a purely elastic pipe wall are also provided to show the difference that viscoelasticity has on the dynamic response. The same parameters are used between the computations of elastic and viscoelastic, except the creep compliance terms J_1, J_2 and J_3 are set to zero for the elastic case.

Table F.1: Parameters used for computing the tapered viscoelastic transmission matrix. Viscoelastic properties of high-density polyethylene used for computations from Soares et al. (2008).

| Parameter	Value	Unit
r_1	10	mm
r_2	12	mm
l	5	m
e	1	mm
ν_p	0.3	-
Axial effect	Anchored upstream	-
E	1.4	GPa
J_1	0.104	GPa^{-1}
J_2	0.124	GPa^{-1}
J_3	0.410	GPa^{-1}
τ_1	0.05	s
τ_2	0.50	s
τ_3	10	s
K	1.5	GPa
ν	100	cSt
ρ	890	kg/m^3

F.3   Conclusions and Recommendations

This Appendix looked at finding the differential equation for flow through tapered viscoelastic transmission lines for application to the TLM approximation. The time domain continuity equation from Covas et al. (2005) was transformed into the Laplace domain and substituted into the momentum Navier-Stokes equation resulting in an overall second order differential
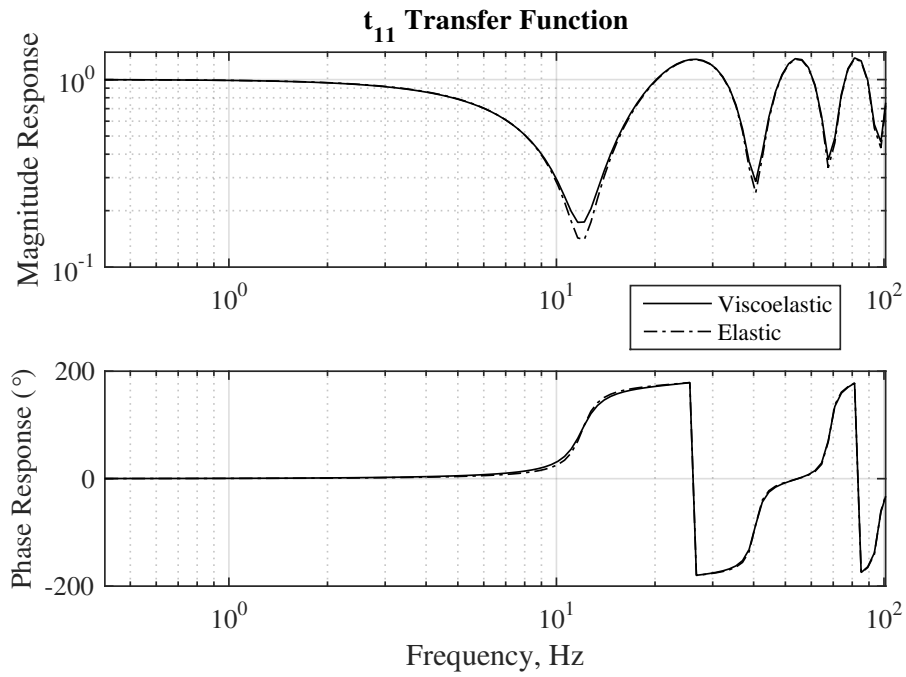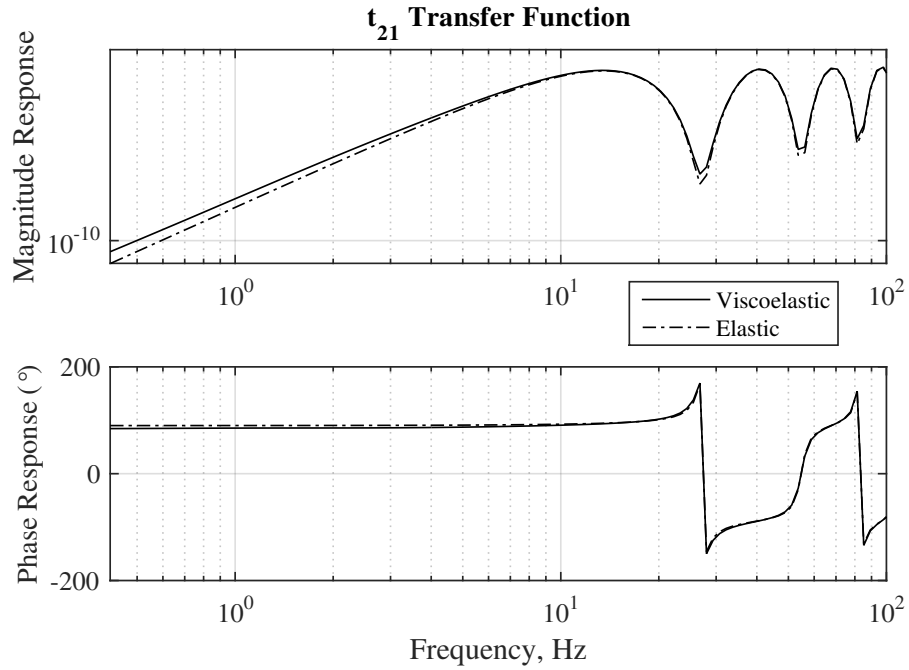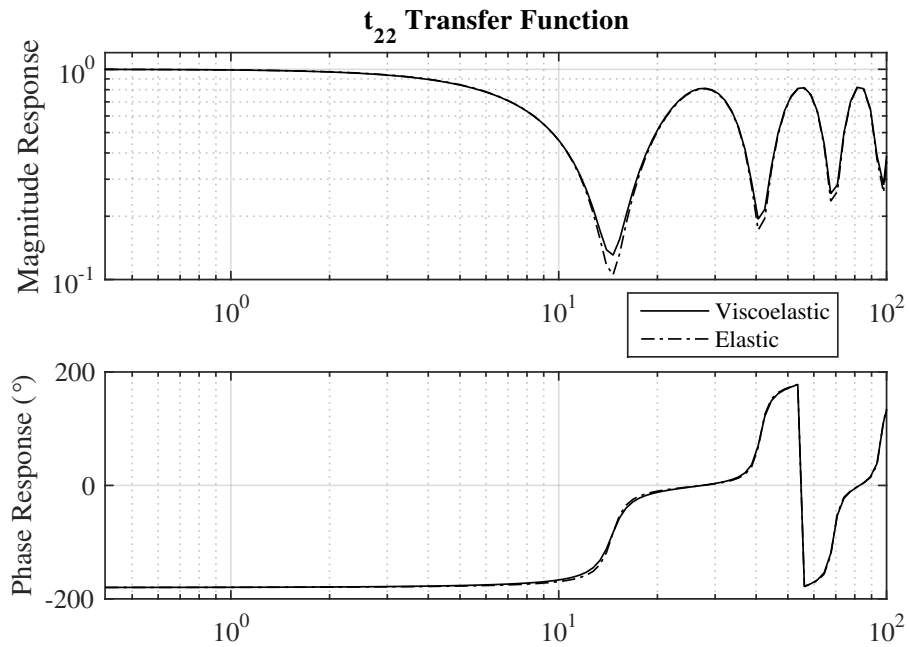
Figure F.3: The t_{11} transfer function in the transmission matrix for the analyzed viscoelastic and elastic tapered transmission line.
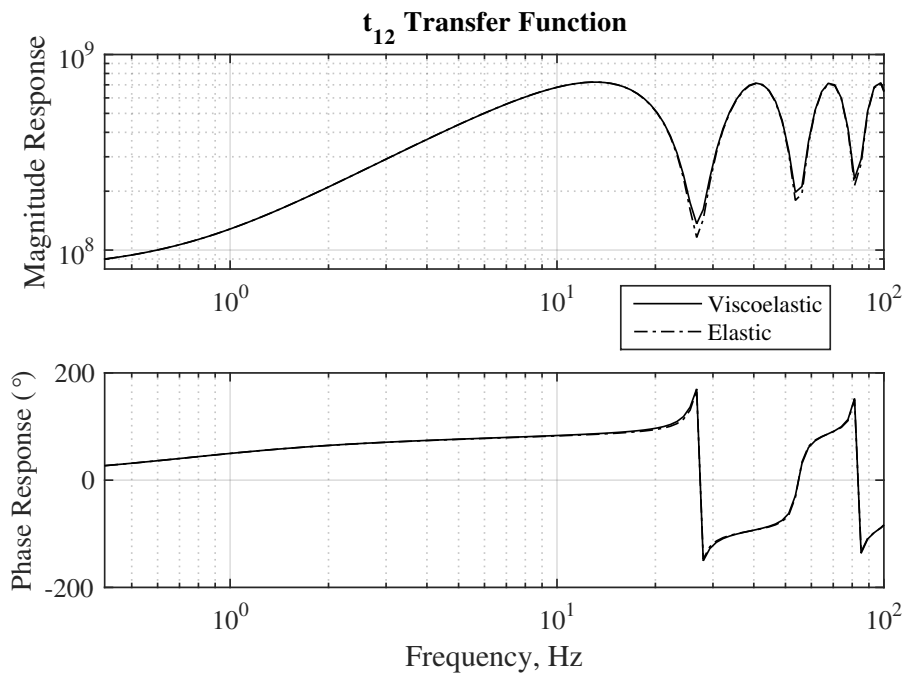
Figure F.4: The t_{12} transfer function in the transmission matrix for the analyzed viscoelastic and elastic tapered transmission line.

Figure F.5: The t_{21} transfer function in the transmission matrix for the analyzed viscoelastic and elastic tapered transmission line.

Figure F.6: The t_{22} transfer function in the transmission matrix for the analyzed viscoelastic and elastic tapered transmission line.

equation. Transmission matrix terms were computed using a boundary value solver and plotted for a pipeline of common hydraulic fluid properties, and viscoelastic properties of HDPE.

Future work on this topic should look at applying the TLM in order to simulate the dynamics quickly in the time domain. The dissipation number, β, and characteristic impedance, Z_c, would need to be derived in order to find and tabulate the TLM weighting factors. This could, however, propose a challenge as the wavespeed in the viscoelastic line is not a constant value due to the frequency dependence of the wall model, an observation also made by Suo and Wylie (1990). The wall model $W(s)$ has its frequency response plotted in Figure F.7. What can be seen is that the magnitude response decreases from a constant value to a lower constant value at fairly low frequency. The phase response also shows changes at low frequency, but remains constant at higher frequencies. At high frequency, the viscoelastic wall model converges to the results of the purely elastic wall. The effect the wall model has occurs primarily at lower frequencies for this pipeline, a point where the pipe doesn't naturally resonate. This explains why the transmission matrix terms plotted in the previous section look very similar between elastic and viscoelastic cases. The largest difference between the two wall models can be seen at lower frequencies. It appears that the inclusion of viscoelastic effects increases the dissipation and damping within the response, which intuitively makes sense due to the presence of viscous dampers inside the Kelvin-Voigt wall model. It is believed that a TLM approximation should be able to fit the numerical solutions for HDPE material presented here. However, this may not be true for other materials in which the viscoelastic dynamics of the wall create non-linearities in the frequency response that cannot be accounted for by the TLM.
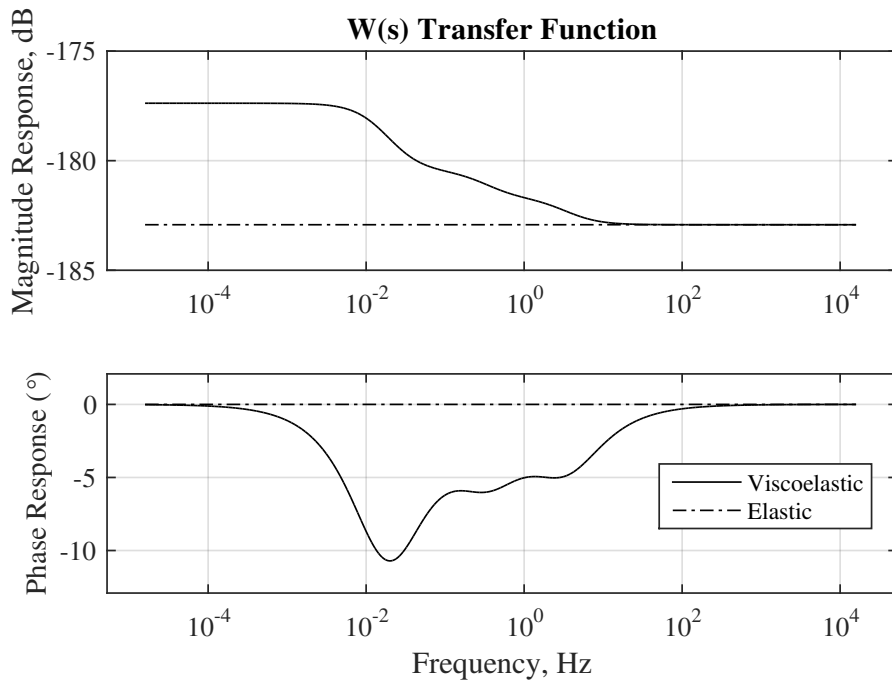
Figure F.7: The frequency response of the wall mechanical model for a viscoelastic and purely elastic pipe wall.